NTNU

Norwegian University of
Science and Technology

Study of impacting droplet on plain and micro-nano enhanced surfaces using Electron Beam Lithography (EBL)

Diego Sanchez Saldana

Petroleum Engineering
Submission date: July 2017
Supervisor: Carlos Alberto Dorao, EPT

Norwegian University of Science and Technology
Department of Energy and Process Engineering

NTNU

Norwegian University
of Science and Technology

Department of Energy
and Process Engineering

EPT-M-2017- 111

MASTER THESIS

For Diego Sánchez Saldaña

Spring 2017

Fabricating and testing of Si nanowires with design characteristics using Electron Beam Lithography (EBL)

Background and objective

The need for high heat flux removal has been triggered by the development of new technologies ranging from computers, data centers, medical applications, electric cars, radars, satellite and lasers, to mention some applications. Today it is recognized that manufacturability is not the limiting factor with regards to the small size of the devices, and that the major challenge is the power dissipation problem, i.e. how to remove the heat from a confined space. A particular alternative is to modify the surface for enhancing heat transfer. In this sense, the fabrication of high height-to-width aspect ratio (HAR) structures play a major role in studying the relationship between the surface characteristics and its heat transfer capability.

The main objective in this work is to develop an optimal procedure for the fabrication of designed nanowires using Electron Bean Lithography EBL and testing of the novel surfaces.

The following tasks are to be considered:

1. Literature study on fabrication of nanowires with focus on alternative techniques and its limitations and potentials.
2. Fabricate and characterize nanowires with a diameter from 100nm to 5000nm and different pitch.
3. Identify the procedure for reproducibility of the samples.

-- ” --

Within 14 days of receiving the written text on the master thesis, the candidate shall submit a research plan for his project to the department.

When the thesis is evaluated, emphasis is put on processing of the results, and that they are presented in tabular and/or graphic form in a clear manner, and that they are analyzed carefully.

The thesis should be formulated as a research report with summary both in English and Norwegian, conclusion, literature references, table of contents etc. During the preparation of the text, the candidate should make an effort to produce a well-structured and easily readable report. In order to ease the evaluation of the thesis, it is important that the cross-references are correct. In

the making of the report, strong emphasis should be placed on both a thorough discussion of the results and an orderly presentation.

The candidate is requested to initiate and keep close contact with his/her academic supervisor(s) throughout the working period. The candidate must follow the rules and regulations of NTNU as well as passive directions given by the Department of Energy and Process Engineering.

Risk assessment of the candidate's work shall be carried out according to the department's procedures. The risk assessment must be documented and included as part of the final report. Events related to the candidate's work adversely affecting the health, safety or security, must be documented and included as part of the final report. If the documentation on risk assessment represents a large number of pages, the full version is to be submitted electronically to the supervisor and an excerpt is included in the report.

Pursuant to "Regulations concerning the supplementary provisions to the technology study program/Master of Science" at NTNU §20, the Department reserves the permission to utilize all the results and data for teaching and research purposes as well as in future publications.

The final report is to be submitted digitally in DAIM. An executive summary of the thesis including title, student's name, supervisor's name, year, department name, and NTNU's logo and name, shall be submitted to the department as a separate pdf file. Based on an agreement with the supervisor, the final report and other material and documents may be given to the supervisor in digital format.

X Work to be done in lab (Water power lab, Fluids engineering lab, Thermal engineering lab)
☐ Field work

Department of Energy and Process Engineering, 13. January 2017

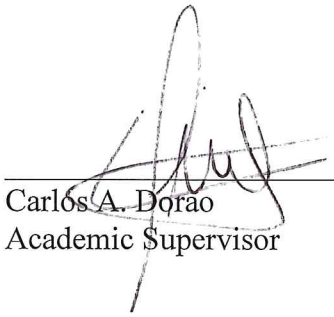

Carlos A. Dorao
Academic Supervisor

Research Advisor:
Manuel Auliano

Acknowledgements

This master thesis report has benefitted immensely from the wisdom, intellectual suport, and practical help of colleagues within the department. I would like to thank the invaluable support of Professor Carlos Alberto Dorao, who was of great support throughout the research of this work. I would also like to thank PhD candidate Manuel Auliano who guided my research, teaching me every step during the process, and Daniel Gonzalez who has carried out the experiments with me. I owe a debt to all the NTNU NanoLab staff for their patience acquainting me to the working process in the cleanroom. The Research Council of Norway is acknowledged for the support to the Norwegian Micro- and Nano-Fabrication Facility, NorFab, project number 245963/F50.

Summary

Compact systems with high power densities are being vastly designed and fabricated in the present. These include electronic devices, CPU chips, telecom equipment, micro-chemical reactors, micro-fuel cell combusts, power semiconductor lasers and radar amplifiers. Yet, the most important problem regarding these devices lies in effective dissipation of the tremendous heat that they produce reaching beyond air cooling limits, therefore liquid cooling will become necessary. Liquid cooling has a limitation in its use, it is called Leidenfrost phenomenon in which, a vapour film is formed in between the liquid and the solid hot surface at a certain temperature and hences a spontaneous reduction in heat transfer. Nanotechnology is allowing for the development of surfaces with special properties that improve the limitation of heat transfer for instance Si nanowires.

The main objective in this work is to identify and fabricate nanostructures for improving the Leidenfrost phenomenon, enhancing the heat transfer performance, and the design and fabrication of an experimental setup for the visualization of Leidenfrost phenomenon identifying the maximum heat flux and the Leidenfrost point. In this project techniques for fabricating the selected structures have been carried out and the structures have been characterized by available equipment at the NTNU Nanolab. Furthermore, design and fabrication of a test section for studying impacting droplets over a micro-nano structure surface has been completed.

Important results uncovered in this work are the following. Description of the facility setup. Plain polished silicon reference Leidenfrost curves and Weber map with water and FC-72 have been defined for a better understanding of the Leidenfrost phenomenon. This, ultimately, allowed for an optimization in the processes of heat transfer. Anomalous wetting characteristics and improvements of limitation in the Leidenfrost phenomenon have been identified for samples with nanostructures compared with plain polished silicon.

Contents

Figures

List of Tables

1. Introduction

1.1 Motivation and background

High power density compact systems and industry applications are currently being vastly designed and fabricated. These include electronic devices, CPU chips, telecom equipment, micro-fuel cell combustors [1], heating surfaces in boilers working on supercritical parameters [2], power semiconductor lasers, and radar amplifiers [3]. This development has posed a major challenge regarding the dissipation of high heat duties from these devices. In the present, heat fluxes generated by electronic circuits can reach a value of about 300 W/cm². Their operation is, however, complicated due to some of the characteristics of electronic circuit such as dimension and permissible working temperature that should be below 85 °C [4]. These high heat fluxes are easily removed by using recent cooling techniques.

Past scholarly studies have explored several solutions to this problem, e.g. single-phase flow through microchannels, micro-porous media, using a sufficiently subcooled fluid to avoid evaporation, doping conventional fluids with nanoparticles to produce nano fluids, cooling with a myriad of impinging liquid jets, as well as impinging droplet sprays with or without partial evaporation of the fluid, to create a very large heat dissipation surface area with micro and nano structures [1]. The use of micro-nano structures can be combined with the use of liquid for cooling to tackle their limitations.

The Leidenfrost phenomenon appears when a pan is heated to 200°C, the water evaporates so quickly that a thin layer of vapor forms between the pan and the water droplet. This temperature, the Leidenfrost temperature, initiates a regime where the low thermal conductivity of the vapor layer inhibits the heat transfer between the hot surface and the liquid. This limits the use of liquid to cold hot surfaces as it prevents the dissipation of heat [5]. The application of random silicon nanowires that delay the occurrence of this phenomenon improving the heat transfer has been found to be a valid solution to this issue. These nanowires, as a nano-structured materials, have interesting physical and chemical properties which can improve the limitation of liquid cooling [6]. The combination of these nanostructures with spray cooling improve boiling

characteristics and reaching a critical heat flux, CHF hereafter, which fulfils the needs of high heat flux removal and protect the heating surface before unexpected failure.[7]

This study investigates the improvement of these nanostuctural surfaces of silicon in the leindenfrost phenomenon. By designing an experimental setup for experiments and reproducing a reference leindenfrost curves of plain polished silicon on different fluids with different Weber number and compare with silicon nanowires, different curves are drawn and discussed.

1.2 Objectives

The main aim of this work is the design and fabrication of an experimental setup for the visualization of the Leidenfrost phenomenon identifying the CHF and the Leidenfrost point, LDF hereafter, and define a reference for this phenomenon by drawing curves of droplet lifetime versus temperature. This is done by testing plain polished silicon with water and FC-72, then comparing the improvements of the CHF and LFD point using nanowires with different geometrical characteristics.

The following sub-objectives are to be achieved:

1. Provide a review of the state-of-the-art of the Leidenfrost phenomenon.
2. Design and fabricate a test facility for studying impacting droplet over a micro-nano structure surface.
3. Plain polished silicon reference Leidenfrost curves of droplet lifetime vs temperature and a Weber map with water and FC-72 to compare with nanowires experiments.
4. Leidenfrost curves of nanowires experiments showing the improvements.
5. Fabrication and characterization of different nanostructured surfaces in the NTNU NanoLab.

1.3 Scope of the work

This work focuses on the experiments of silicon nanowires fabricated. Plain polished silicon Leidenfrost experiments with water and FC-72 will be carried out in order to compare the improvement in the Leidenfrost phenomenon of the rough samples with silicon nanowires of different geometrical characteristics.

1.4 Structure

Chapter 2 introduces a review of Leidenfrost phenomenon, Weber map and basic concepts for the further understanding of the phenomenon.

Chapter 3 explains the Leidenfrost phenomenon and the importance of the Weber map.

Chapter 4 describes general aspects relative to the fabrication of the nanostructures tested.

Chapter 5 specifies the facility setup in order to visualize the Leidenfrost phenomenon.

Chapter 6 presents final results and a subsequent discussion.

Chapter 7 offers a conclusion for this work and identifies the challenges remaining.

2. Theory and background

2.1 Leidenfrost phenomenon history

The Leidenfrost phenomenon, also known as film boiling, occurs when a liquid comes into contact with a solid that is at a temperature above the liquid's boiling point. Upon contact, a layer of vapor forms between the liquid-solid interfaces, creating a barrier between the two. There are many examples of this phenomenon, even in day-to-day life (water "dancing" around in a pan while boiling) [8].

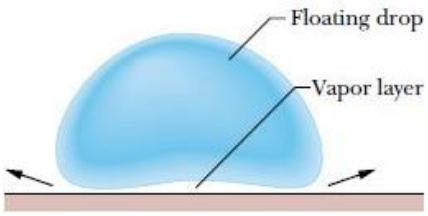

Figure 1- A Leidenfrost phenomenon, drop in cross section [9]

The process of film boiling is attributed to the doctor and theologian Johann Gottlob Leidenfrost (1715-1794) who first described the effect in his manuscript *A Tract About Some Qualities of Common Wate*r in 1756. Here the phenomenon is explained in depth by looking at the case of a hot frying pan and water droplets. If a pan is heated to 200°C, the water evaporates so quickly that a thin layer of vapor forms between the pan and the water droplet, this temperature is called Leidenfrost temperature. It is at this point when the Leidenfrost regime starts as the low thermal conductivity of the vapor layer inhibits heat transfer between the hot surface and the liquid. The vapor also causes the water droplets to "dance" around in the pan as the vapor propels it in different directions. The droplets evaporate over a certain amount of time, taking longer if the pan is heated to a temperature above boiling, but below the Leidenfrost point. When the temperature of the cooling surface drops below the critical temperature, the vapor film collapses and the system enters a nucleate-boiling regime, which can result in vapor explosions that are particularly detrimental in certain contexts, such as in nuclear power plants. [10]

Due to this detrimental aspect, the Leidenfrost effect has focused the attention of many physicists with an interest in drops. It appeared that the drops in the Leidenfrost state are

convenient to manipulate fluids and particles, and are a good example of the ability of drops to be used as micro-reactors such as micro heat exchangers [39]. However, many things are still to be understood, especially when the drops are pushed towards their limits. There is still a lot to be studied about the Leidenfrost Point, especially regarding the temperature in which the drops can experience this effect on a given substrate [11].

In order to explain this knowledge gap about Leidenfrost phenomenon, experiments have been carried out focusing in different aspects of the phenomenon. In 1966, Wachters and Westerling [12] conducted pioneering experiments involving drop impact on a heated wall within the film boiling regime. Since then, great strides have been made, aided by new advances in both instrumentation and computational tools. Overall, numerous parameters can influence this process, including drop parameters (diameter, Ddrop, impact velocity, Vdrop, and physical properties of liquid, such as saturation temperature, Tsat, density, ρf, viscosity, μf, and surface tension, σ, surrounding gas parameters (pressure, temperature, properties, velocity, and flow configuration), and wall characteristics (wettability, diffusivity, surface roughness, and wall temperature, Tw) [13].

Parameter	Observation/References
Size of liquid mass	• LFP independent of liquid mass size (Gottfried et al. 1966 and Patel and Bell, 1966) • LFP increased with droplet volume (Nishio and Hirata, 1978)
Method of liquid deposition	• LFP differed between steady state drop size technique using a pipet and the transient sessile drop technique (Godleski and Bell, 1966). • LFP increased with droplet velocity (Patel and Bell, 1966, Yao and Cai, 1988; Klinzing et al. 1993; and Labeish, 1994). • LFP did not differ between sessile and impinging drops ($u_0 < 5$ m/s) (Bell, 1967 and Nishio and Hirata, 1978).
Liquid subcooling	• Liquid subcooling had little effect on LFP for water on polished aluminium, brass and stainless steel, but did cause an increased LFP on Pyrex (Baumeister et al. 1970). • Subcooling increased drop lifetime but did not influence the LFP (Hiroyasu et al. 1974). • Subcooling raise the LFP for water and other fluids at high pressures where both sensible and latent heat exchange are significant (Emmerson and Snoek, 1978).
Solid thermal properties	• LFP increases as solid thermal capacitance decreases (Patel and Bell, 1966; Baumeister et al., 1970; and Nishio and Harata, 1978). • Baumeister and Simon (1973) developed a LFP correlation accounts for solid thermal properties. • LFP independent of solid thermal diffusivity (Bell, 1967 and Emmerson, 1975).
Surface conditions	• Gottfried et al. (1966) estimated thet the vapor layer beneath a film boiling sessile water drop was on the order of 10 μm , which is on the same length scale as surface aspirates on machine finished surfaces (Benardin, 1993). Thus, rough surfaces in comparison to polished surfaces would be expected to require a higher LFP to support a thicker vapor layer to avoid liquid-solid contact for a sessile drop (Bradfield 1966). • LFP increased as surface roughness and fouling increased (Baumeister et al., 1970); Baumeister and Simon, 1973; and Nishio and Hirata, 1978). In contrast, Bell (1967) claimed tha surface oxide films had a negligible effect on the LFP for droplets. • LFP increased with increasing surface prosity (Avedision and Koplik, 1987). • LFP decreased with increased advancing contact angle in pool boiling (Kovalev, 1966; Unal et al,. 1992; and Labeish, 1994 and Ramilison and Lienhard, 1987).
Pressure	• LFP increased with pressure for various fluids (Nikolayev et al., 1974; Hiroyasu et al., 1974; and Emmerson, 1975; Emmerson and Snoek, 1978) • $(T_{leid} - T_{sat})$ found to remain constant for various pressures (Hiroyasu et al., Emmersion, Nishio and Hirata, 1978, and Testa and Nicotra, 1986). • Rhodes and Bell (1978) observed $(T_{leid} - T_{sat})$ for Freon-114 to be constant over a reduced pressure range of 0.125 to 0.350 and found it to decrease with increasing pressure above this range. Klimenko and Snytin (1990) reported similar findings for four inorganic fluids.

Table 1. Review of the existing literature. Summary of the influential LDF parameters [13]

Taking into account these influential parameters in LDF and, despite significant advances in experimental, theoretical and computational research in understanding the interfacial behaviour of the drop from the moment of impact, there are many inconsistencies concerning some of the most important aspects of the impact process and consequent heat transfer, especially in regard to critical heat flux, transition boiling, and the Leidenfrost point. This thesis aims to develop a better understanding of these aspects of the phenomenon.

2.2 Basic concepts

2.2.1 Structure definition

To characterize the structures and know what properties they have it is crucial that we define two parameters, the surface roughness and the contact surface fraction. These are calculated using three different areas of our structure: the top surface area, the projected surface area, and the real surface area. These are therefore further defined with the following subscripts t, p and a for cylindrical pillars on a plain surface fabricated in this work [14].

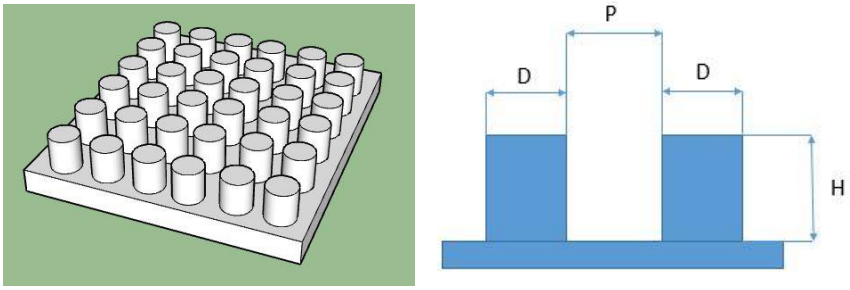

Figure 2 - Cylindrical pillars. Diameter, Pitch and Height

Cylindrical pillar:

$$A_p = (P + D)^2 \quad (1)$$

$$A_t = \frac{\pi D^2}{4} \quad (2)$$

$$A_a = A_p + \pi D h \quad (3)$$

With these areas we can calculate now the roughness ratio r and the contact surface fraction f:

$$f = \frac{A_t}{A_p} \quad (4)$$

$$r = \frac{A_a}{A_p} \quad (5)$$

2.2.2 Wettability

Wetting refers to the ability of a droplet to maintain contact with a surface; that is, to spread out and adhere when it is deposited in it. Wettability, the degree of wetting of a surface, depends on the balance between adhesive and cohesive forces [14]. When a liquid is deposited on a surface it can wet the surface completely, it may not be at all wetting, or a state in between, depending on surface energy. Contact angle is used to measure the wetting properties of the surface. If a liquid is brought in contact or partially in contact with the substrate, but does not form a film on the substrate, the state is called the Wenzel mode, Figure 2. If the drops do not make any contact with the substrate, the surface is non-wetting. This state is also called the Cassie mode, Figure 2 [15].

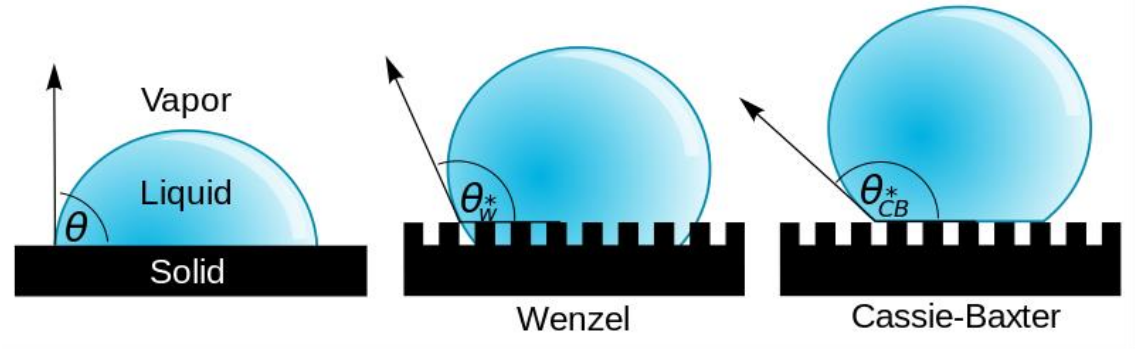

Figure 3 - Wezel mode and Cassie-Baxter mode droplet deposition [15]

2.2.3 Contact angle

Young et al. first proposed that the contact angle θ of the droplets is determined by the equilibrium at the three-phase contact line where the liquid, gas and solid intersect [16]:

$$\cos\theta = \frac{\gamma_{sv}-\gamma_{sl}}{\gamma_{lv}} \qquad (6)$$

Where γ_{sl} , γ_{sv} and γ_{lv} are the solid-liquid, solid-vapor and liquid-vapor surface tensions, respectively. However, Young's equation does not take into account the contribution of roughness, surface chemistry, dissolutions or swelling, as it assumes ideal solid surfaces.

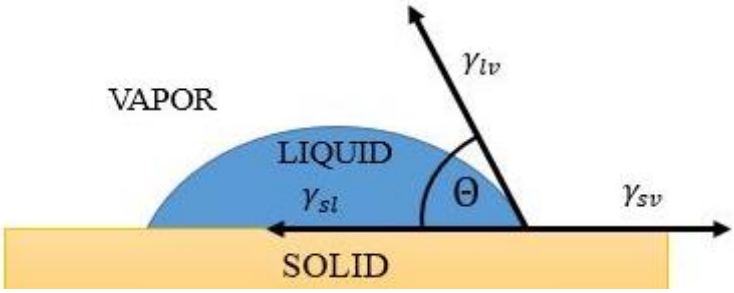

Figure 4 – Contact angle of a droplet in equilibrium between the different phase's Surface tensions at the respective boundary

2.2.4 Contact Angle Hysteresis

Contact angle hysteresis is the difference between an advancing contact angle and a receding contact angle. Measuring said contact angle has shown that it remains stationary if the liquid is not disturbed or its liquid dynamics are not altered. If a liquid has a determined contact angle, and more liquid is injected in it, the contact angle will increase, but the boundary between the three phases will remain stationary until it advances outward suddenly. Also, if the amount of liquid is reduced, the contact angle recedes but the three-phase boundary will remain in the same position until it recedes inward suddenly. The contact angle that takes place just before the three-phase boundary advances or recedes is called advancing contact angle and receding contact angle respectively.

$$\Delta\theta = \theta_a - \theta_r \qquad (7)$$

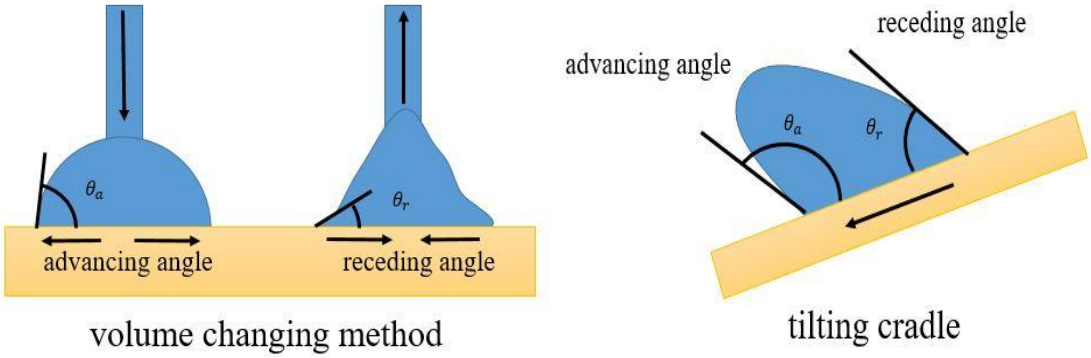

Figure 5 – Methods to measure the dynamic contact angles, volume changing method and tilting cradle method

Contact angle hysteresis is linked to droplet mobility. When a droplet is on a tilted surface, the static contact angles of the different limits of the surface start to change until the front and the back contact angles reach the advancing and receding contact angles. After that

happens, the three-phase boundary starts to move, so the whole droplet will move downwards through the surface. The lower the contact angle is, the higher mobility the droplets will have on the surface [17].

2.2.5 Spreading parameter

A droplet will completely wet the substrate if S > 0, i.e. μe = 0°. When S < 0, i.e. μe > 0° partially wet the substrate, or not wet the substrate at all [18].

$$S = \gamma_{sv} - (\gamma_{sl} + \gamma_{lv}) \quad (8)$$

2.2.6 Surface classification

Surfaces can be classified by the contact angle. Four types can be defined: Hydrophilic, hydrophobic, super hydrophilic, and super hydrophobic.

In general, the assumption is that when the contact angle is higher than 90 or 150 degrees, the surface is hydrophobic or super hydrophobic respectively, and it will repel water. While if the contact angle is lower than 90 or 5 degrees, the surface is hydrophilic or super hydrophilic respectively, and it will have affinity with water. It can be observed experimentally that when a liquid is placed on a super hydrophobic surface the droplet will tend to form almost spherical droplets. In contrast, if we place a liquid in a super hydrophilic surface, it will tend to form a thin film over the surface [19].

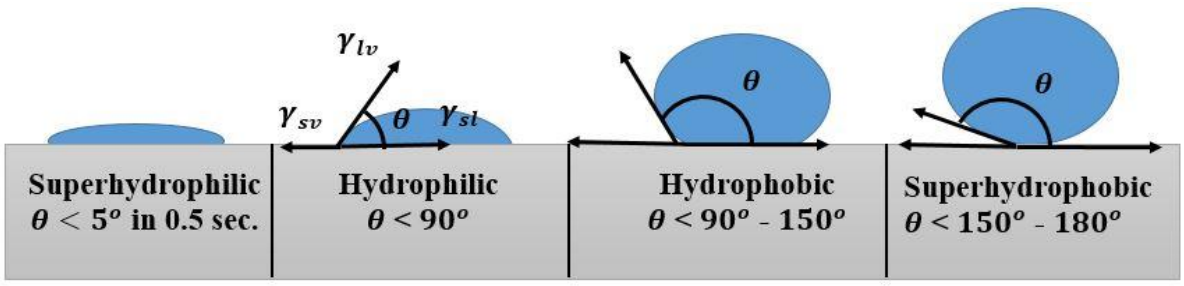

Figure 6 - Contact angle Surface classification

2.2.7 Droplet Morphology

It has been claimed in section 2.2.2.4. that by knowing the contact angle, knowledge of the droplets behaviour on a surface can be defined. However, Young's equation assumes an ideal solid surface and hereby neglects some important properties of real surfaces and its consequences. Wenzel and Cassie continued Young's work by extending the wetting study to rough and porous surfaces. Yet it considers droplets in different states of wetting in relation with the surface roughness.

In the Wenzel [20] state, the droplet completely wets all the rough area, so there are no air bubbles between the liquid and the solid. In this state, the Wenzel equation amplifies the contact angle by a factor r, where f is the surface roughness fraction:

$$\cos(\theta_w) = r\cos(\theta_e) \qquad (9)$$

Cassie and Baxter [21] developed another model considering that the droplet is in contact only with the tips of the roughness, so there is an air interface between some parts of the solid and the liquid. It is shown that the contact angle in this case is defined by:

$$\cos(\theta_c) = f(\cos\theta_e + 1) - 1 \qquad (10)$$

These two droplet morphologies are named the Wenzel and Cassie states respectively. In both cases, the roughness amplifies the chemistry characteristics of the surfaces. Thus, a hydrophobic flat surface becomes more hydrophobic when roughness is added and it becomes more hydrophilic if the flat surface is hydrophilic. In practice, it usually occurs that these models are not fully implemented as droplets do not present any of both morphologies, instead, they are in a medium point between them, which is shown in section 2.2.2 Wettability and Figure 2 in the different states of the drop.

Even though both states can coexist in rough surfaces, the Wenzel state is less desirable due to its higher adhesion to the surface compared to the Cassie state. Because of this, a lot of studies have focused on the Cassie state to achieve a very low adhesion in super hydrophobic surfaces leading to interesting properties such as self-cleaning or anti-icing ones [22].

When a droplet is in the Cassie state, it can make a transition to the Wenzel state and vice versa. The limit between these two states is the so called critical contact angle [23] and can be obtained equalizing Wenzel and Cassie-Baxter equations

$$cos\theta_{cr} = \frac{f-1}{r-1} \qquad (11)$$

The Cassie state is thermodynamically more stable when the physical contact angle θ_p is bigger than the critical contact angle, it is approximated with the static contact angle in a smooth surface. The Wenzel state is more stable when the physical contact angle is smaller than the critical one.

2.2.8 Weber

The Weber number is the ratio of the inertia force and surface tension. For a droplet with density ρ, velocity before impact v^2, its characteristic length e.g. the initial droplet diameter D_0 and surface tension σ the Weber number is,

$$We = \frac{\rho v^2 D_0}{\sigma} \qquad (12)$$

We is an important parameter when comparing contact angle measurements and a droplet's evaporation lifetime on a heated surface due to their dependence of the inertia force [24]. We ~1 is therefore often used.

This thesis defines a Weber map for different fluids, the corresponding Weber number is calculated from $We = 2\rho g H D_0/\sigma$, derived by substituting 2gH for v^2 in the definition. (g corresponding to the gravity and H to height from which the droplet is released)

3. Boiling and behaviour of the droplet (Leidenfrost curve and Weber map)

Application of the new technology of heat flux removal is a consequence of research for enhancement of the heat transfer by the forced convection (for gases), and heat reception during the pool boiling. The main parameter for determining boiling is its characteristic curve, which shows a relation of absorbing heat flux to temperature difference (overheating degree). This overheating is defined as a temperature difference between heating surface (Tsurf), and saturation temperature for the liquid (Tsat). The regime of boiling, where the heat fluxes in temperature, desired from the heat transport point of view, is determined by nucleate boiling and it goes to its limited value called the critical heat flux (CHF). The CHF point on the boiling curve divides the process between nucleate boiling and film boiling. [7]

This section will address the classical pool boiling curve as a plot of heat flux, q'', versus excess temperature, ΔT= Tsurf - Tsat. As the value of the excess temperature increases, the curve traverses four different regimes:

- Natural or free convection
- Nucleate boiling
- Transition boiling
- Film boiling

Different experimental methods may be used to define the pool boiling curve; constant temperature control and constant heat flux control are the two most commonly cited.

A typical boiling curve for saturated pool boiling of water at atmospheric pressure for a temperature-controlled environment is shown is Figure 7.

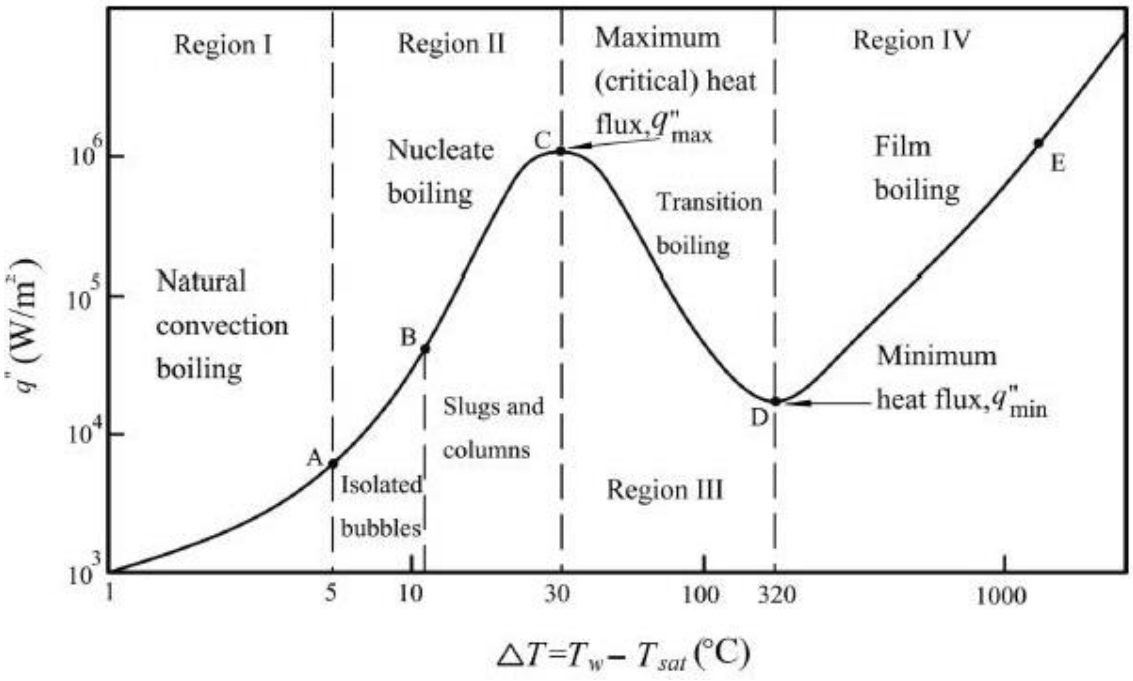

Figure 7 - Boiling curve for saturated pool boiling of water dividing in regions [25]

When the excess temperature ΔT is less than 5ºC, no bubbles form. Instead, heat is transferred from the solid surface to the bulk liquid via natural convection.

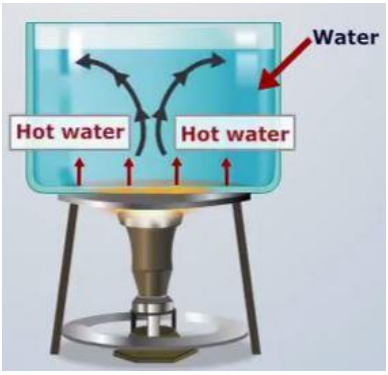

Figure 8 – Natural convection regime, heat transferred from the solid surface to the bulk liquid via natural convection [26]

When the excess temperature increases beyond 5ºC, the system enters the nucleate boiling regime – Point A on Figure 7, vapor bubbles are generated at certain preferred locations on the heater surface called nucleation sites; these are often microscopic cavities or cracks on the solid surface.

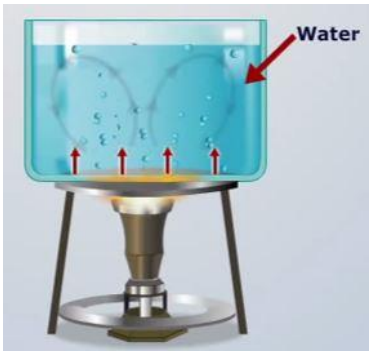

Figure 9 - Nucleate boiling regime, vapor bubbles starts to be generated [26]

As the excess temperature increases beyond point B Figure 7, additional nucleation sites become active and more bubbles are generated. The higher density of bubbles lead to an interaction between them.

Bubbles from separate sites now merge to form columns and slugs of vapor, thus decreasing the overall contact area between the heating surface and the saturated liquid.

Consequently, the slope of the boiling curve begins to decrease and the heat flux eventually reaches a maximum value, q'' max, referred to as the critical heat flux.

Figure 10 – Maximum heat flux, more bubbles are generated and contact area decreases [26]

As the temperature increases beyond the critical heat flux point, the rate of bubble generation exceeds the rate of bubble detachment from the source of heat.

Bubbles from an increasing number of sites merge to form continuous vapor films over portions of the surface, further decreasing the contact area between the heating source and the saturated liquid.

These vapor films are, nonetheless, not stable as they can detach from the surface, leading to the restoration of contact with the liquid and resumption of nucleate boiling.

Under unstable conditions, the surface temperature may fluctuate rapidly, so the excess temperature shown on the ΔT-axis of Figure 7 between points C and D should be regarded as an average value.

Since the boiling in this regime combines unstable film with partial-nucleate boiling types, it is referred to as the region of transition boiling.

Figure 11 – Transition boiling regime, continuous vapor film is formed and further decrease of the contact area [26]

When the excess temperature becomes high enough to sustain a stable vapor film, the heat flux reaches its minimum value, q'' min. This point, the Leidenfrost temperature, marks the upper temperature limit of the transition boiling regime.

At temperatures above the Leidenfrost temperature, the bulk liquid and the heating surface are completely separated by a stable vapor film, so boiling in this regime is known as film boiling.

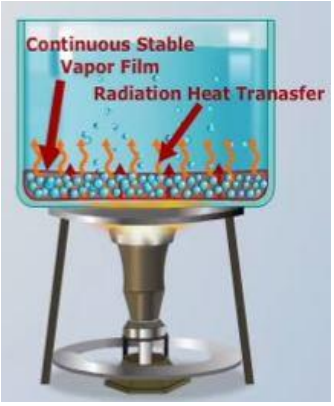

Figure 12 – Film boiling regime, stable vapor film is generated and a significant loss of heat transfer is present [26]

The phase change in film boiling occurs at a liquid-vapor interface, instead of directly on the surface, as in the case of nucleate boiling.

Pool boiling continues in this regime until the surface temperature reaches the maximum allowable temperature of the heating surface (melting point of the heated surface material). Beyond that point, the heating surface can melt and cause a potentially catastrophic failure. [25]

Thus study analyses this theoretical claim by studying the impact of a droplet on a hot surface. The heat transfer in drop impingement on a heated wall is strongly influenced by the magnitude of wall temperature, relative to the liquid's saturation temperature. When Tw is below Tsat, the heat transfer is dominated by heat conduction from the wall to the liquid. Evaporation, due to mass transfer along the liquid–gas interface, as claimed at the start of the chapter, takes place with the pool boiling experiment in a vessel. It must be taken into account that some parameters such as drop-wall contact area, contact angle, and heat flux vary greatly during the impact. When Tw begins to exceed Tsat, the drop boils on the heated wall, and small bubbles form inside the drop, which grow and merge, but do not separate from the wall. This bubble behaviour is distinctly different from that encountered in pool boiling, where bubbles are quickly removed from the wall by buoyancy. Moreover, bubble size, evolution, distribution, and merger greatly influence

flow dynamics and drop heat transfer. At even higher wall temperatures, when Tw exceeds the Leidenfrost temperature, a thin micrometer-scale vapor layer quickly forms between the drop and the wall, which greatly decreases liquid–solid contact and culminates in substantial deterioration of heat removal from the wall. Depending on impact momentum, the drop may bounce, break up, or roll on the wall, further complicating the heat transfer process.

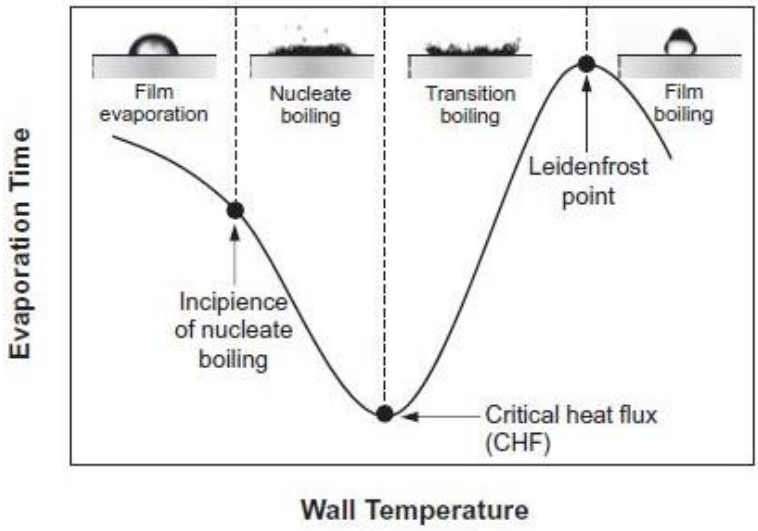

Figure 13 – Heat transfer regimes associated with a drop impinging a hot wall [27]

Clearly, wall temperature plays a crucial role in the study of drop impingement on a heated wall, influencing both impact dynamics and heat transfer performance. Based on evaporation, the lifetime of a single drop at different wall temperatures identifies four distinct evaporation regimes: film evaporation, nucleate boiling, transition boiling, and film boiling, as shown in Figure 13. The Leidenfrost point is especially important, resulting in the longest evaporation time.

Because of drastic differences among the four evaporation regimes, efforts have been made to quantify transition boundaries between regimes using both hydrodynamic and heat transfer considerations. Bernardin [28] pointed out that Tw and the impact Weber number are the two most important parameters governing impact behaviour and heat transfer. They provided comprehensive maps covering both impact dynamics and heat transfer regimes for low and high Weber numbers (We = 20, 60, and 220). Later, Bernardin [29] also incorporated the influences of surface roughness in their maps. They reported

that surface features influence boiling regimes in two major ways: (a) inducing breakup of the spread film at high wall temperatures corresponding to film boiling and high-temperature region of transition boiling, and (b) increasing nucleation site density at lower wall temperatures corresponding to nucleate boiling and lower temperature region of transition boiling [27].

4. Fabrication of Si nanowires

4.1 General process patterned Si nanowires

4.1.1 General view of the process patterned Si nanowires

Fig. 14 shows a scheme of the process followed for the desire fabrication of Si nanowires.

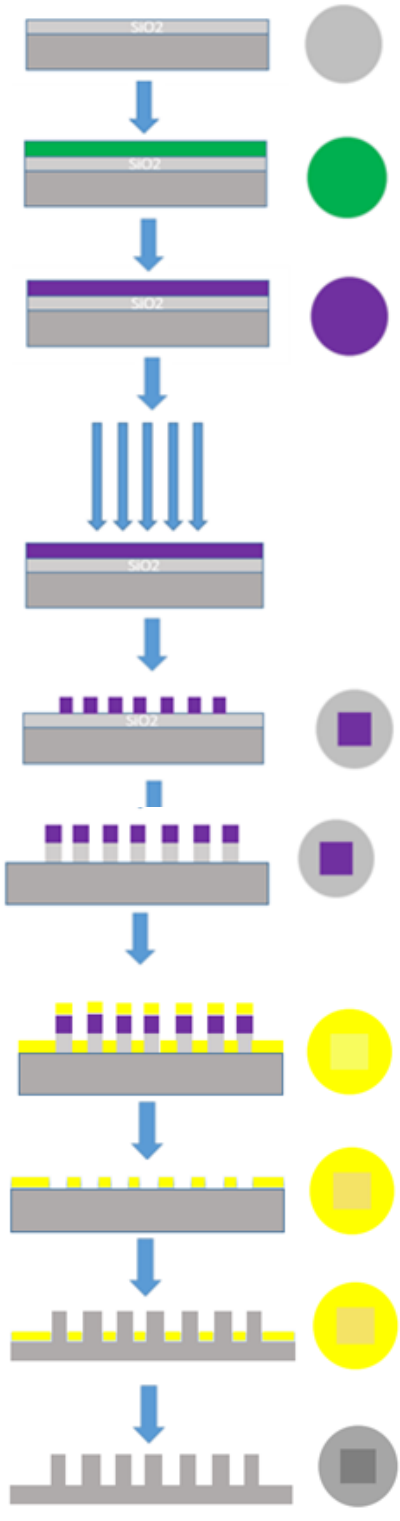

1 – Cleaning

2 – Dehydration

3 – Plasma cleaning

4 – Pre-soft baking before spin coating

5 – Photoresist spin coating

6 – Checking thickness

7 – Pre-exposure soft baking

8 – EBL Elionix exposure

9 – Development

10 – HF Elimination of SiO2 layer

11 – AJA E-beam evaporator

12 – Lift off

13 – Etching

14 – Gold removing

Figure 14 - General view of the process

4.1.2 Recipe patterned nanowires

The recipe established in this process has been developed through articles regarding fabrication. Following the step of development, the remaining part of the recipe was introduced by Manuel Auliano, PhD student in the NTNU, who joined the project after having explored previous literature regarding fabrication [30]. This allowed for the creation of a new recipe for the fabrication of nanowires.

4.1.3 Process step by step

4.1.3.1 Cleaning

The first step in the process is cleaning the Si wafer, ensuring it is not contaminated to allow for positive, non-corrupted results. The work was developed on an ISO 5 or 6 room and vibration reduced zones at VCF-level. These characteristics were needed due to instruments' requirements. This environment was also sterile, considering that dust, hair, skin oils, etc. can affect the nanoscale procedures and harm the work. Some items like plastic carriers and tweezers must be as clean as possible every time to minimize contamination during all the process.

The wafer is cleaned by splashing the wafer with acetone until the whole wafer is covered. Then it is showered with isopropanol (IPA) and deionized water. Instantly after the wafer is dried with N2 until there are no droplets on the surface.

4.1.3.2 Dehydration

The wafer is heated up in a hot plate. To ensure that the back of the wafer is not contaminated by other particles that may be in the hot plate, we use our own clean silicon wafer.

4.1.3.3 Plasma cleaning

Plasma cleaner (Femto, Diener Electronic) is used to remove all the organic contaminants in the surface resulted from a reaction with O2. With this step, the surface becomes more hydrophilic and resists potential adhesion.

4.1.3.4 Pre-soft baking before spin coating

The wafer is then heated on a hot plate at higher temperature. To ensure that the surface of the wafer has the proper conditions for the deposition of the photoresist, our own clean silicon wafer is again used to put on our sample and avoid contamination. During this step, all the OH bonds are thermally cracked promoting resist adhesion.

4.1.3.5 Photoresist spin coating

It is used as negative photoresist, so the resist further exposed to EBL Elinoix will not be removed after the electron beam lithography process. A spin coater is used to create a thin layer of photoresist on the Si wafer. First, the wafer is placed on the chunk of the spinner and when it is centered, vacuum is applied so the wafer cannot leave the chunk. Then, photoresist is applied at the center of the wafer with a pipette. The pipettes are not re-usable, once the resist is applied they must be emptied and cleaned properly.

Figure 15 - Spin coating

4.1.3.6 Checking thickness

To make sure that the thickness necessary has been attained, the reflectometer is used to measure reference wafer and compare this with the wafer and photoresist. If the thickness is too high, the process ought to be repeated as too much photoresist can fall and bend together, hindering the continuation of the process.

4.1.3.7 Pre-exposure soft baking

When the photoresist layer is applied in the surface, it must be soft baked to evaporate the solvent and densify the layer. Then the wafer is cooled down in a cool plate.

Figure 16 – Pre-exposure soft baking

4.1.3.8 EBL Elionix exposure

Before using EBL, a file in CleWin 5, a layout editor designed program, ought to be created. The desired pattern is designed considering that the part exposed is going to remain after applying the developer.

In this part, one can only control the diameter and the pitch of the nanowires.

Parameters should be selected within the range for proper operation for the photoresist.

Figure 17 - EBL exposure

4.1.3.9 Development

In this step, the non-exposed areas unwanted in the sample are removed. The developer is used to fulfill that objective. The use of two beakers, one with enough developer to immerse the wafer, and the other is under a tap, full of water and with the tap slightly open, encourages a laminar flow on the surface of the water going out of the beaker.

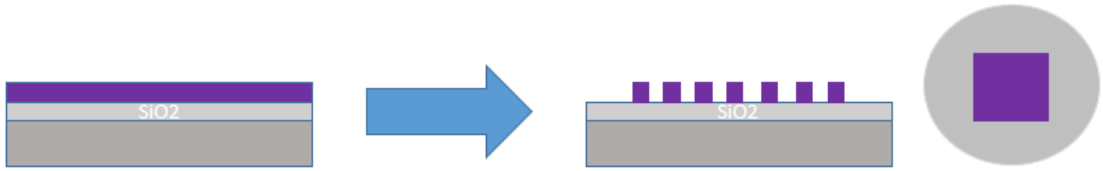

Figure 18 – Development

4.1.3.10 HF Elimination of SiO2 layer

The sample is immersed in a beaker with a solution of HF, the objective of this step is to eliminate the native layer of SiO2 to increase the addition of the metal layer needed for the process. It has been discovered that without this, after the lift off, all the layer is removed, so this step is required.

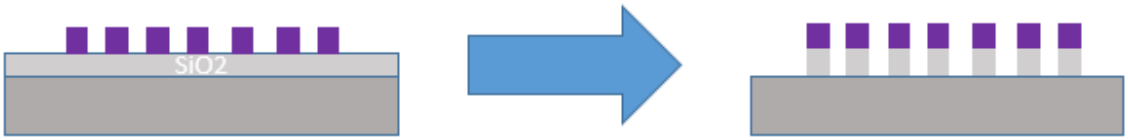

Figure 19 - HF elimination of SiO2 layer

4.1.3.11 AJA E-beam evaporator

This step must be done as soon as possible after the HF due to the native layer of SiO2 grows at room temperature, while it is in contact with the oxygen it suffers an oxidation, letting the SiO2 grow [31].

The layer of SiO2 produce problems in the lift off due to bad addition.

For this process, a layer of gold was introduced. This is easy to etch and control with HF solution.

Figure 20 – Gold deposition

4.1.3.12 Lift off

For the lift off, PG Remover was used. When in immersion mode, a two-bath system is recommended to reduce the possibility of redeposition of removed resist. The first bath removes the bulk of the resist and the second, cleaner bath removes remaining traces of material. When the 1st stripping bath has become loaded with resist, it can be replaced with the 2nd 'drag-out' bath to increase bath yield. Remover baths should be changed when removal rate drops significantly and may be measured by the number of wafers processed [32].

It is important to make sure there is not residual part of the photoresist as it can affect the growth of the nanowires in the previous step. The reaction of the organic material with chemicals reactants during etching and removing gold can also be dangerous.

Figure 21 - Lift off (SiO2 layer can be suppressed due to the small thickness)

4.1.3.13 Etching

After deposition, HF is used for etching the layer of gold and the chemical reaction of the HF with the Gold (Au). The pattern is immersed, and metalized silicon substrate into a solution of hydrofluoric acid and hydrogen peroxide

In the first step, the hydrogen peroxide is decomposed to water at the metal surface and in the process transfers holes to the silicon via the metal. Next, the hole-rich silicon, now

in an oxidized state, reacts with the hydrofluoric acid to form the soluble species H2SiF6 and hydrogen gas.

Etching proceeds anisotropically directly below the metal, and the metal sinks into the silicon, resulting in a patterned metal film with an array of nanowires in a single step. Metal-assisted chemical etching is possible with both thin and thick metal films [33].

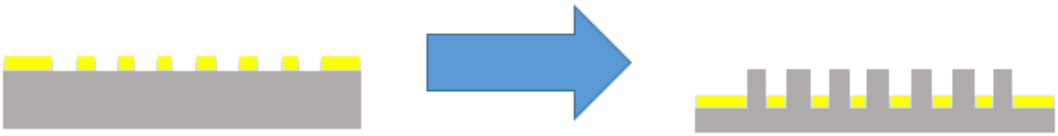

Figure 22 - Etching HF

4.1.3.14 Gold removing

A common gold etchant is used to remove the layer of gold on the top of the wafer, the etchant rate depends on the operating condition. The wafer is then submerged in the gold etchant solution, and after gold is removed, it is cleaned by rinsing the wafer with ethanol and dry on a hot plate.

Figure 23 - Gold is removed with standard gold etchant

4.2 General process of random nanowires

This is the general description of random Si nanowires described by Manuel Auliano [6].

A thin layer of silicon nitride is deposited by Plasma Enhanced Chemical Vapor Deposition (PECVD) on the etched side to prevent silver deposition. Then the silicon wafer is ultrasonicated with acetone and isopropanol for 15 minutes at room temperature to remove contamination from organic grease, then rinsed several times with DI water and dried with nitrogen. After being dipped in a 5% HF solution for 2 minutes in order to obtain H-terminated surfaces, the sample is immediately soaked in a freshly prepared dilute solution of 0.005 M silver nitrate (AgNO3) and 4.8 M HF for 1 minutes at room temperature and then rinsed with DI water to remove the silver dendrites. They were then immediately immersed into the solution of 4.8 M HF and 0.5 M H2O2 at room temperature: the height of Si NWs is effectively controlled by adjusting the etching time. After the etching, the sample is rinsed with DI water, dried and then then soaked for 10 minutes in a concentrated 10 M solution of nitric acid (HNO3) to remove the silver dendrites. Finally, the sample is rinsed with DI water and dried with nitrogen [6].

4.3 Characterization

Once the sample is produced, we need to characterize the structures fabricated and check if some errors were made during the process followed with further improvement of it. The characterization is done with a Focused Ion Beam (FIB) microscope under high vacuum conditions. The sample must be placed in the holder with some adhesive tape to ensure that will not fall. This is the time to control that the sample has not defects after the etching process, as well as measure the height obtained. To do so, one ought to select a tilting angle of 30 degrees because of the easy trigonometric operation to measure heights. It is very important that the wafer does not crash in the lens. Z=18mm has to be selected and the eucentric height has to be found to better control the testing.

5. Experimental setup for Leidenfrost phenomenon visualization and experimental method

This chapter describes the setup arranged to achieve the visualization of the boiling process and experimental method.

5.1 Experimental setup design

A high-speed digital camera (photron fastcam SA3) is used for this purpose. Video recording is set up at different frames per second (fps) 500 fps and 10000 fps. This enables the study of the behaviour of the droplet when impacting with the hot surface, shutter speed, light, and other parameters which are adjusted in order secure the good quality of the image. See Appendix B datasheets for device details.

A syringe pump is used in order to control the droplet velocity, the settings are adjusted to let the drop release by its own gravity, and having every droplet tested the same conditions of volume and velocity. Volume and speed are setting in the syringe pump.

The needle of the syringe is 0.8 mm of diameter and 22 mm of length, kept for every experiment in order to keep the same conditions of the experiments, and to be able to compare and discuss different result due to the properties of the fluids.

A DAQ (Data Acquisition) is connected to the 3 thermocouples in order to control the data of the temperature in time, this data collected is processed in the computer through Matlab and Labview. Thanks to this two programs, data of temperature in time is processed and set to achieve a Leidenfrost curve.

An 56mm x 56mm x 35mm brass block for testing 2" wafer samples have been designed with the software Autodesk Inventor (Autodesk Inc., U.S.) and fabricated by the engineering department at NTNU EPT to fit together with an optical tensiometer (Attension Theta, Biolin Scientific, Sweden) for studying impacting droplets over plain polished silicon and nanostructure surface. See Appendix A for detailed drawings.

The brass block, for 2" wafer samples, is designed to hold 4 cartridge heaters, 3 thermocouples and is insulated by 10mm thick SFC-2 (Bagges AS, Norway) walls on all sides and underneath. Four 50mm long 500W cartridge heaters (RAC2506-50L10Ø500W, Lojer Components, U.K.) have been delivered by Lojer Components. The temperature 1.5mm below the top surface of the brass block is monitored by 1 K-type thermocouples (KMQSS-IM050U-150, Omega, U.K.) delivered by Omega Engineering, and 2 more of them on the top surface positioned with own made holders and OT-201 OMEGATHERM Thermally Conductive Silicone Paste [5]. See Appendix A for detailed drawings.

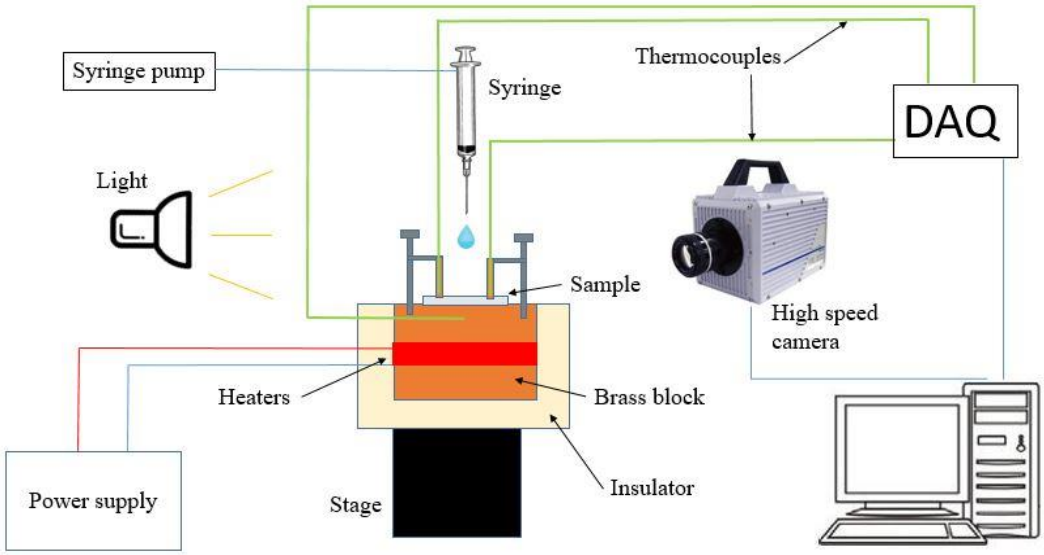

Figure 24 – Facility setup for the Leidenfrost experiments

5.2 Validation

In this part, improvements of the facility are commented, it has been divided in different sections:

a. Glue
b. Information presentation
c. Thermocouples

a. Glue

OT-201 OMEGATHERM Thermally Conductive Silicone Paste is used to improve the contact of the thermocouples with the surface, improving the measurements of the temperature, this glue is a thermally conductive, “Heat Sink” silicone grease. It has a very high thermal conductivity coupled with high insulation resistance and high dielectric strength. Glue is used in this study as it has been deemed for continuous use between -40°F and +392°F (40°C and 200°C). The limit of temperature is overpassed, regarding other articles in this field [34] the used of this paste is secured for the range of temperatures in this work. See Appendix B for details.

Figure 25 - OT-201 OMEGATHERM Thermally Conductive Silicone Paste

A comparison between the measurements with glue and without silicone grease has been carried out. Figure 26 shows a comparison between the measurements of the surface temperature of the brass block for testing 2’’ wafers, in blue one thermocouple with silicone grease and another one, the orange, without silicone grease.

As it is shown in the plan, for the four points there are a difference of 7ºC, 14ºC, 11ºC, 16ºC respectively. The use of silicone grease shows an improvement in accuracy of the

measurement of the surface temperature. Figure 27 evidences this in showing the development of the silicone grease use.

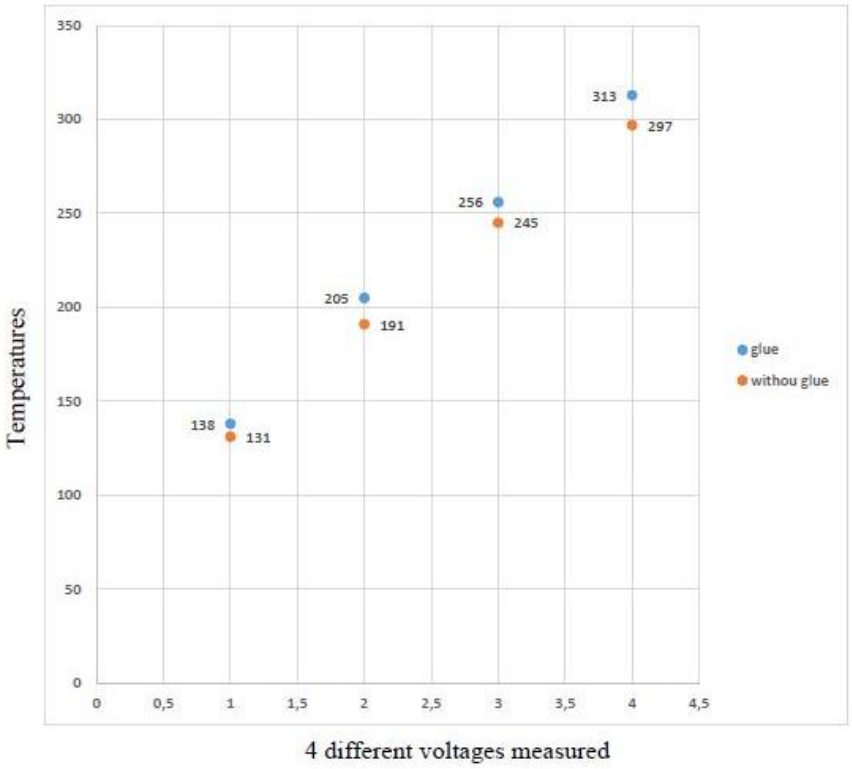

Figure 26 - Comparison of measurements with silicone grease and without silicone grease

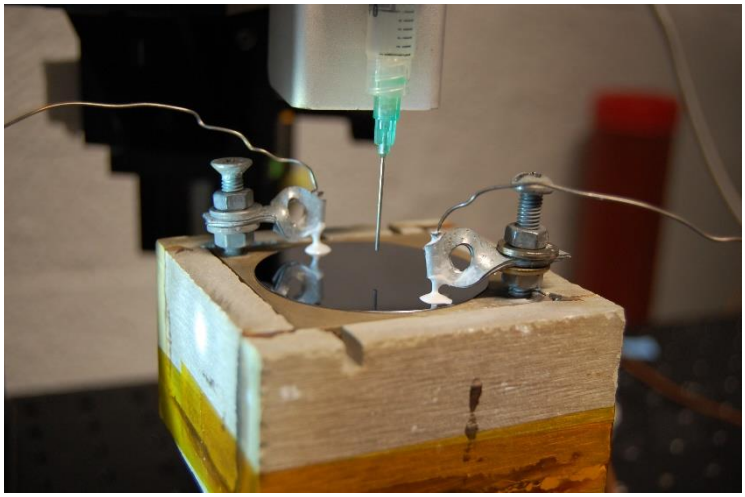

Figure 27 - Development of the silicone grease use

b. Information presentation

An improvement of the code in Matlab has been achieved and a plot log/log is presented in order to have a better visualization of the data, both plots are presented: the old oe and the actual one.

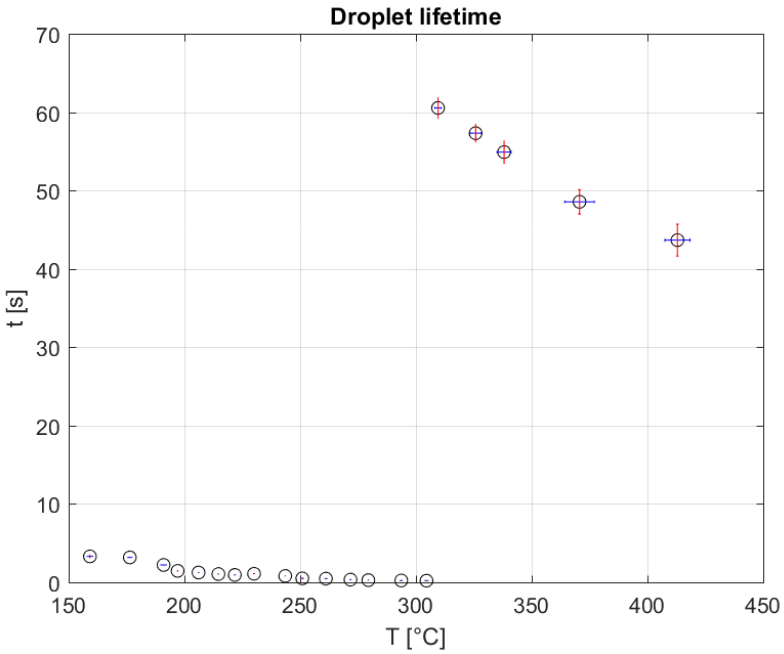

Figure 28 - Initial plot, droplet lifetime vs temperature of the surface, curve for water with a distance of 25 mm from the surface to the syringe

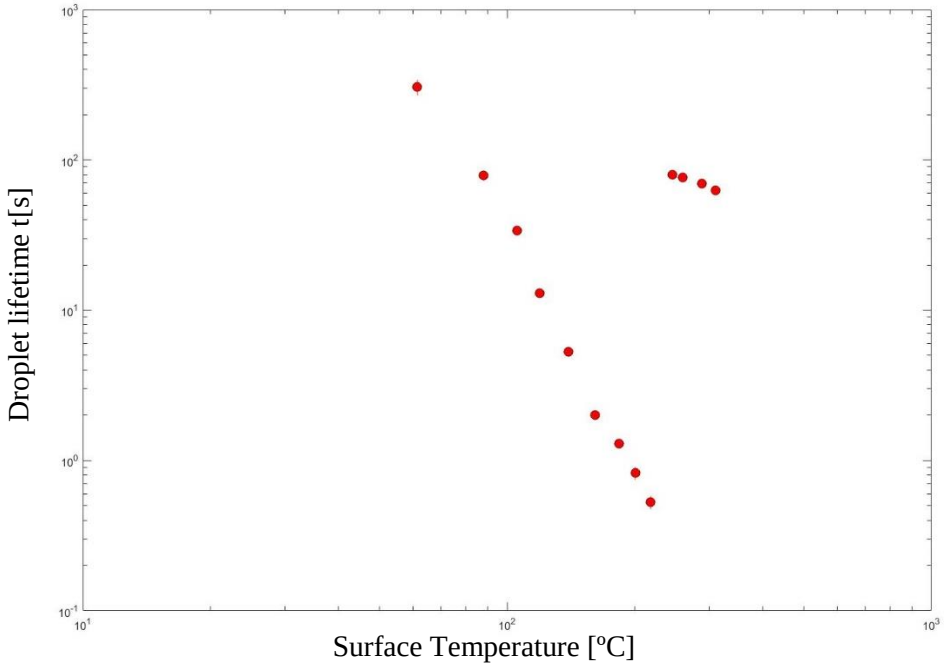

Figure 29 - Final presentation of the data, plot of droplet lifetime vs temperature of the surface, curve for water with a distance of 25 mm from the surface to the syringe

c. Thermocouples

A different way to control the surface temperature of the sample has been studied, an improvement in the use of glue has been shown and the correct use of the thermocouples with a perpendicular position toward the sample have allowed the obtaining of accurate data.

A logbook was created in order to control, compare and collect the data from all experiments for further analysis. The data was contrasted in every experiment and an improvement of experiments is performed, making the experiments faster and easier while also gaining accuracy.

A correlation between temperatures in the surface of the sample and inside the brass block was carried out showing that in every experiment there is a different relation between both temperatures. Thus, plotting the surface temperature through a correlation is not always accurate. In this work, measurements were carried out with two thermocouples attached to the surface, to check and control the surface temperature. Samples with nanowires also show a change in their properties, this proves a correlation between the surface temperature and the temperature inside the brass block is not valid.

Figure 30 and Figure 31 show the correlation of two experiments and it is not found the same relation between surface temperature and inside the block temperature.

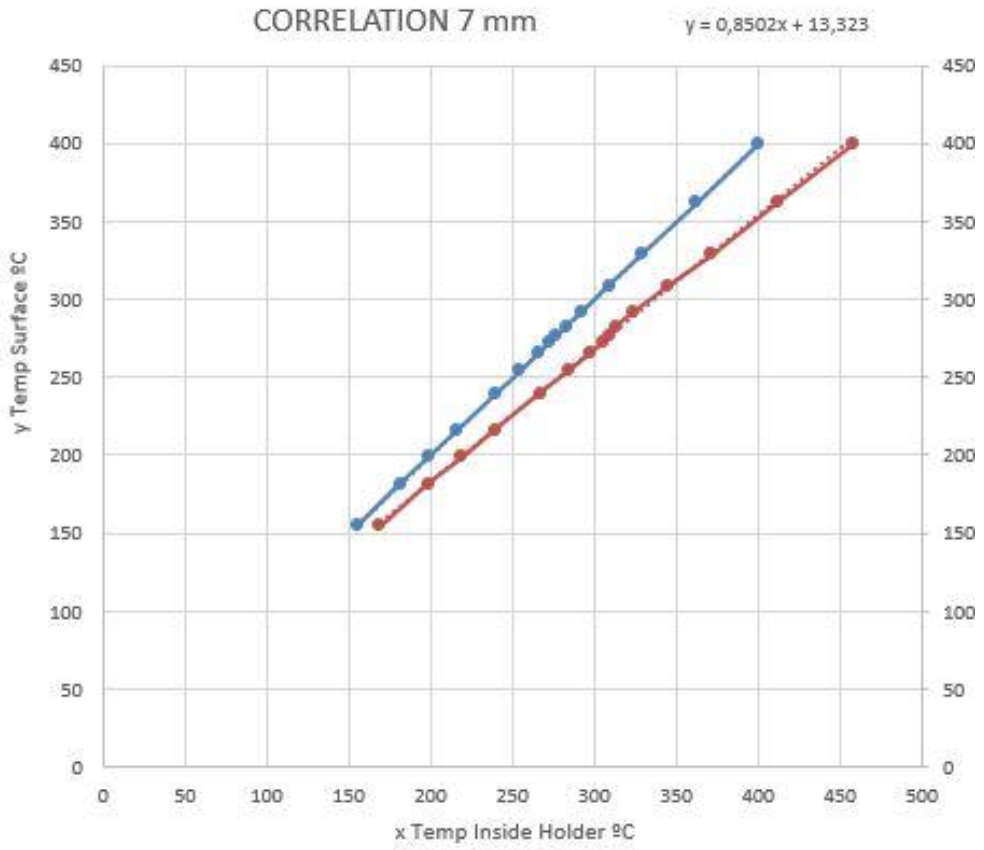

Figure 30 – Correlation of Surface temperature and the inside of the brass block temperature in the droplet fall height of 7mm experiment with water

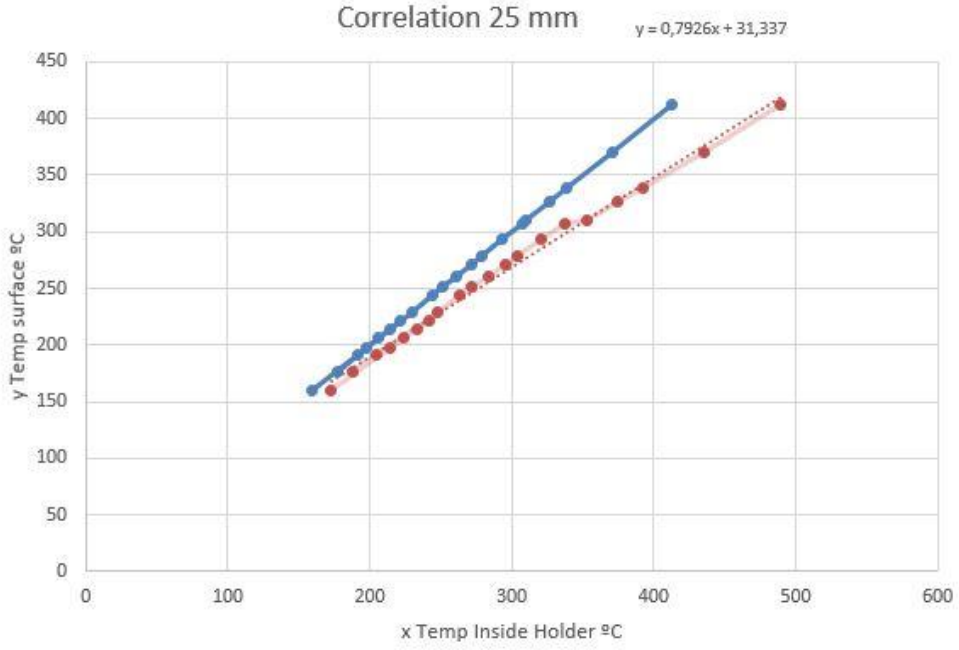

Figure 31 - Correlation of Surface temperature and the inside of the brass block temperature in the droplet fall height of 25mm experiment with water

6. Results and discussion

This section presents the main results and discussions regarding the fabrication and testing of the nanowires described in this project.

The following main results of this work are:

1. Reference LDF curve and Weber map on plain polished silicon
    a. Water
    b. FC-72
    c. Comparison both fluids
2. Fabrication of nanowires
    a. Patterned nanowires
    b. Random nanowires
    c. Microstructures with random nanowires
3. Improvements of different nanostructures in comparison with plain polished silicon
    a. Changes in CHF and LDF
    b. Differences of behaviour

6.1 Reference LDF curve and Weber map on plain polished silicon

A Leidenfrost reference curve is presented in this work for water and FC-72 at different heights and changes in LDF and CHF are discussed. Moreover, a Weber map studying the behaviour of the droplet in contact with a hot surface of the different fluids is represented and discussed.

a. Water

Leidenfrost phenomenon is studied in this part for water. Data is collected from experiments and presented in plots of droplet lifetime versus temperature of surface, the vertical error bars represent the standard deviation of droplet lifetimes recorded at each temperature, while the horizontal ones represent the error on the surface temperature considered by taking into account the two thermocouples used to measure the surface temperature. A delay of the CHF point and the LDF point while the height is increasing is shown and, consequently, there is a delay in the Leidenfrost curve while increasing the Weber number with water due to the relation Weber number with the height by substituting 2gH for V^2, $We = 2\rho g D_0 H/\gamma$. Plots of different height are presented. Experiments have been carried out in different days, this makes the experiments reliable due to the repeatability of the experiments, data collected in different days that follow a trend in the results. Due to the repeatability of this work, precision is presented in the result, but it is compared the lack of exactitude regarding the Leidenfrost phenomenon in previous investigations [12]. There is a lack of accuracy about the exact LDF, related to the different influential parameters of the Leidenfrost phenomenon explained in the section 2.1. Leidenfrost phenomenon history in Figure 1.

There is a switch on the LDF, for heights 5mm and 7mm the LDF point counting the temperatures of the surface are 254.1ºC and 257.3ºC respectively, as the height is increasing the LFD point surfers a delay in temperature, for 16 mm of height the LDF point is 267.5ºC, 10 degrees more than the lower height of 5 mm and 7 mm, and for the heights of 25 mm, 50 mm and 75 mm, temperatures are 310.4 ºC, 303 ºC and 296.6 ºC respectively. For the CHF, there is also a delay when height where the droplets are realising towards the surface is increased, which increases the point of the maximum heat transfer as well.

Reference	T_{leid}(ºC)	Surface Material	Notes
Blaszkowska and Zakrzewka (1930)	157	Silver	
Borishansky and Kutateladze (1947)	310 255	Graphite	T_f = 20 ºC T_f = 85 ºC
Borishansky (1953)	222 194 250 237	Brass Brass Copper Copper	T_f = 20 ºC T_f = 20 ºC T_f = 20 ºC T_f = 20 ºC d_0 = 4.5 mm
Tamura and Tanasawa (1959)	302	Stainless steel	
Gottfried (1962)	285	Stainless steel	T_f = 25 ºC 3.7 < d_0 < 4.3
Betta (1963)	245	Not given	4.6 < d_0
Lee (1965)	280	Not given	7.8 < d_0
Godleski and Bell (1966)	320	Stainless steel	T_{leid} = 264 ºC for extended liquid masses and 161 ºC for transient technique
Gottfried et al. (1966)	280	Stainless steel	
Kutateladze and Borishanski (1966)	250	Not given	
Patel and Bell (1966)	305	Stainless steel	0.05 < V < 410 ml extended masses
Baumeister et al. (1970)	515 305, 325 230,235 >200 235 155 265 <184	Pyrex (3-4 rms) Stainless steel (3.4 rms) Brass (3-4 rms) Brass fresh polish (3-4 rms) Aluminum (3-4 rms) Alum. Fresh pol. (3-4 rms) Aluminum (25 rms) Gold fresh polish	d_0 = 0.39 mm d_0 = 0.39 & 2.25 mm d_0 = 0.39 & 2.25 mm d_0 = 2.25 mm d_0 = 0.39 & 2.25 mm d_0 = 0.39 mm d_0 = 2.25 mm d_0 = 2.25 mm
Emmerson (1975)	282 316 284	Stainless steel	LFP also given for pressures of 210, 315, 420, and 525 kPa
Xiong and Yuen (1991)	280-310	Stainless steel	

Table 2 - Summary of Leidenfrost temperatures for water (P = 1 atm) as reported in the literature [13]

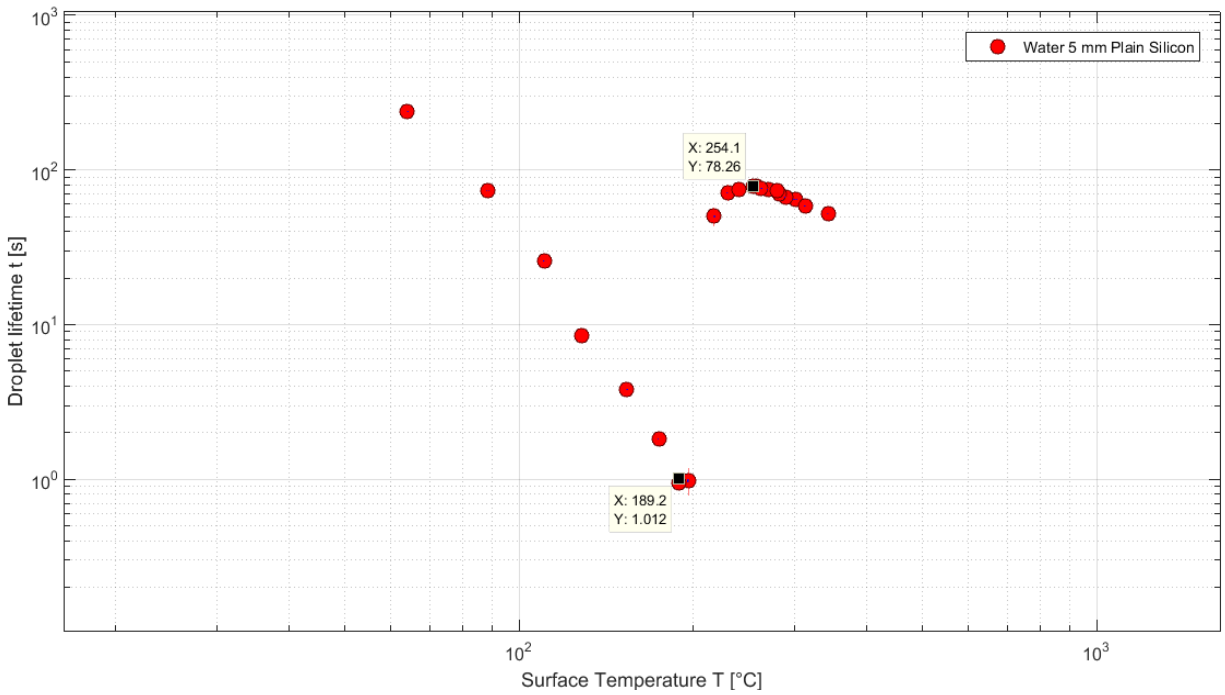

Figure 32 - Water LDF curve for droplet fall height of 5 mm on plain polished silicon

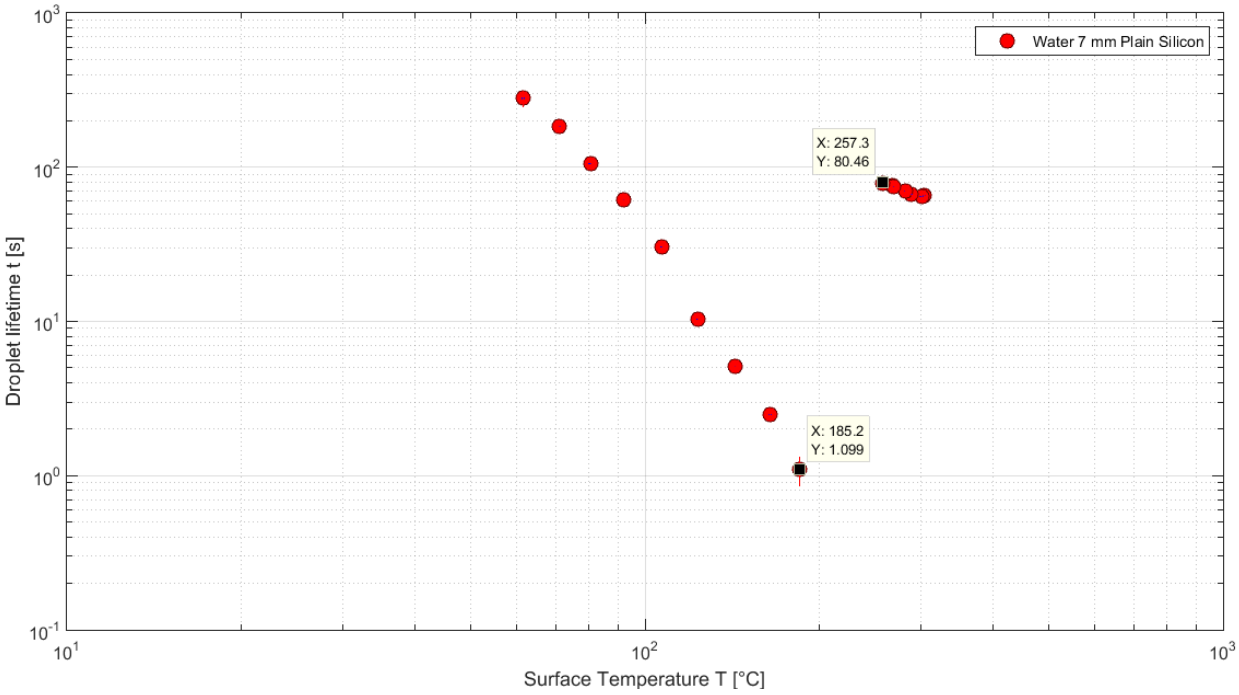

Figure 33 - Water LDF curve for droplet fall height of 7 mm on plain polished silicon

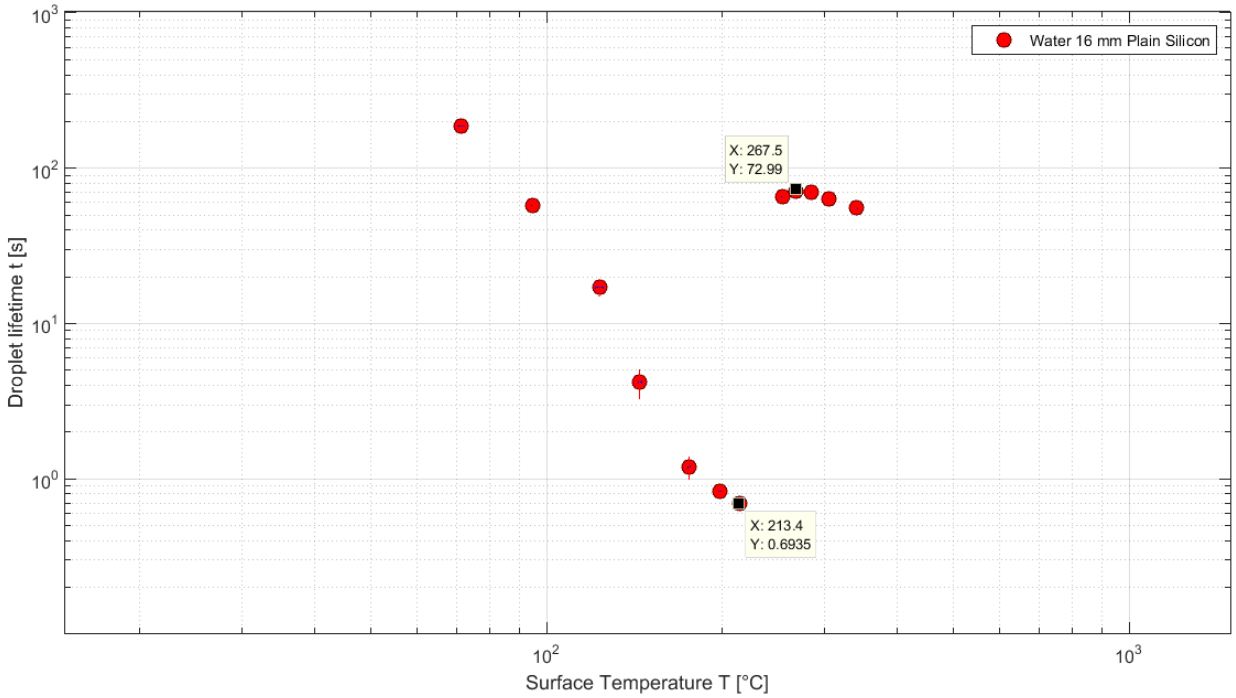

Figure 34 - Water LDF curve for droplet fall height of 16 mm on plain polished silicon

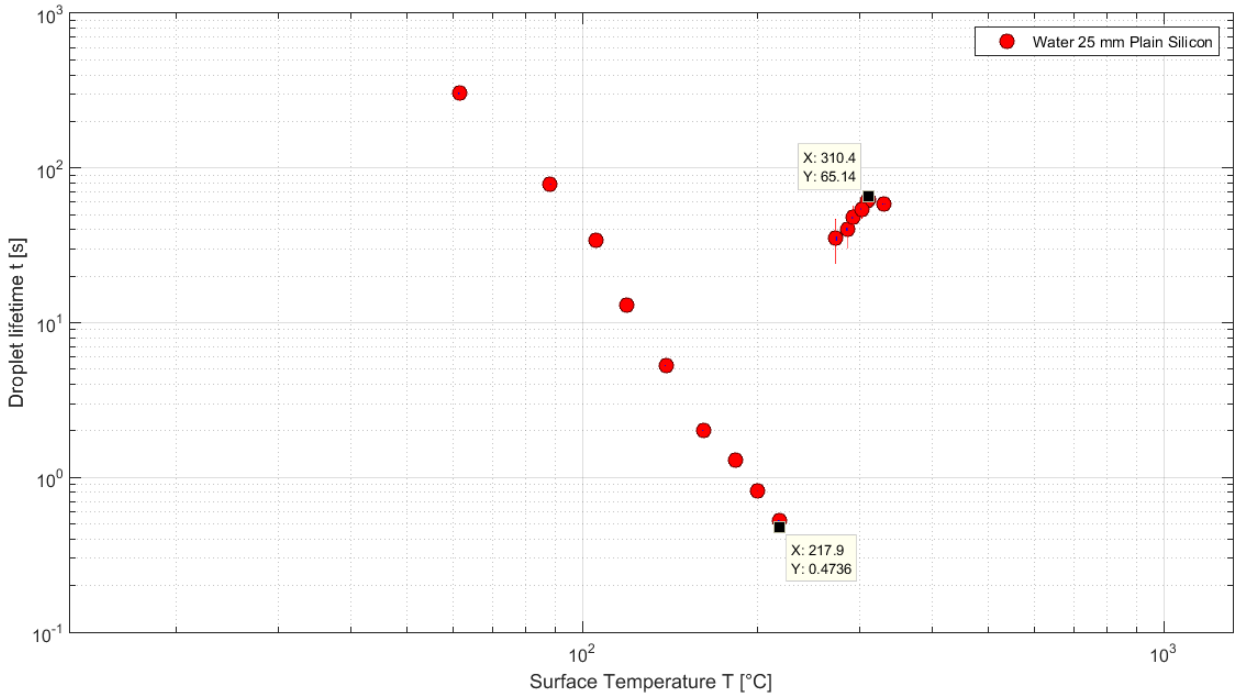

Figure 35 - Water LDF curve for droplet fall height of 25 mm on plain polished silicon

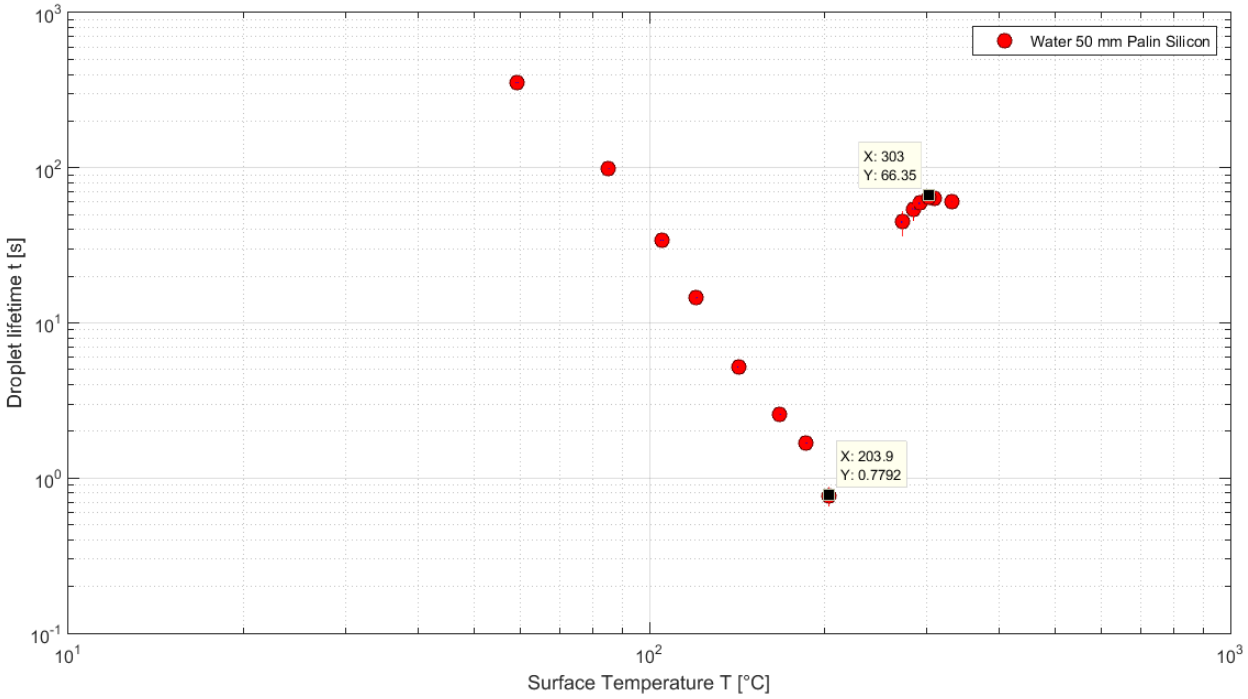

Figure 36 - Water LDF curve for droplet fall height of 50 mm on plain polished silicon

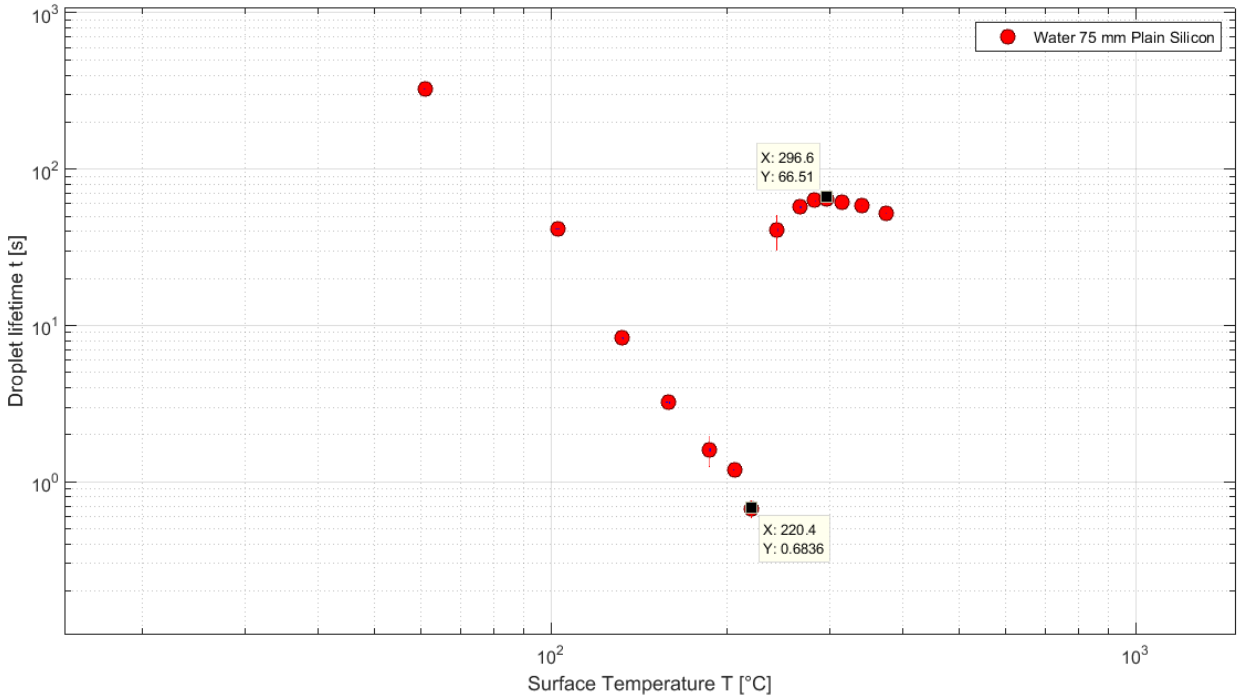

Figure 37 - Water LDF curve for droplet fall height of 75 mm on plain polished silicon

A difference in the behaviour is explained in this Weber map for water on plain polished silicon. Different behaviours have been classified by: Deposition, Deposition with secondary Atomisation, Atomisation, Rebound.

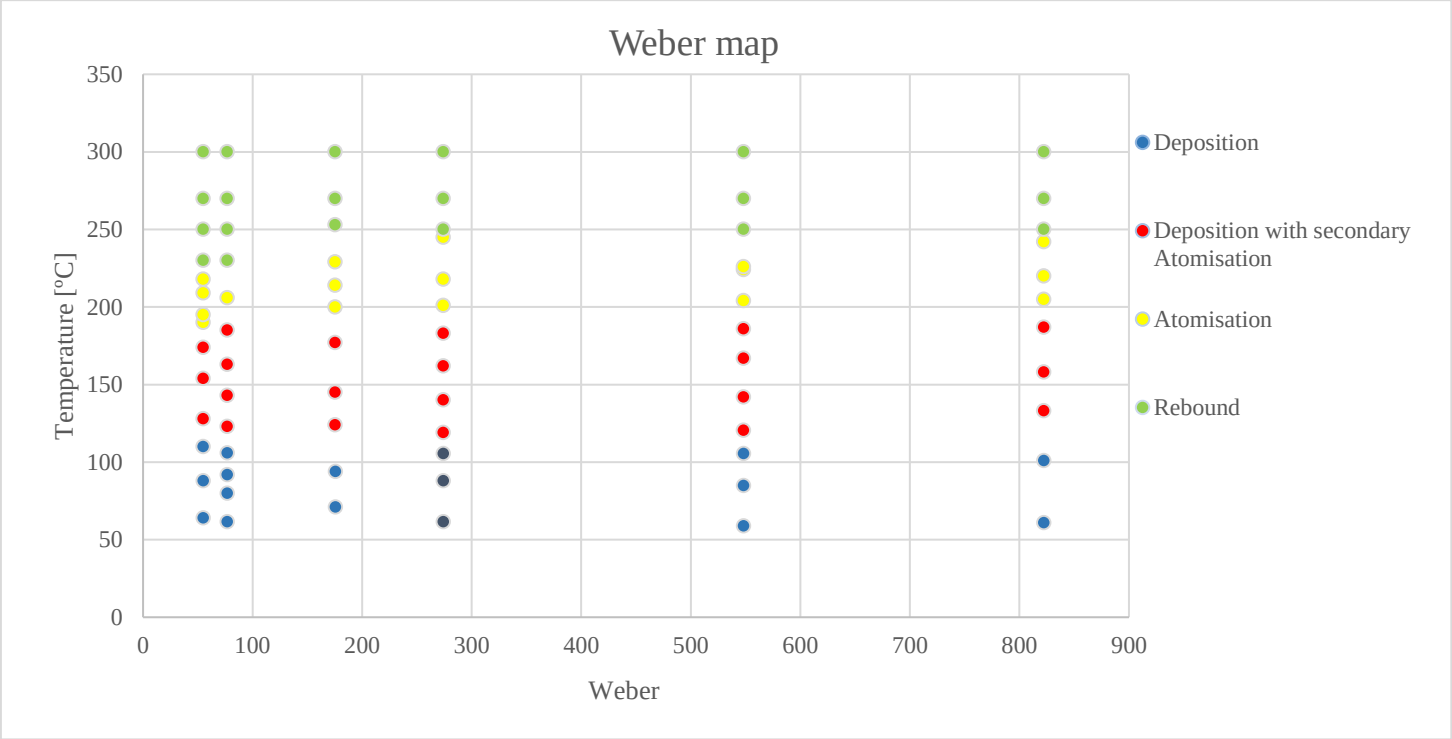

Figure 38 - Impact regime map for water droplets impacting on a heated, polished silicon surface. Regimes mapped with respect to the Weber number and the temperature of the surface are: Deposition (blue points), deposition with secondary atomisation (red points), atomisation (yellow points) and rebound (green points)

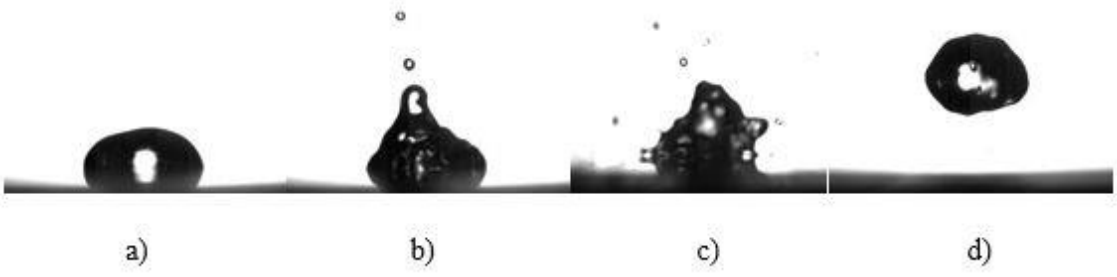

Figure 39 - Impact regimes for water on plain polished silicon: a) Deposition, b) Deposition with secondary atomisation, c) Atomisation, d) Rebound

Figure 40 - Behaviour of water on plain polished silicon droplet Impact for We = 175, from Impact to 120 ms: The droplet impingement history for a Weber number of 175. The surface temperatures are; 71°C, 94°C, 124°C, 177°C, 200°C, 229ºC and 253ºC. We = 275; Δt = 8 ms and 2 frames to show their behaviour

b. FC-72

The Leidenfrost phenomenon is studied in this part for FC-72 fluid. Data is collected from experiments and presented in plots of droplet lifetime versus temperature of surface, the vertical error bars represent the standard deviation of droplet lifetimes recorded at each temperature while the horizontal ones represent the error on the surface temperature considered by taking into account the two thermocouples. For FC-72 a delay of the CHF point and the LDF point while the height is increasing is not shown contrary to water. Plots of different height are presented and the LDF and CHF are presented in the plot. The exactitude of this experiment with FC-72 is contrasted with the Table 3. The different result shown in the literature is related to the different influential parameters of the Leidenfrost phenomenon explained in the section 2.1. Leidenfrost phenomenon and history in Figure 1.

Liquid	Chemical formula	Density ρ [10^3 kg/m^3]	Boiling temperature T_B [°C]	Leidefrost temperature[(a)] T_L [°C]	Liquid dynamic viscosity μ_L [mPa s]	Vapor dynamic viscosity[(b)] μ_v [10^{-2} mPa s]	Liquid thermal conductivity[(c)] k_v [W/K]	Surface tension σ [mN/m]
FC 72	C_6F_{14}	1.68	56	116	0.64	1.10	n/a	10.0

Table 3 – Properties of FC-72 [35]

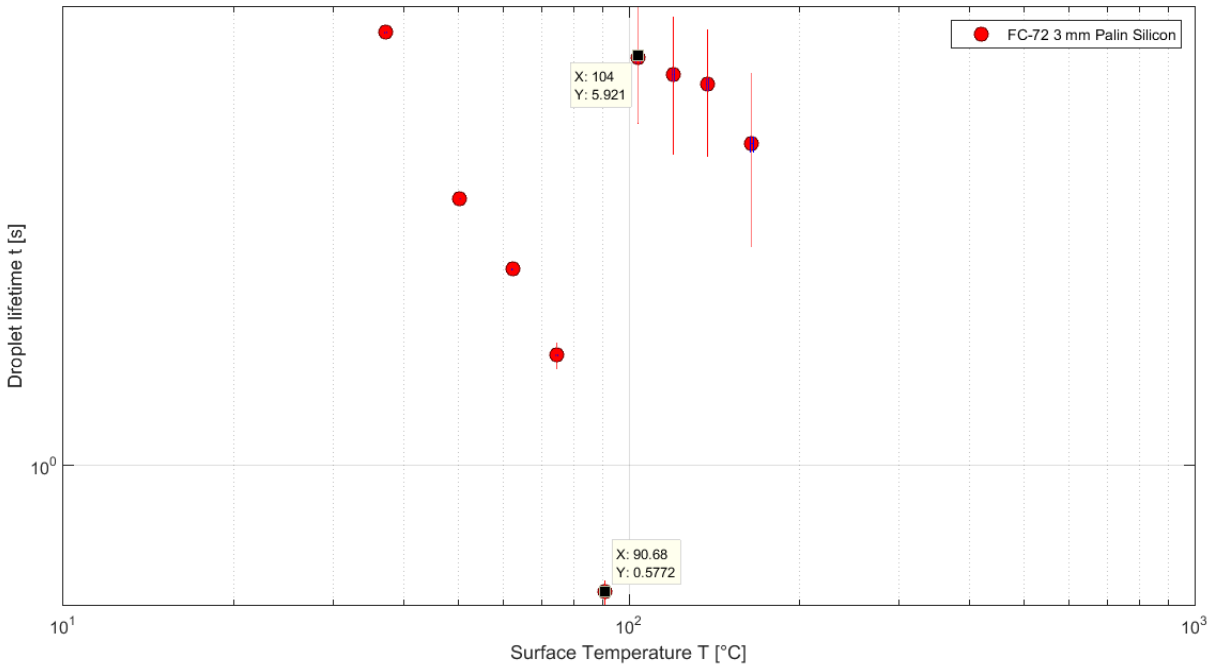

Figure 41 - FC-72 LDF curve for droplet fall height of 3 mm on plain polished silicon

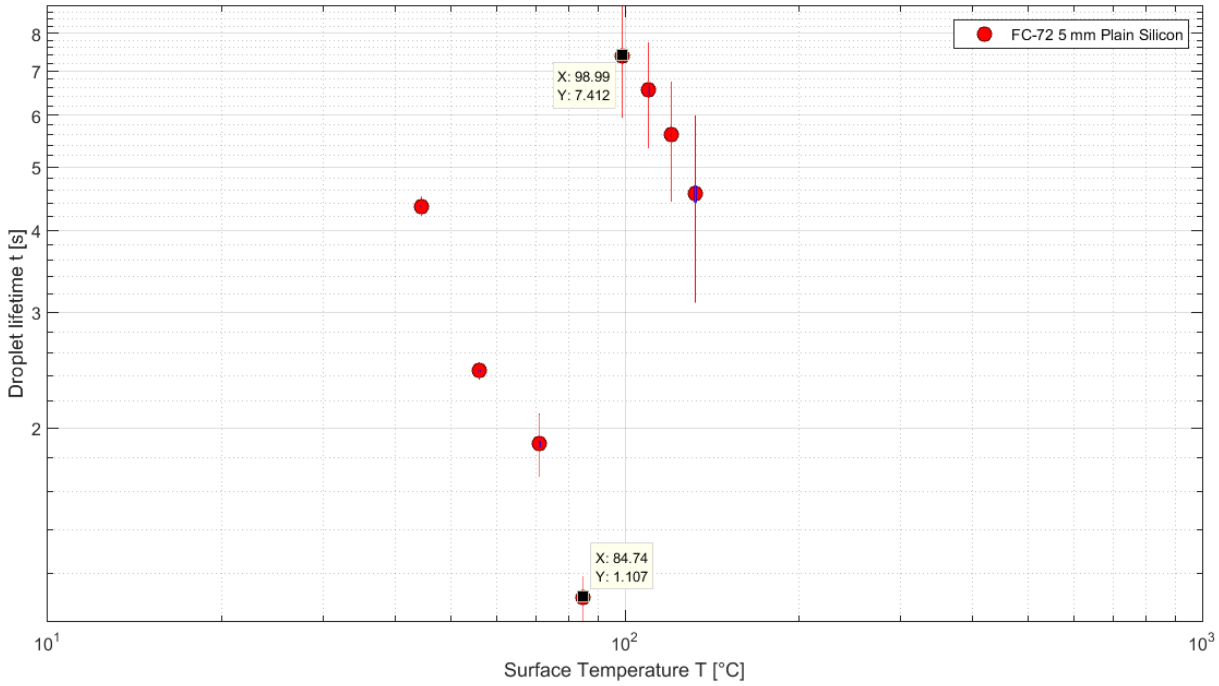

Figure 42 - FC-72 LDF curve for droplet fall height of 5 mm on plain polished silicon

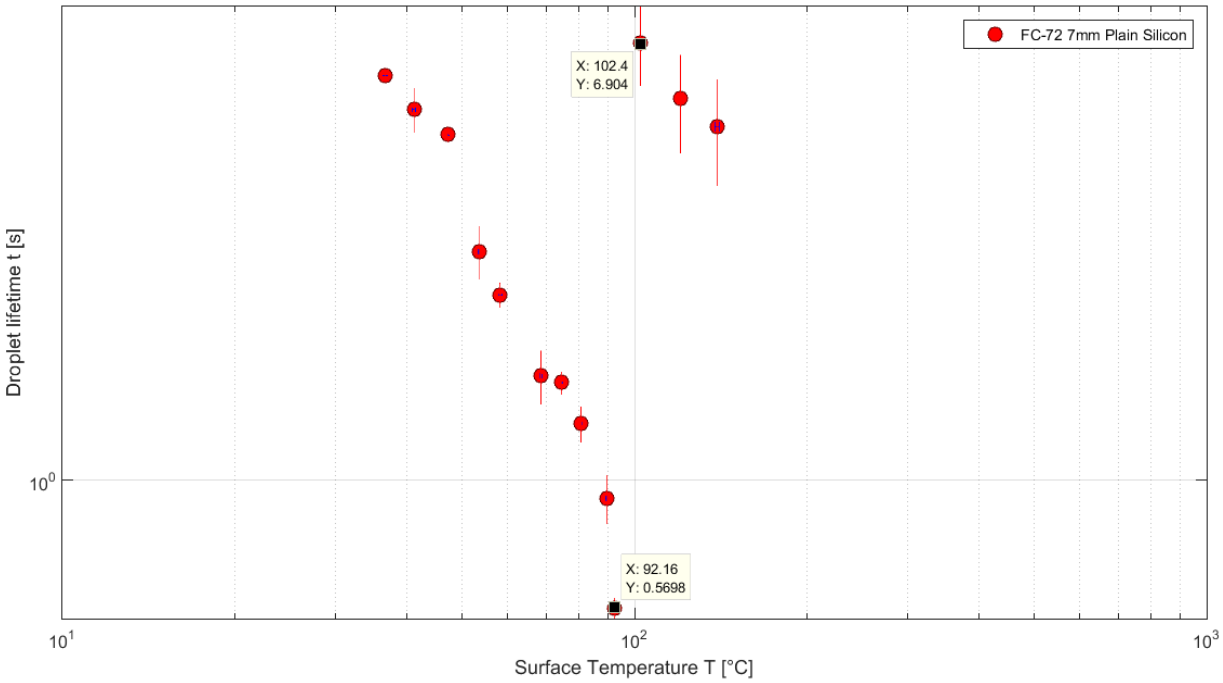

Figure 43 - FC-72 LDF curve for droplet fall height of 7 mm on plain polished silicon

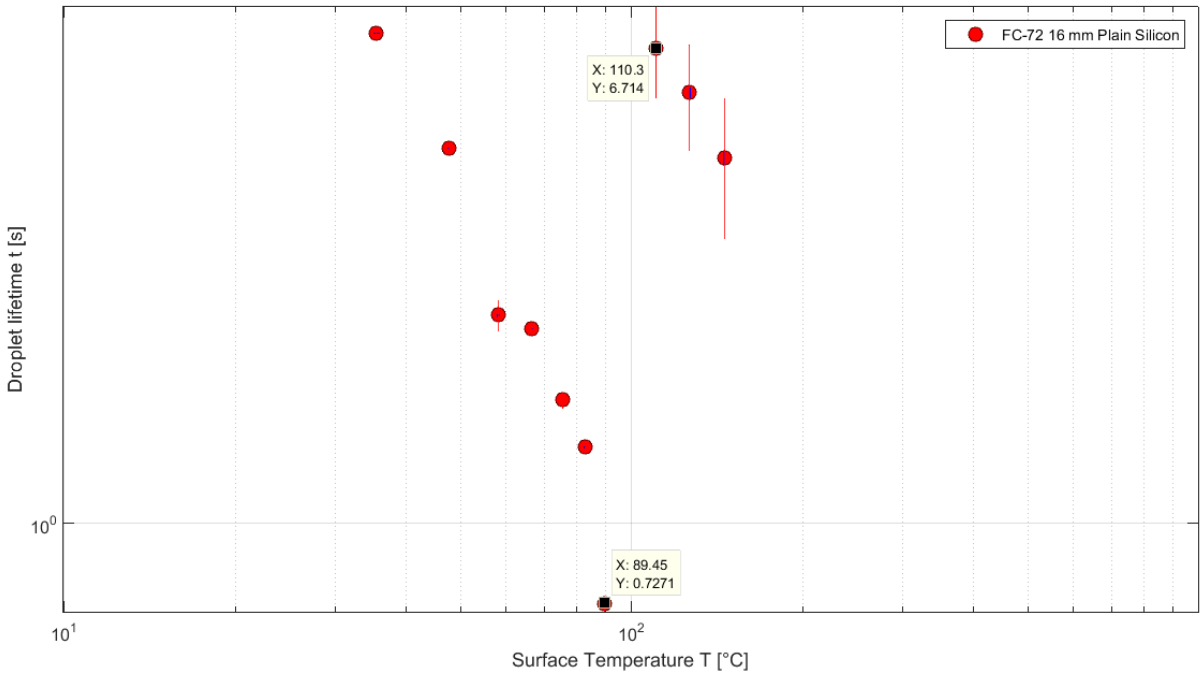

Figure 44 - FC-72 LDF curve for droplet fall height of 16 mm on plain polished silicon

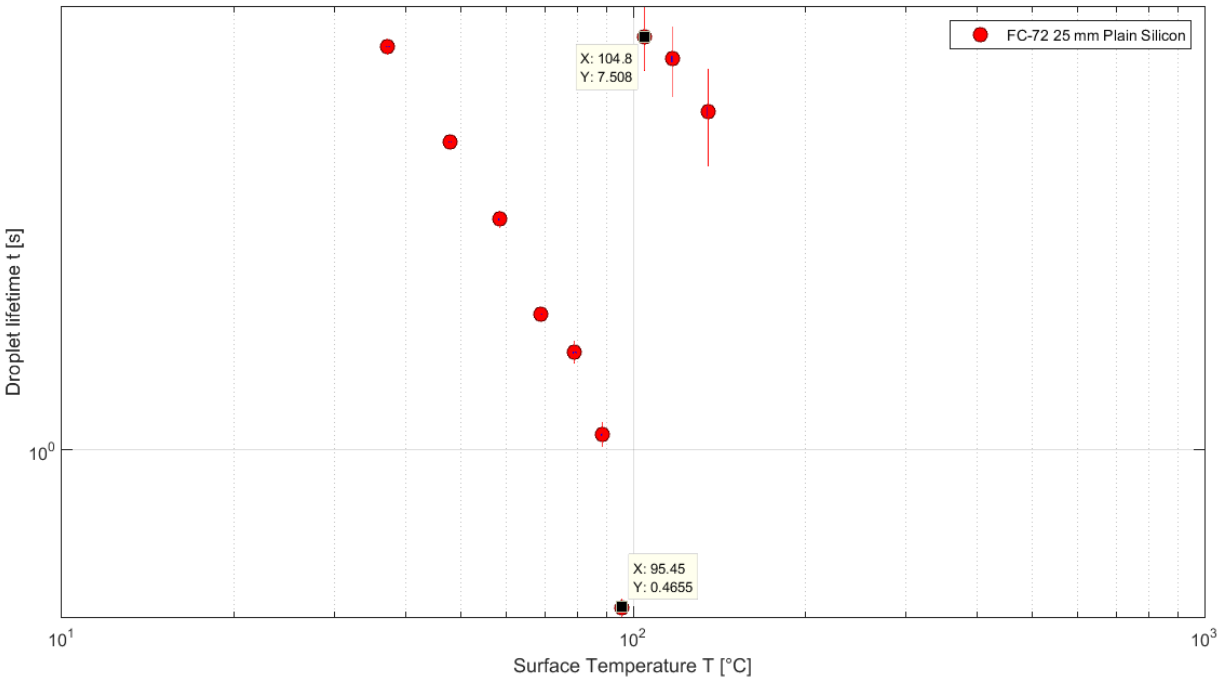

Figure 45 - FC-72 LDF curve for droplet fall height of 25 mm on plain polished silicon

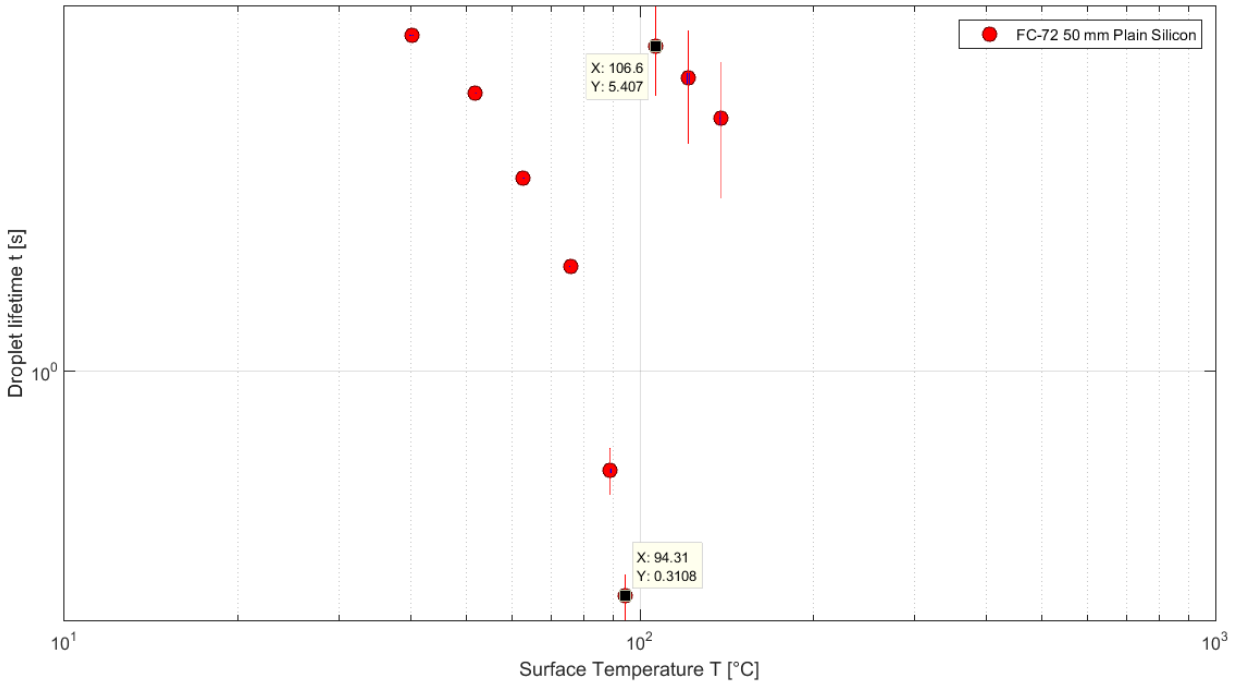

Figure 46 - FC-72 LDF curve for droplet fall height of 50 mm on plain polished silicon

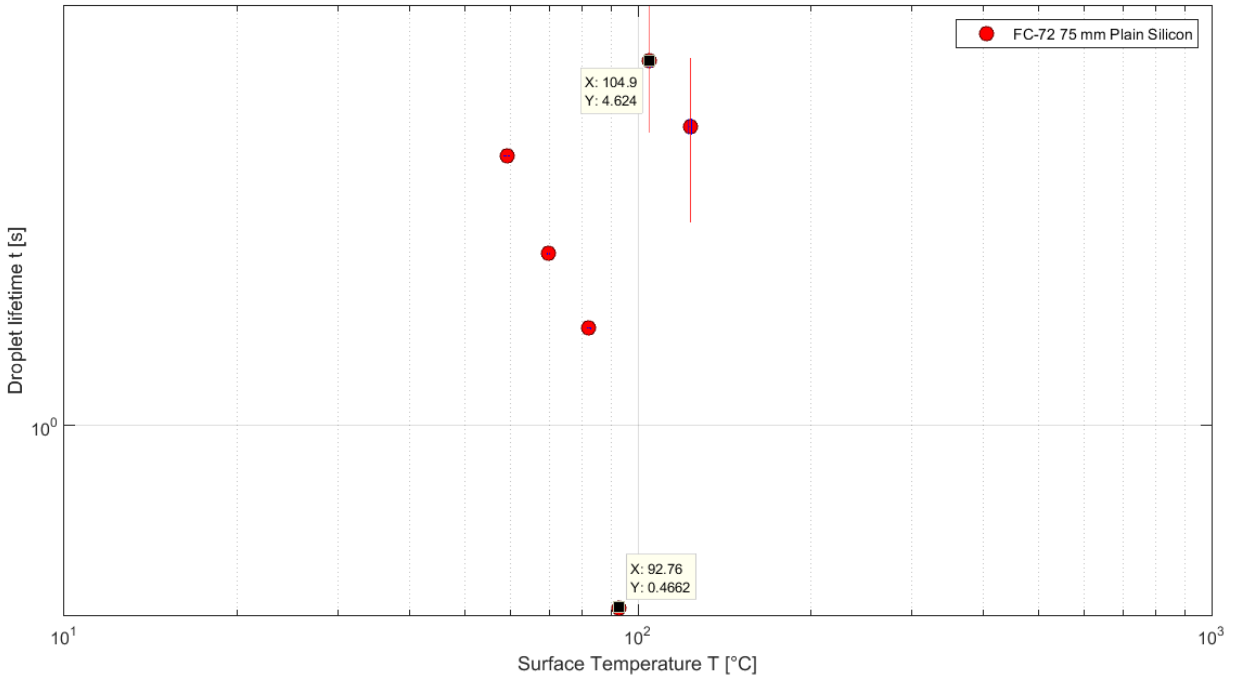

Figure 47 - FC-72 LDF curve for droplet fall height of 75 mm on plain polished silicon

A difference in the behaviour is explained in this Weber map, different behaviours of FC-72 on plain polished silicon have been classified by: Deposition, Breakup/Splashing and Rebound.

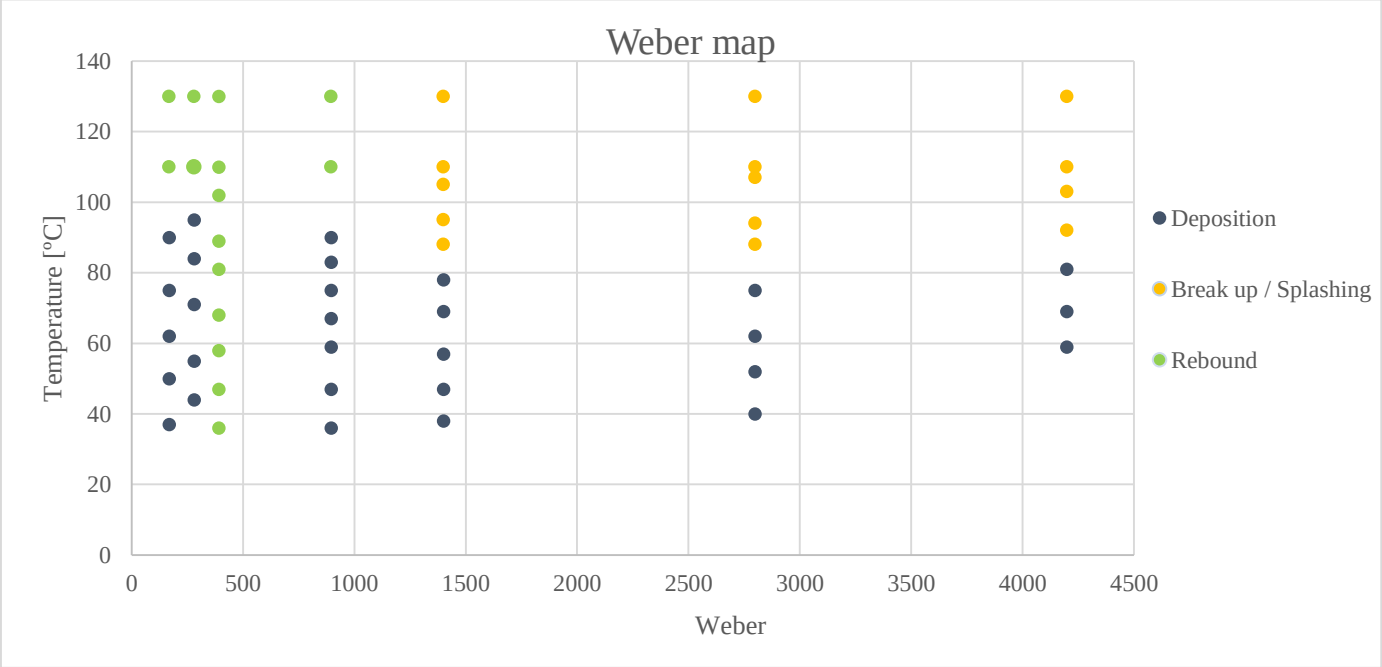

Figure 48 - Impact regime map for FC-72 droplets impacting on a heated, polished silicon surface. Regimes mapped with respect to the Weber number and the temperature of the surface are: deposition (blue points), breakup/splashing (red points), rebound (green points)

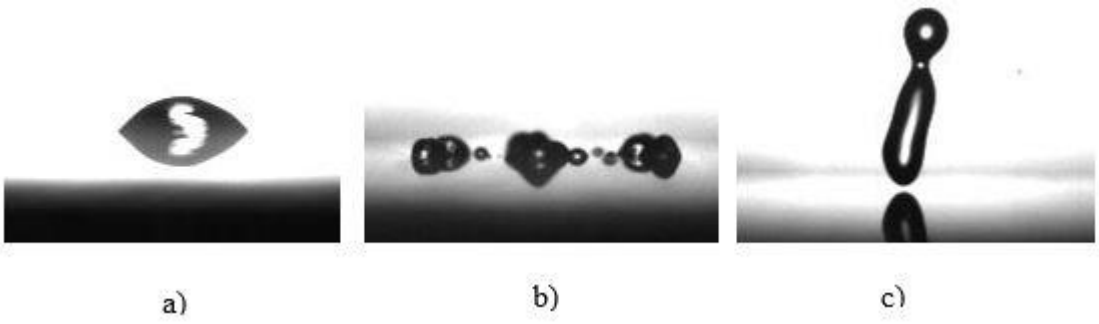

Figure 49 - Impact regimes for FC-72 on plain polished silicon: Deposition (a), Breakup/Splashing (b), Rebound (c)

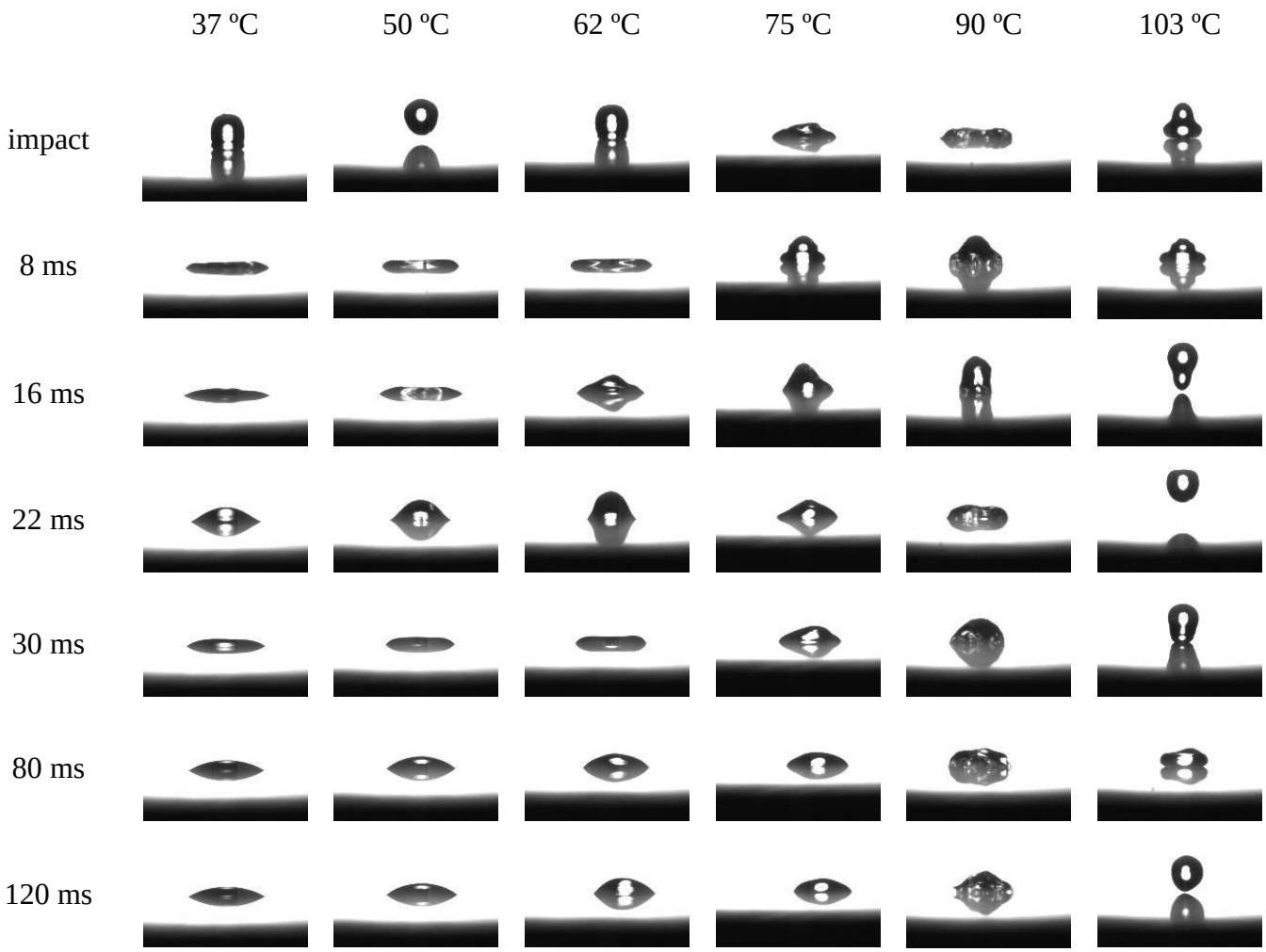

Figure 50 - Behaviour of droplet Impact on plain polished silicon for We = 168, from Impact to 120 ms: The droplet impingement history for a Weber number of 168. The surface temperatures are; 37°C, 50°C, 62°C, 75°C, 90°C and 103ºC. We = 168; Δt = 8 ms

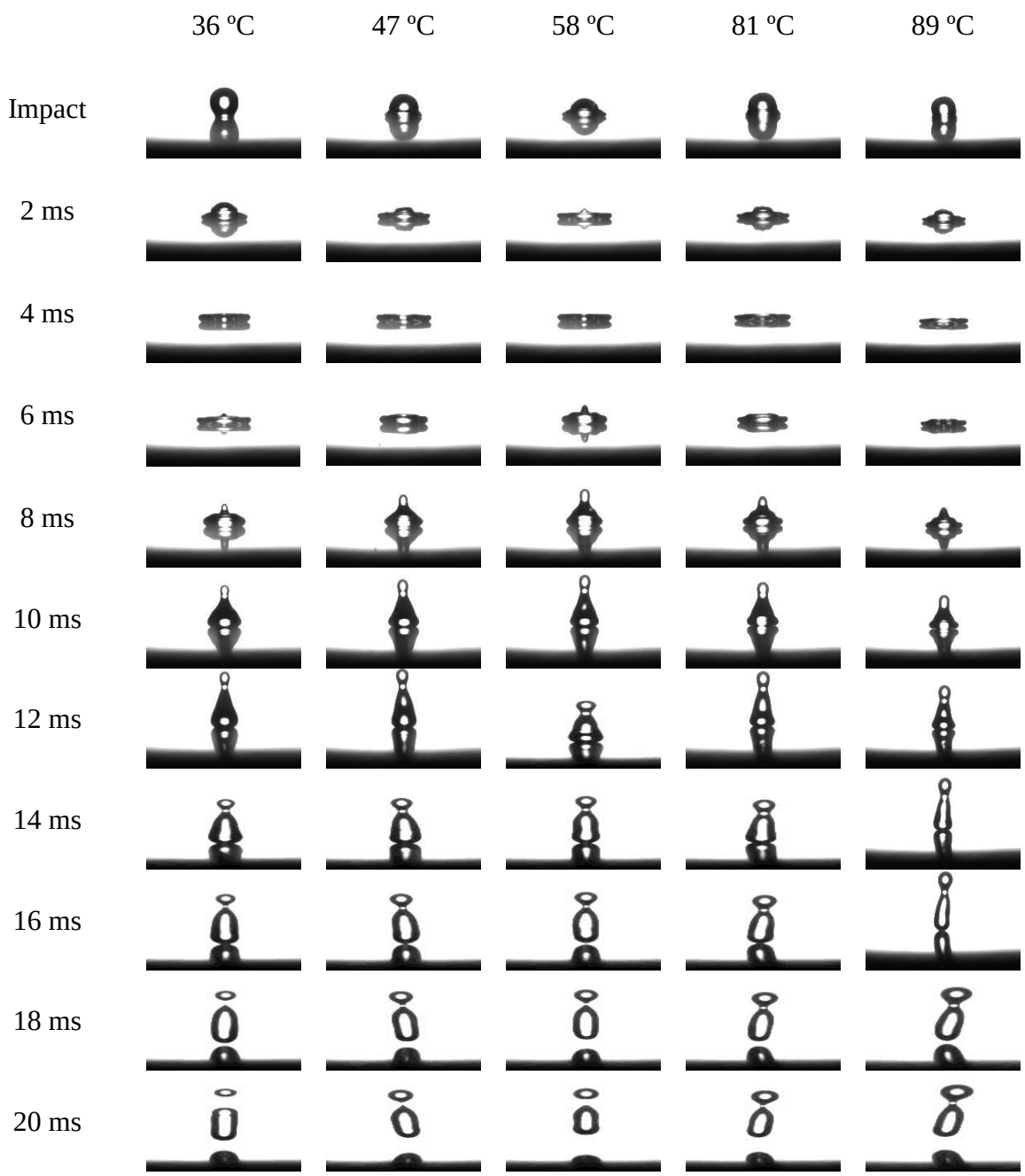

Figure 51 - Behaviour of droplet Impact on plain polished silicon for We = 392, from Impact to 20 ms: The droplet impingement history for a Weber number of 392. The surface temperatures are; 36°C, 47°C, 58°C, 81°C and 89°C. We = 392; Δt = 2 ms

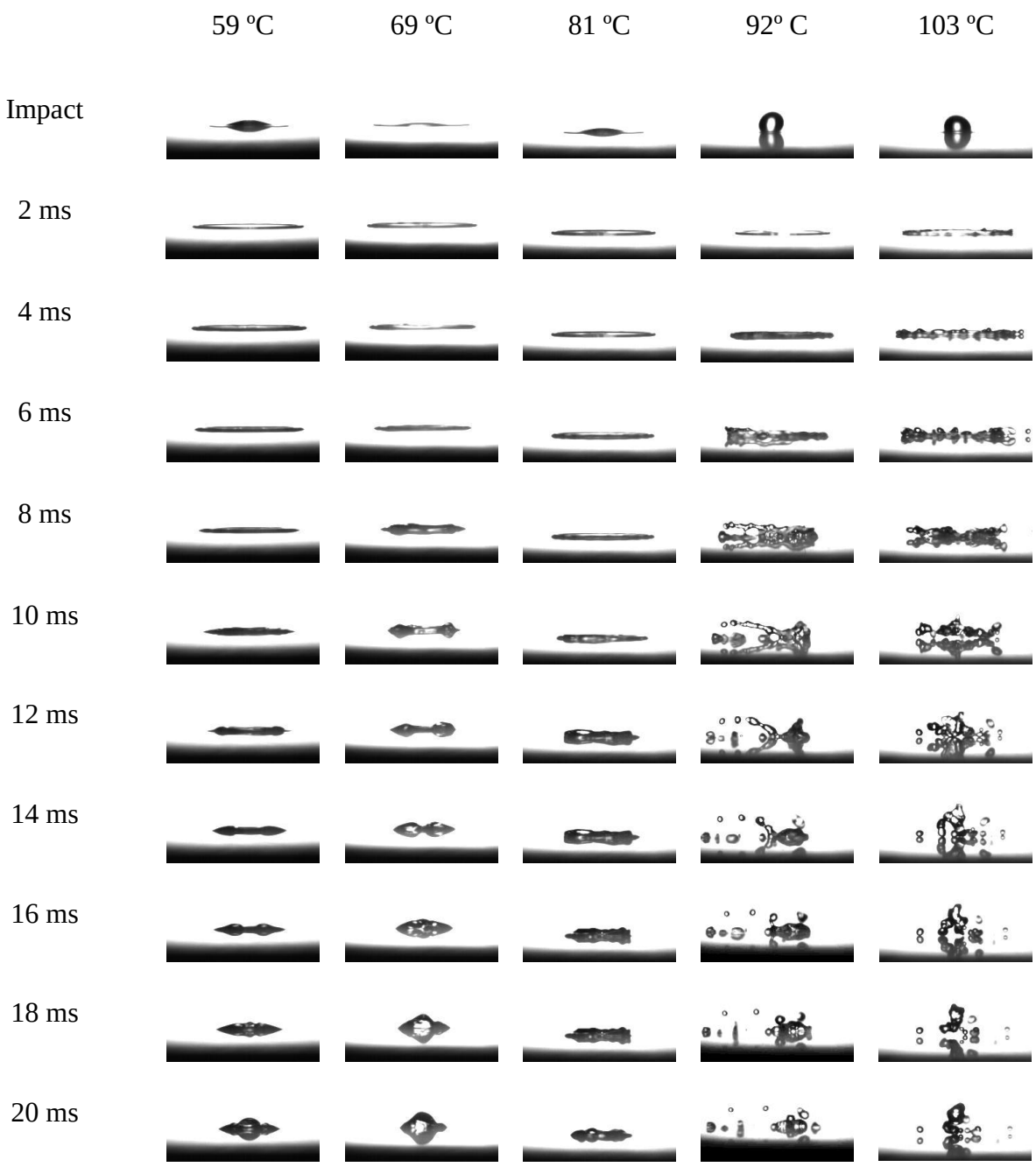

Figure 52 - Behaviour of droplet Impact on plain polished silicon for We = 4198, from Impact to 20 ms: The droplet impingement history for a Weber number of 4198. The surface temperatures are; 59°C, 69°C, 81°C, 92°C and 103ºC. We = 4198; Δt = 2 ms

It becomes clear that there is a difference in time regarding the lifetime of the droplet due to the splashing of the droplet increasing the height, which is plotted in the Figure 53 where different images of the different splits are shown. The bar error of the point above LDF is bigger than point below LDF due to measurements carried out by eye and with a chronometer.

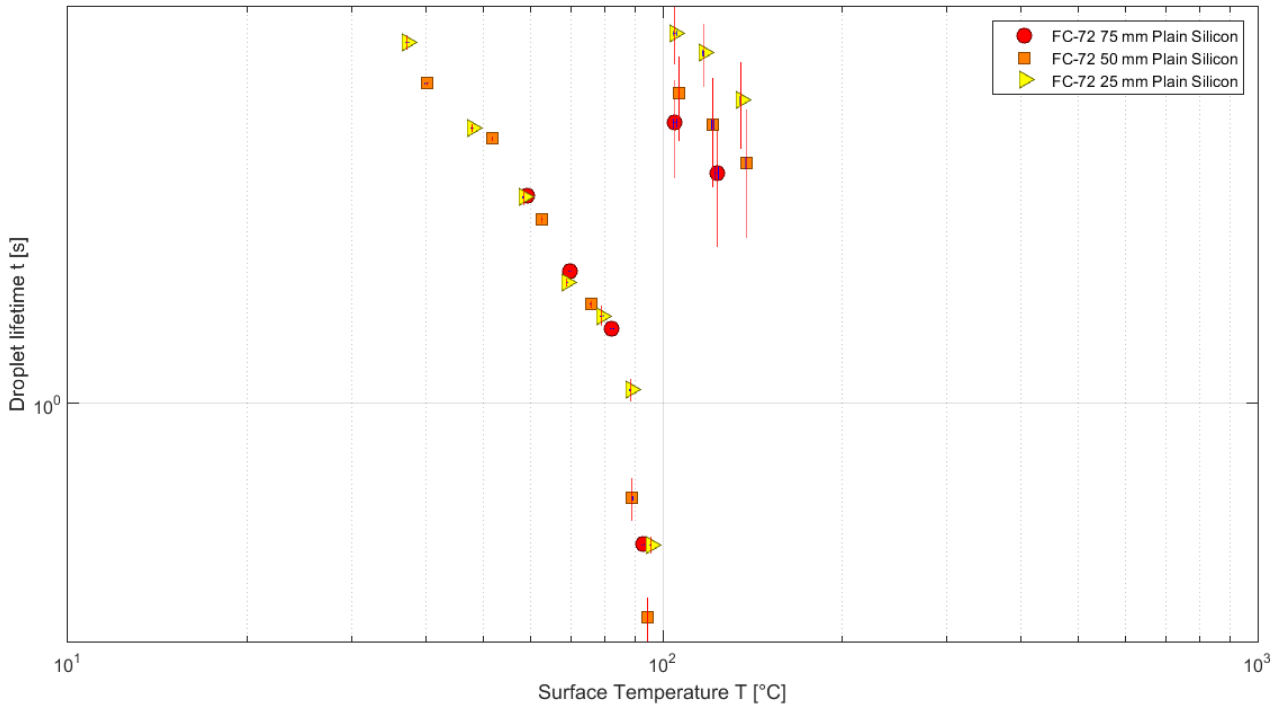

Figure 53 – FC-72 LDF curves, droplet fall height of 75mm, 50mm and 25mm on plain polished silicon

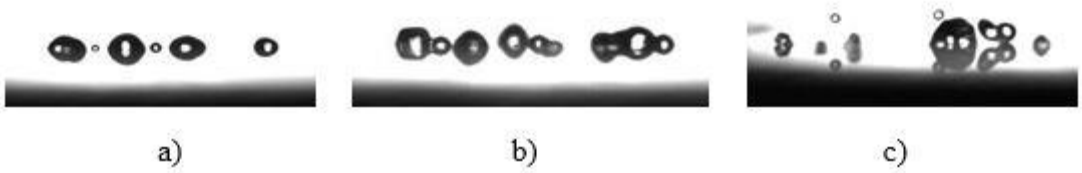

Figure 54 - Different split droplet fall height of a) 25mm, b) 50mm and c) 75mm on plain polished silicon

c. Comparison of both fluids

FC-72 is a dielectric fluid and it has some disadvantages versus water, the evaporation enthalpy for dielectric fluids is lower (88kJ/kg) than water (2256kJ/kg).

But it has some advantages, to evaporate water below 100ºC one needs to apply a higher pressure to archive the evaporation. At an atmospheric pressure FC-72, it can be evaporated around 60ºC- easier than water.

FC-72 is an electric isolator, an advisable property for cooling in the field of electric devices, although FC-72 has worse thermophysical properties in comparison with water [36]. It has been demonstrated that FC-72 has some good cooling properties in comparison with water [37]

The heat transfer advantage of using water is mainly associated with the superior thermophysical properties of this fluid. However, in addition to the large fluid saturation temperature at atmospheric conditions, direct cooling of electronics are frequently not possible using water due to the incompatibility of the fluid with electrical components.

Dielectric fluids like FC-72 are used to cool such electronic devices, especially in direct contact cooling applications. Because of the poor thermal transport properties of such fluids, it is often necessary to employ forced convective heat transfer schemes to augment pool boiling heat transfer rates for high flux chip cooling.

These schemes take the form of microchannel convective boiling and jet impingement and spray impingement boiling.

Deionized water has superior thermal properties, including an enthalpy of vaporization that is two orders of magnitude larger than most dielectric and heat transfer fluids (see Table I), and hence, it has the potential for use in high flux cooling applications. While the saturation temperature of water at atmospheric pressure is larger than the maximum temperature limit permissible in electronics cooling, the temperature constraint can be met by lowering the working system pressure.

The main downside to using water for electronics cooling stems from the difficulty in keeping this fluid dielectric, thereby precluding direct contact with chip electrical interconnects in current packaging technology. One possibility that permits use of water is an indirect cooling approach wherein the cooling fluid is contained within a heat sink located on top of a chip using a TIM. [38].

In Figure 55, it is shown the differences of the LDF curve of water and FC-72, the differences shown are the different droplet lifetime for the same temperature due to the properties of the fluids, for FC-72 the boiling point is 56 ºC and for water it is 100 ºC at atmospheric pressure. For water CHF and LDF are higher than FC-72 due to their boiling point and properties that affect the behaviour of a droplet of each fluid with the hot wall, for example different behaviours of water and FC-72. Water presents atomisation and a lack of FC-72, this can be explained with the properties of superficial tension, density and viscosity of the fluids.

Different diameter of the falling droplet from the syringe is due to FC-72, which presents higher density, viscosity and lower superficial tension. Contrary water droplets remain more time in the point of the syringe and achieve higher diameter of the falling droplet due to higher superficial tension and lower density and viscosity.

For electronic cooling, water needs to be under pressure to achieve CHF in temperatures that allow devices to reach the working temperature limit around 85 ºC. Water also lacks the proper properties for direct electronic cooling due to the fact that water is an electricity conductor. Water, however, does have better properties for the heat transfer than FC-72 due to its higher evaporation enthalpy.

FC-72 has better properties to interact with electronic devices and can be used in atmospheric conditions due to it reaches CHF around 90 ºC. This is the proper situation for limit working temperatures of electronic devices, but not for heat transfer which has shown that FC-72 has worse properties in comparison with water.

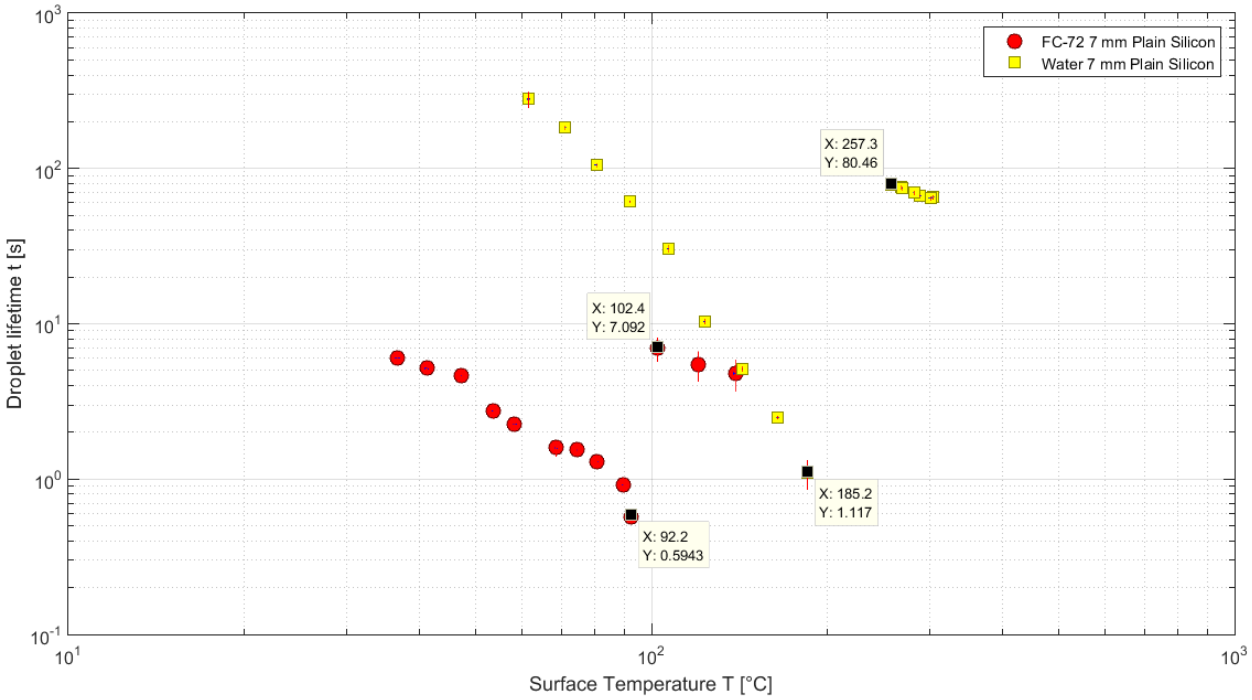

Figure 55 - LDF curves of FC-72 and water for the same droplet fall height of 7 mm on plain polished silicon

6.2 Fabrication of nanostructures

a. Patterned nanowires

Figure 56 shows an array of conical Si nanowires after etching with diameter 800 nm, pitch 2 μm and the measurement of the height is 2 - 3 μm, the bottom part between nanowires is gold to be removed.

Nanowires presented a bended shape due to the reduction of diameter in the top part, which made them weak. The shape of this nanowires results from the concentration of HF used in the etching step. It is used more concentration of HF, this change in solution changed the etching rate. The etching time of theses nanowires is 30 min at room temperature, and the final shape of the nanowires presented a conical shape, the diameter from bottom to the middle of the nanowire was considerably bigger than diameter from middle to top.

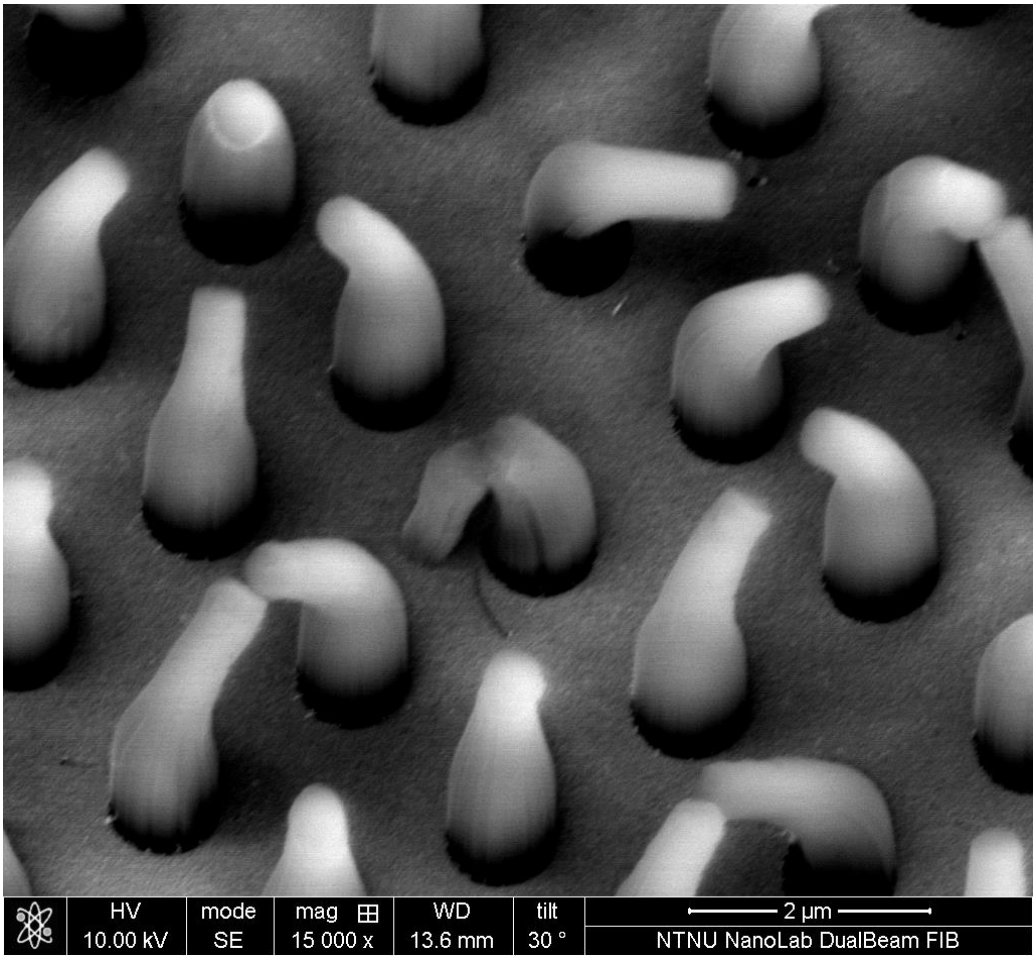

Figure 56 – Conical Si nanowires after etching – Diameter 800 nm Pitch 2 μm tilted 30º

Picture 57 show, Si nanowires with diameter 800 nm, pitch 10 μm, and height between 300 – 500 nm after etching and the bottom part between nanowires is gold to be removed.

Picture 58 show a single Si nanowire from the array of Figure 57, it is shown the height and the size of this nanowire, the top part is not focus due to the small size of the nanowire.

The solution of the etching step was then changed, by using a smaller concentration of HF with different thickness of gold. The etching time was 10 min at room temperature, and the result was a regular shape along the nanowires, cylindrical nanowires. The etching rate became more controllable and the solution attacked the top part of the nanowire less. Resulting from this, the desired cylindrical shape was achieved in the nanowires.

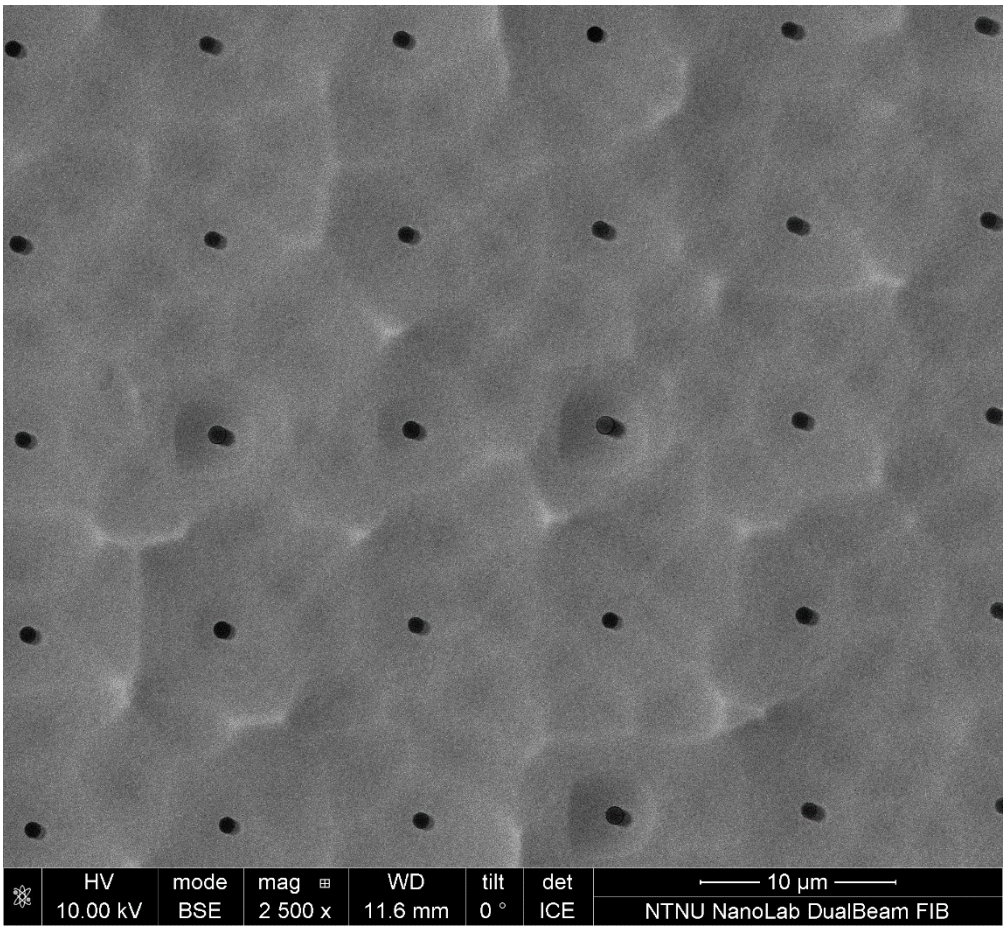

Figure 57 - Si Nanowires after etching Diameter 800 nm Pitch 10 μm top view

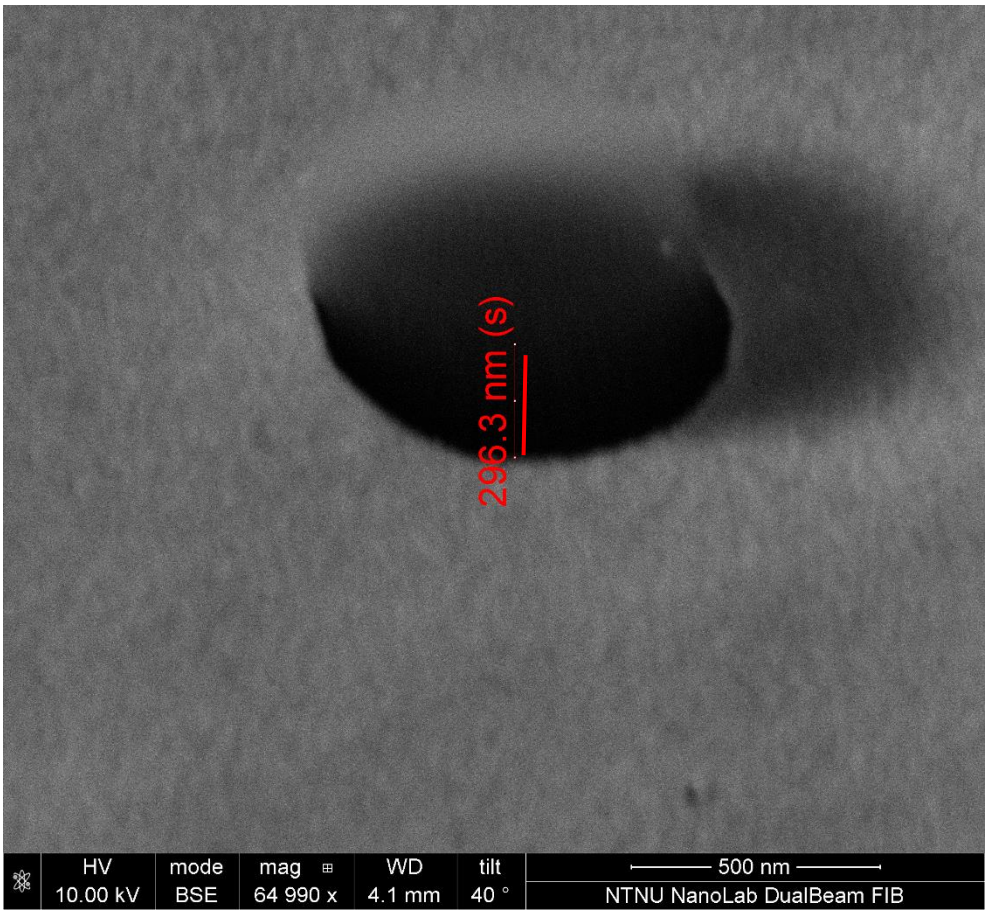

Figure 58 - Single Si nanowires after etching Diameter 800 nm Pitch 10 C tilted 40º

Figures 59 and 60 show the result after etching of Si nanowires with diameter 200 nm, pitch 625 nm, and height between 300 – 500 nm. The bottom part between nanowires is gold to be removed. The same procedure as in pictures 57 and 58 was carried out, an etching time of 10 min in the solution of HF with less concentration to finally attain a cylindrical shape along the nanowires.

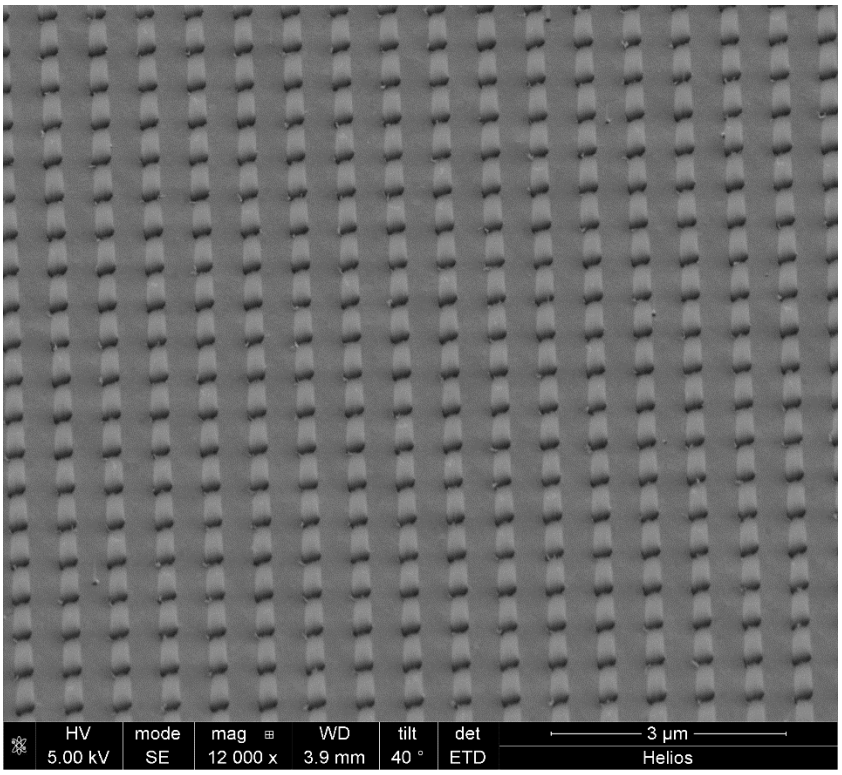

Figure 59 - Big area, Si Nanowires after etching Diameter 200nm Pitch 625 nm tilted 40º

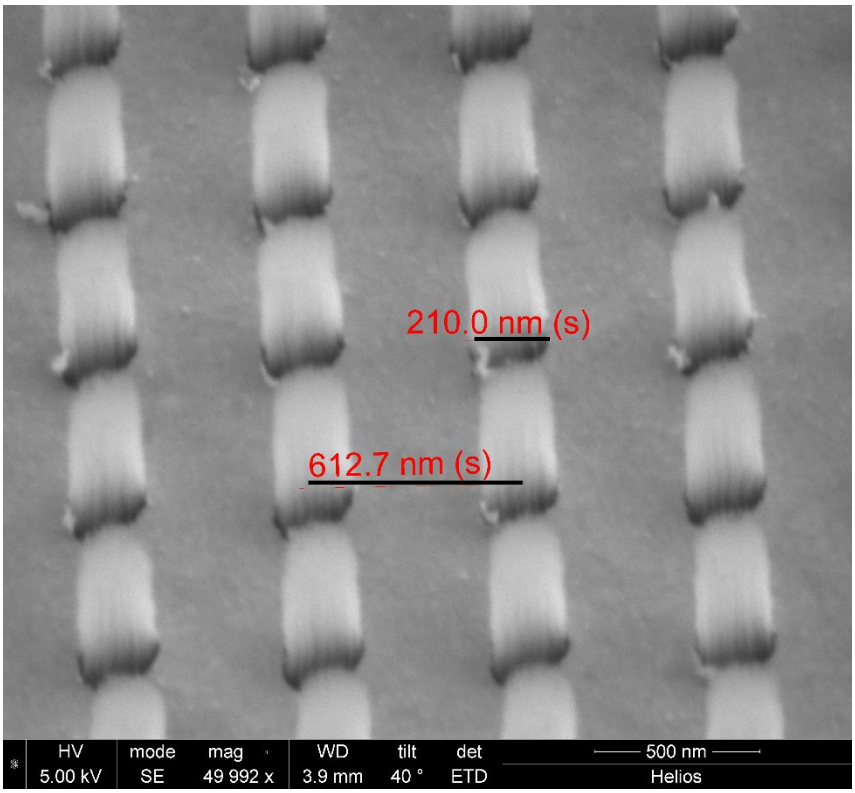

Figure 60 - Measurements of Si nanowires after etching Diameter 200 nm Pitch 625 nm tilted 40º

Figures 61 and 62 show the result after etching of Si nanowires with diameter 200nm, pitch 625nm, and height 2 – 4 μm. The bottom part between nanowires is gold to be removed. The same procedure as in pictures 57 and 58 was followed however it was left in the solution for 30 minutes with less HF concentration. The shape was controlled as a result of the concentration of the solution, achieving cylindrical shape along the nanowires.

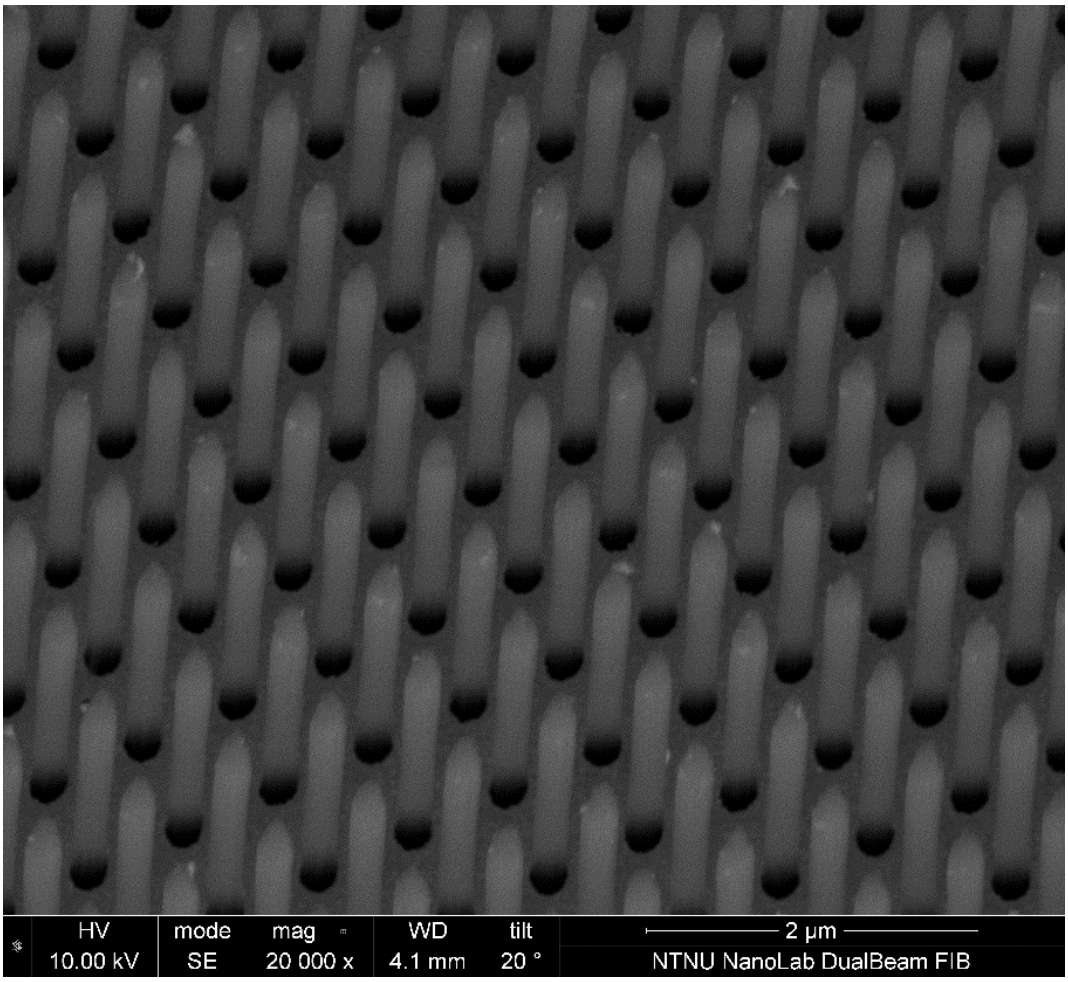

Figure 61 – Si nanowires after etching Diameter 200 nm Pitch 625 nm tilted 20º

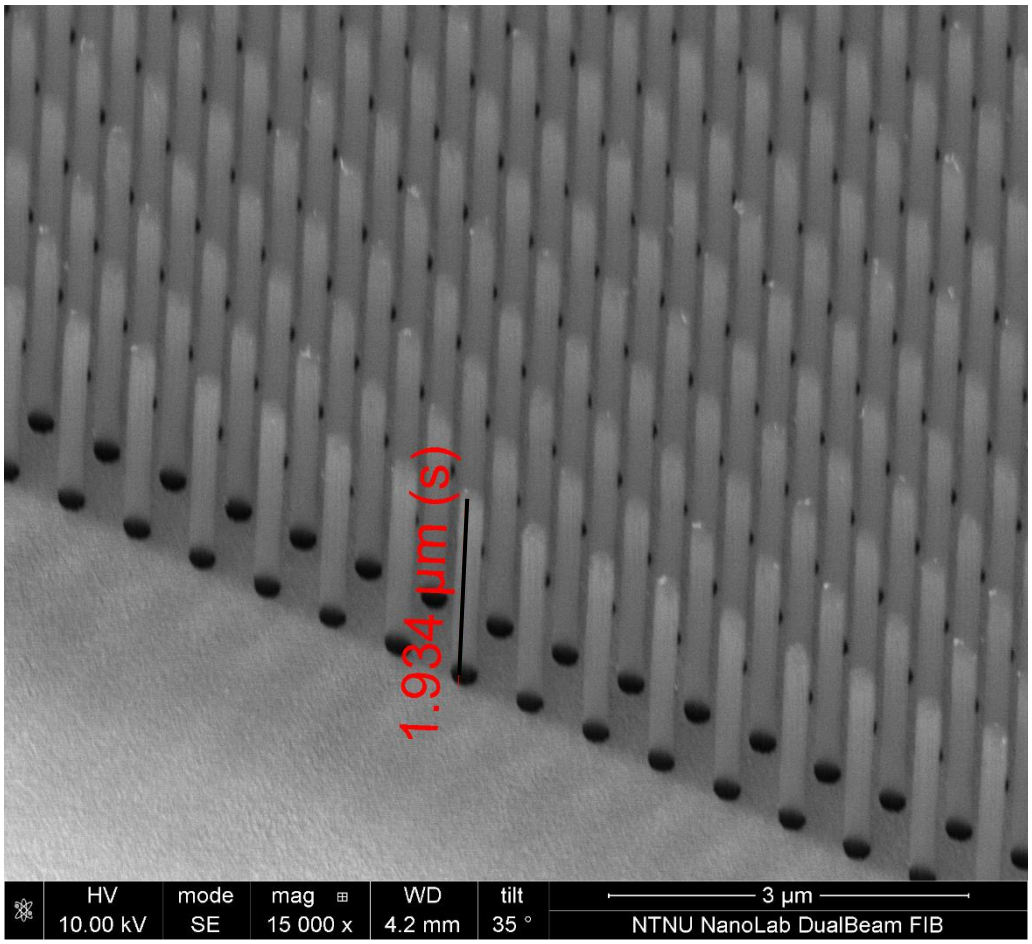

Figure 62 - Measurements of Si nanowires after etching Diameter 200nm Pitch 625 nm tilted 35º

Figure 63 and 64 show a different result in the etching part, where bending occurred in the final result due to the height of the nanowires and the way the sample was dried. Nanowires with smaller diameters tend to bend when the determinate aspect ratio is achieved. A solution to this was then investigated: In order to avoid bending, rather than using water to clean the wafer after the etching step, isopropanol (IPA) was used, improving the final result. It was left to dry in a hot plate instead of using N2, this way we avoid abruptness when drying.

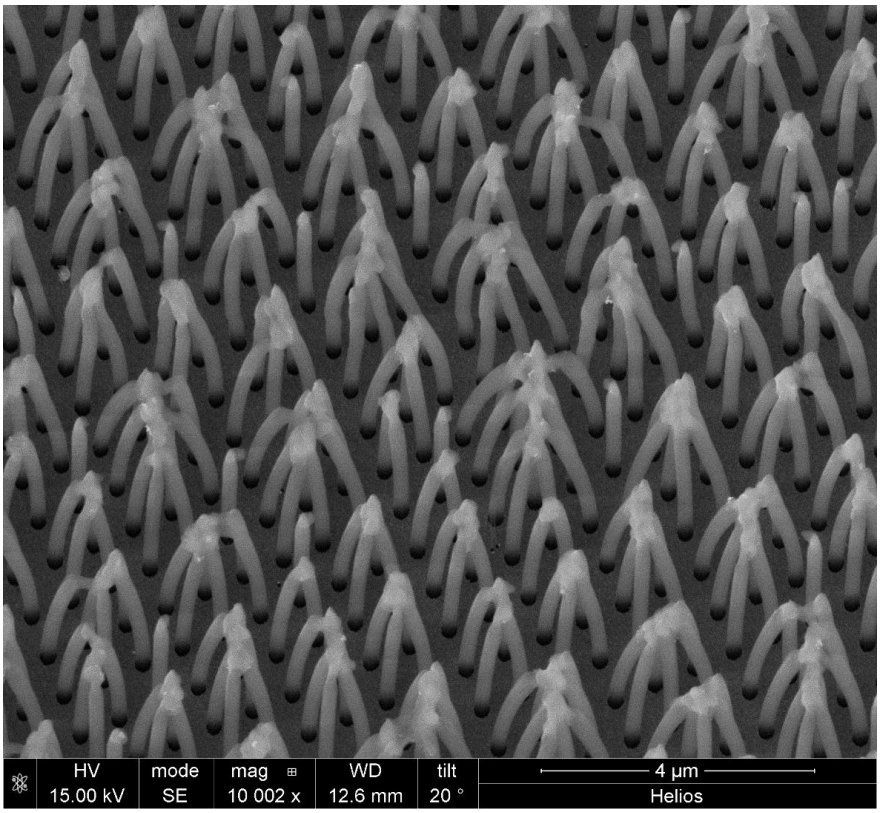

Figure 63 – Bended Si nanowires after etching Diameter 200 nm Pitch 625 nm tilted 20º

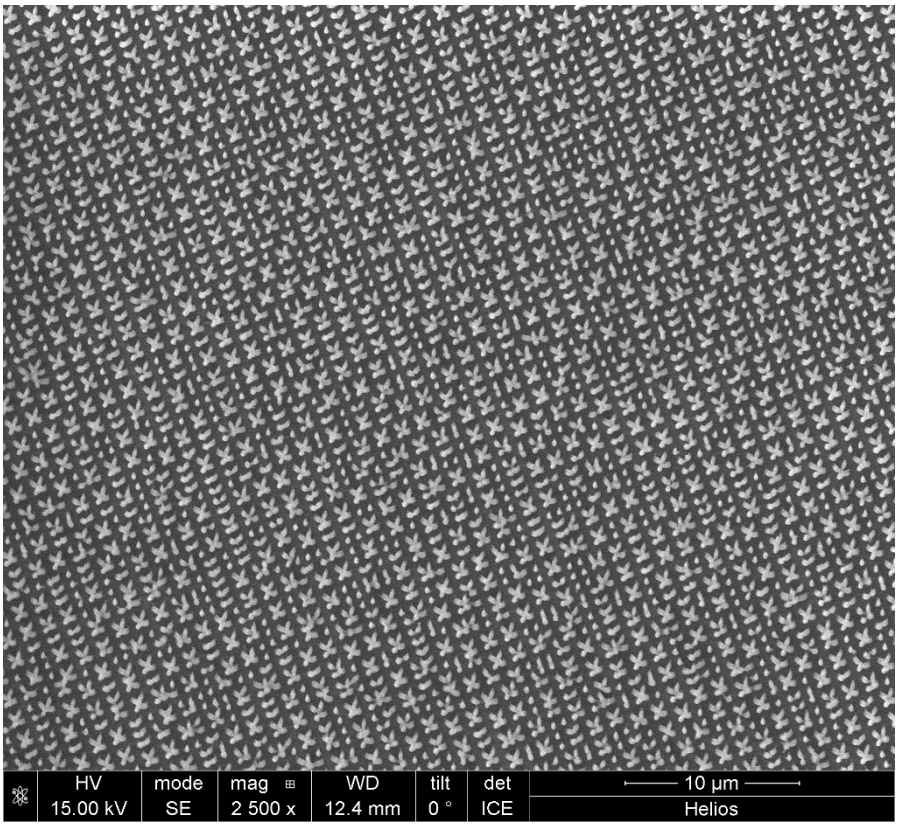

Figure 64 - Bended Si nanowires after etching Diameter 200 nm Pitch 625 nm, top view

Figure 65 and 66 show a different result in the etching part, where bending occurred in the final result due to the height of the nanowires and the way the sample was removed from the solution of HF. Nanowires with smaller diameters tend to bend when the determinate aspect ratio is achieved. Different group regions can be distinguished as random regions. A solution to this was then investigated: In order to avoid bending, rather than using water to clean the wafer after the etching step, isopropanol (IPA) was used, improving the final result. It was left to dry in a hot plate instead of using N2, this way we avoid abruptness when drying.

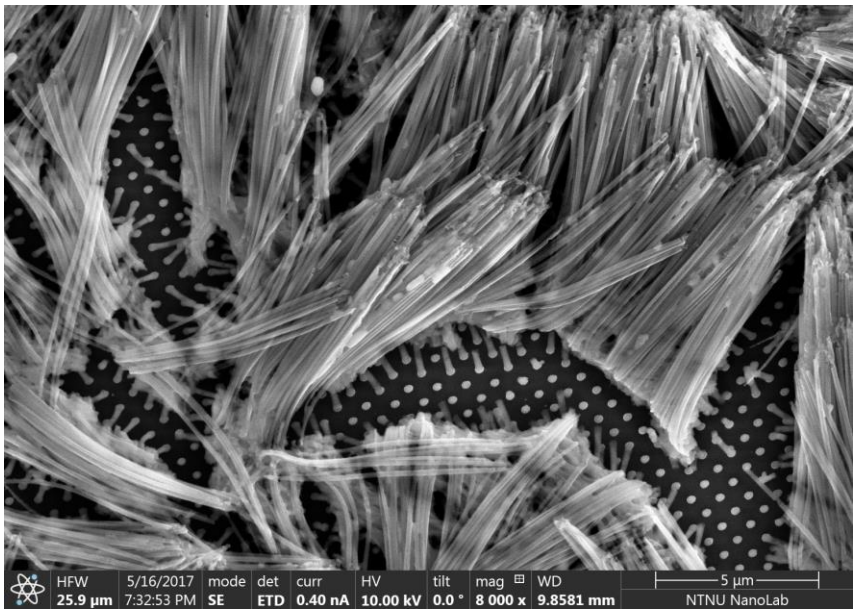

Figure 65 - Bended Si nanowires after etching Diameter 200 nm Pitch 625 nm, top view

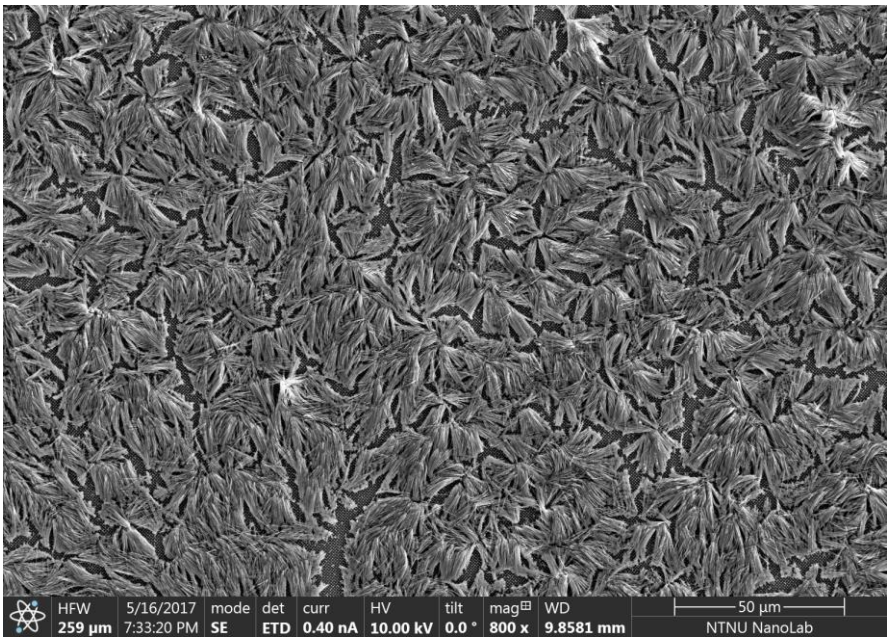

Figure 66 - Bended Si nanowires after etching Diameter 200 nm Pitch 625 nm, top view

Figure 67 and 68 show a different result in the etching part, where bending occurred in the final result due to the height of the nanowires and the way the sample was removed from the solution of HF. Nanowires with smaller diameters tend to bend when the determinate aspect ratio is achieved. Different group regions can be distinguished as a pyramidal region.

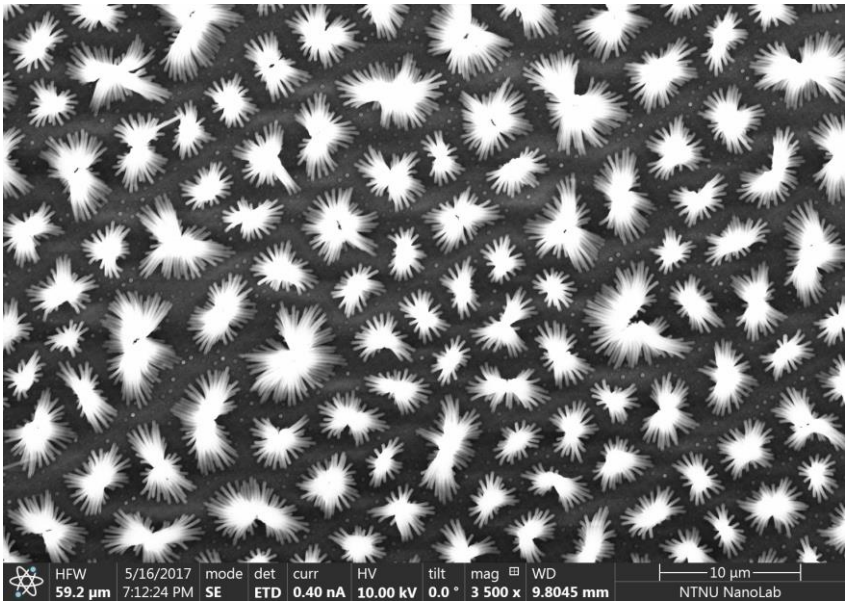

Figure 67 - Bended Si nanowires after etching Diameter 200 nm Pitch 625 nm, top view

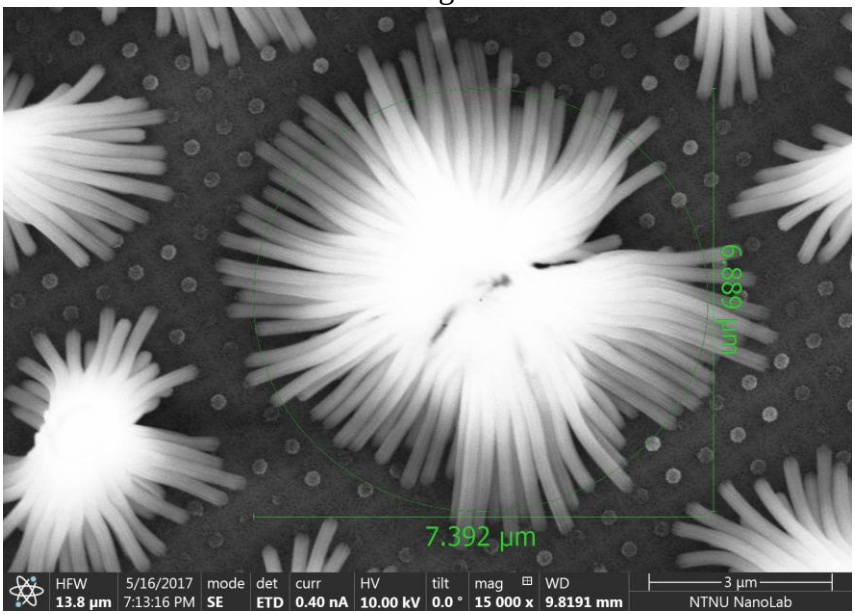

Figure 68 - Bended Si nanowires after etching Diameter 200 nm Pitch 625 nm, top view

Figure 69 and 70 show a different result in the etching part, where bending occurred in the final result due to the height of the nanowires and the way the sample was removed from the solution of HF. Nanowires with smaller diameters tend to bend when the determinate aspect ratio is achieved. Different group regions can be distinguished as random regions.

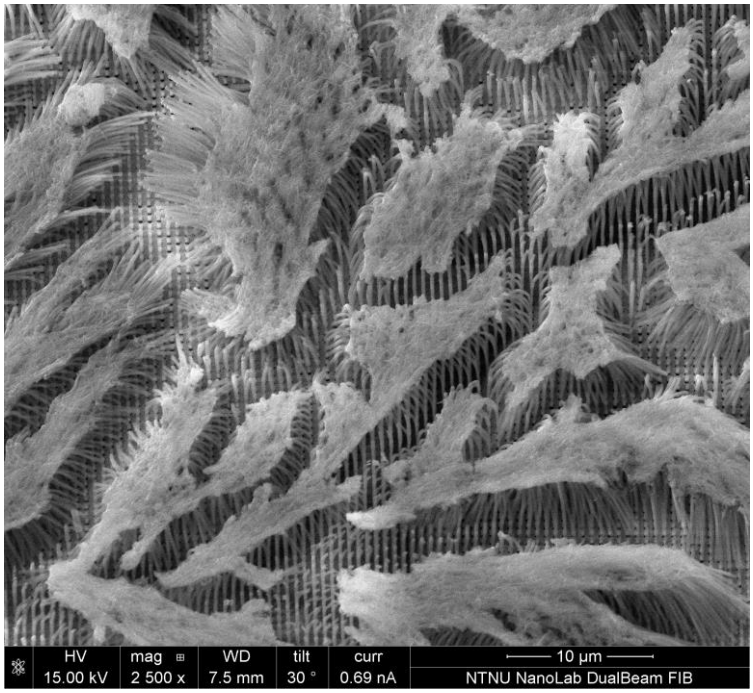

Figure 69 - Bended Si nanowires after etching Diameter 200 nm Pitch 625 nm, tilted 30º

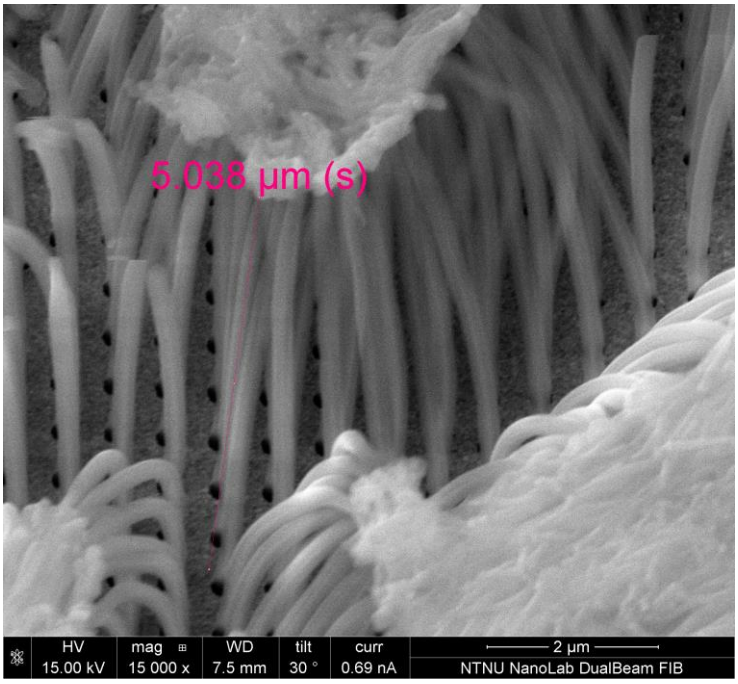

Figure 70 - Bended Si nanowires after etching Diameter 200 nm Pitch 625 nm, tilted 30º

b. Random nanowires

Figure 71 and 72 show a different result in the etching part, nanowires grow randomly after etching due to the silver layer on top of the Silicon wafer. Si random nanowires present additional microscale cavities and pores that increase the nucleation cavity density and the surface roughness. Also, Si random nanowires provide a strong capillary wicking due to the nanoporosity.

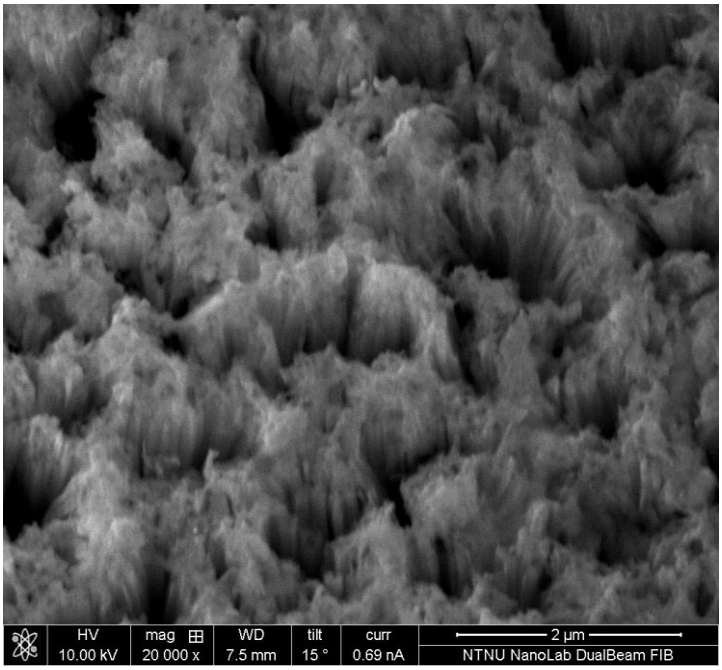

Figure 71 - Random Si nanowires after etching, tilted 15º

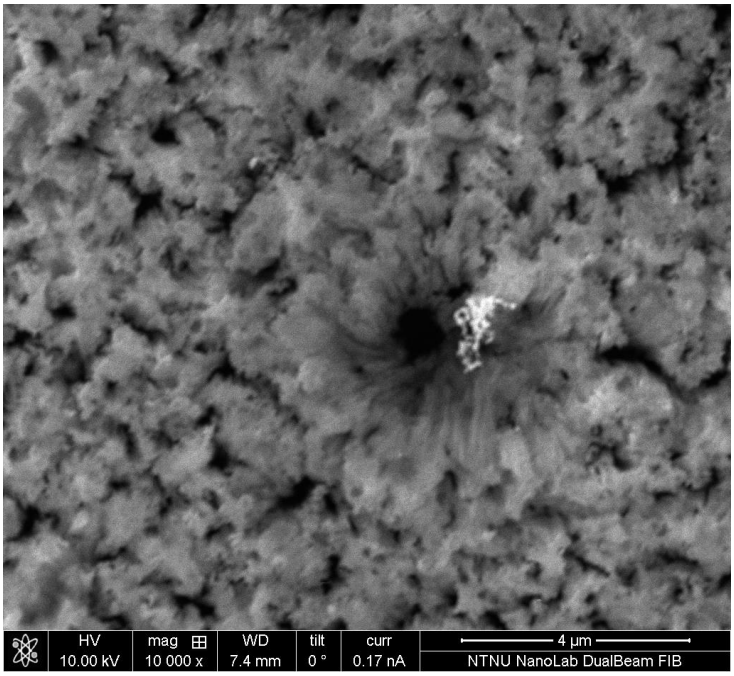

Figure 72 – Cavity between random Si nanowires after etching, top view

6.3 Improvements of different nanostructures in comparison with plain polished silicon

a. Patterned nanowires

Figures 73, 74, and 75 show a comparison of the Leidenfrost curves for different surfaces, plain Si and Si nanowires Diameter 800 nm, Pitch 2 μm and height 2 μm approximately with same fall droplet height, 7mm, 25mm and 50 mm respectively. It is shown that the droplet lifetime reduces slightly when increasing the temperature until a temperature where a sudden jump is observed.

Figure 76 shows the different LDF points achieved in these experiments. It is possible to observe that the micro-structured surface presents a higher LFP for all the heights. The observed results suggested that sub-micron surfaces could improve the spray cooling performance. The shift in the LFP compared to the plain Si can be attributed to the properties of the processed surface.

The sub-micron tapered pillars make the surface more hydrophilic that avoids the Leidenfrost phenomenon. The larger roughness provided by the pillars yields an increase in the effective heat transfer area.

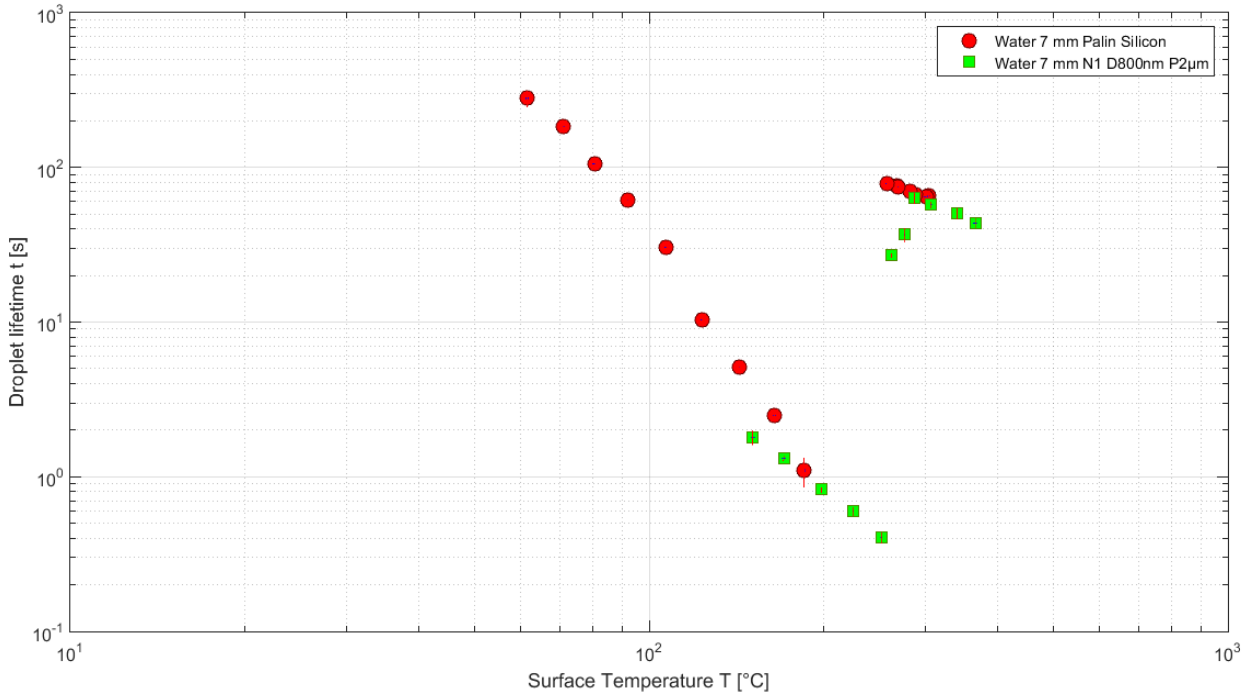

Figure 73 - LDF curves of Patterned Si nanowires Diameter 800 nm Pitch 2 µm and plain polished silicon as surface, droplet fall height of 7 mm

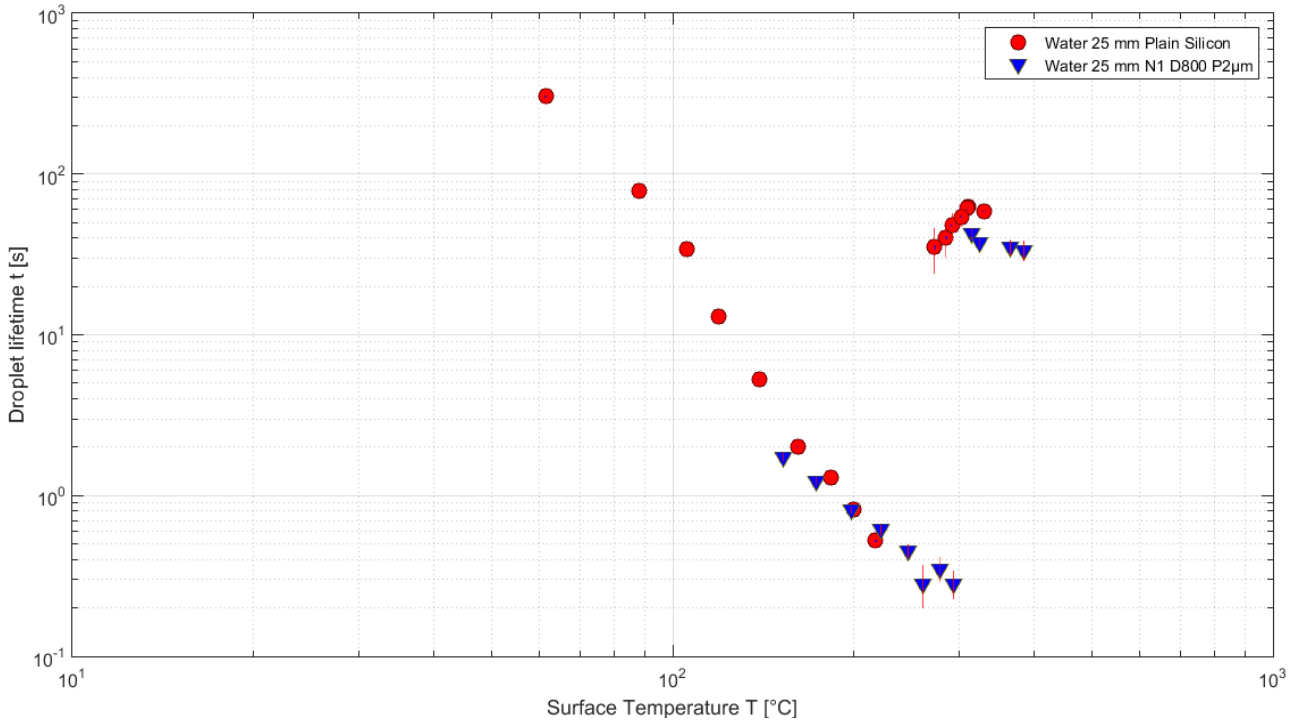

Figure 74 - LDF curves of Patterned Si nanowires Diameter 800 nm Pitch 2 µm and plain polished silicon as surface, droplet fall height of 25 mm

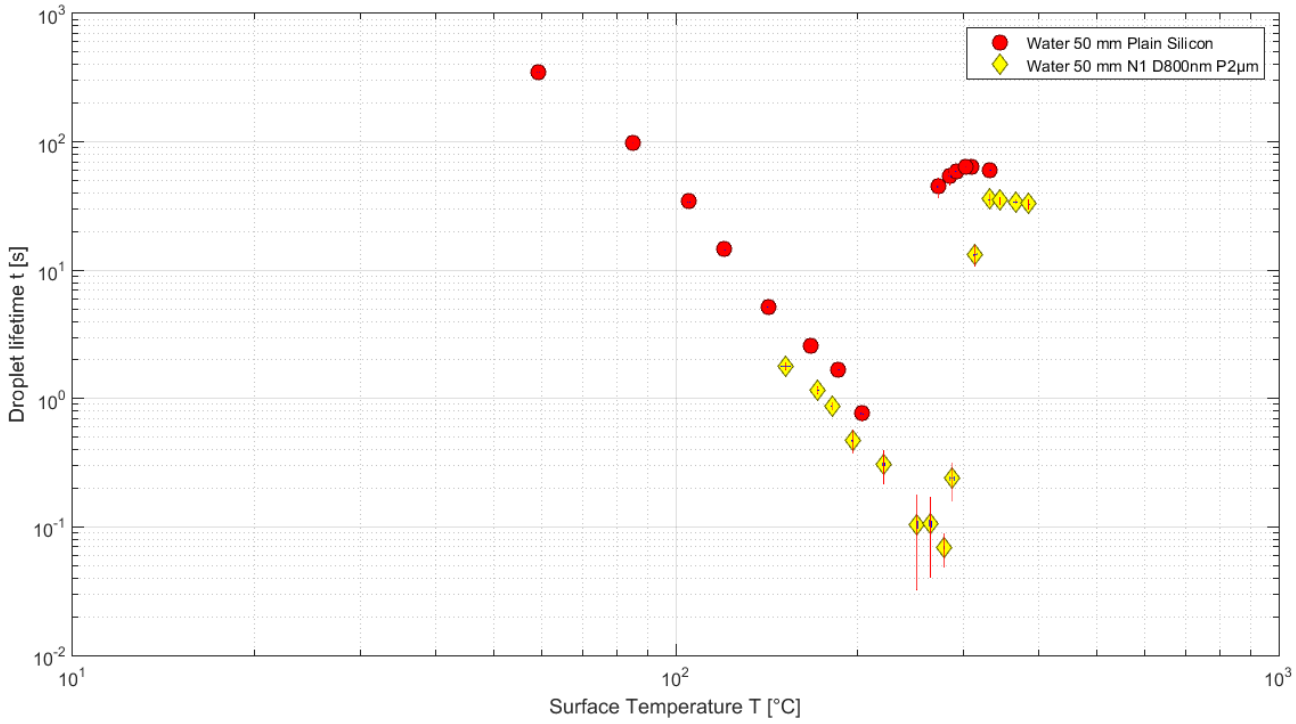

Figure 75 - LDF curves of Patterned Si nanowires Diameter 800 nm Pitch 2 µm and plain polished silicon as surface, droplet fall height of 50 mm

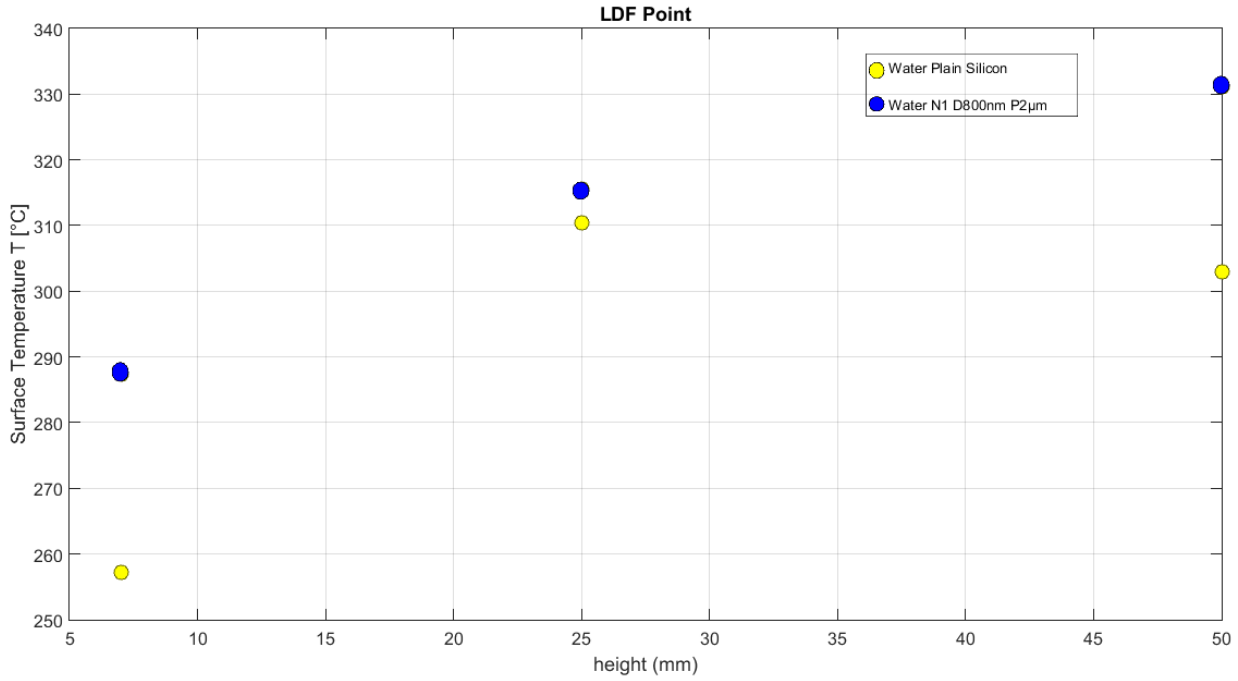

Figure 76 – Water LDF points for different surfaces and different fall droplet heights

Figure 77 – a) water contact angle on Si nanowires Diameter 800 nm Pitch 2 μm Height 2 μm b) water contact angle on plain polished silicon

b. Si random nanowires

Figure 78 shows a comparison of the Leidenfrost curves for different surfaces, plain Si and Si random nanowires with 7 mm fall droplet height.

It is possible to observe that the micro-structured surface presents a higher LFP for all the heights. The observed results suggested that sub-micron surfaces could improve the spray cooling performance. The shift in the LFP compared to the plain Si can be attributed to the properties of the processed surface.

The random nanowires make the surface more hydrophilic that delays the Leidenfrost phenomenon. The larger roughness provided by the pillars yields an increase in the effective heat transfer area.

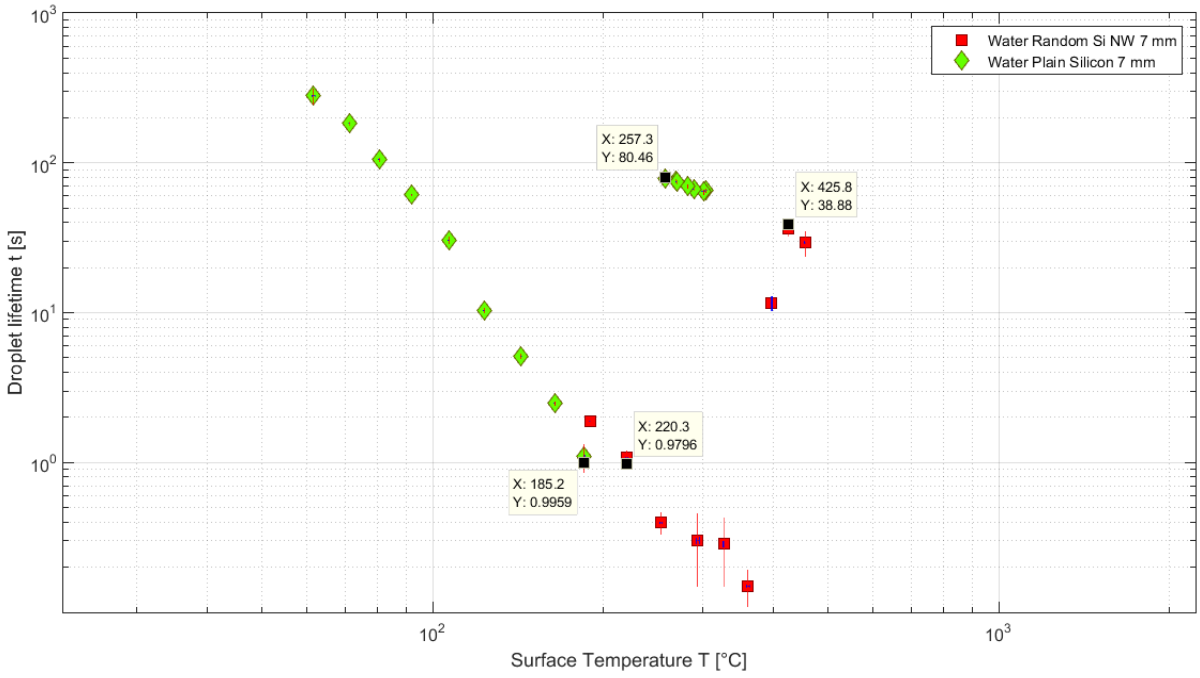

Figure 78 - LDF curves of Si random nanowires and plain polished silicon as surfaces, droplet fall height of 7 mm

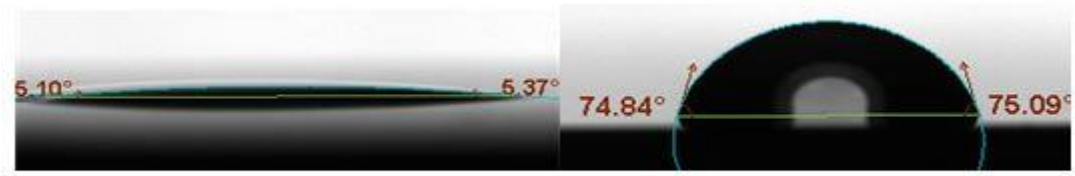

a) b)

Figure 79 – a) water contact angle on Si random nanowires

b) water contact angle on plain polished silicon

7. Conclusion

7.1 Summary

This master thesis report has shown the design and fabrication of an experimental setup for the visualization of the Leidenfrost phenomenon by identifying the CHF (critical heat flux) and the LDF (Leidenfrost point), and defining a reference of the Leidenfrost phenomenon by drawing curves of droplet lifetime versus temperature testing plain polished silicon with water and FC-72. An improvement of the CHF and LFD point using nanostructures with different geometrical characteristics has been demonstrated.

A working recipe or the fabrication of nanostructures has been developed allowing the acquisition of a working, uncomplicated means for these to be obtained in the laboratory. Finally, the design of the samples was successfully achieved without important defects in the structures.

The final result, as it is presented in the chapter 6 of results, are: water and FC-72 plain polished silicon reference Leidenfrost curves of droplet lifetime vs temperature and a Weber map describing droplet behaviour, Leidenfrost curves of droplet lifetime vs temperature of nanostructures experiments and general information about fabrication and characterization of different nanostructured surfaces accomplished in in the NTNU NanoLab.

7.2 Recommendation for further work

Further development could include the investigation of the fabrication process changing the photoresist and trying to get smaller diameters and smaller pitches. Moreover, trying to improve the result to avoid some problems experienced, looking for the proper thickness for etching in order to save material, finding a proper way to perform the final etching step, using nanoimprinting for an optimization of the process and changing the concentration in the solution in order to get same changes in the shape of the nanowires would be some interesting developments future work could take into account.

Fabrication of different samples and a development of pool boiling facility can be investigated focus on new experiments in order to draw a direct pool boiling curve with the heat flux versus with pool boiling experiments.

Further tests can be done with the different samples produced. Same experiments carried out in this project can be done changing experiment conditions such as size of liquid mass, method of liquid deposition, liquid subcooling, solid thermal properties, surface conditions, pressure as explained in section 2.1 on the Leidenfrost phenomenon history in table 1.

REFERENCES

[1] Thome, J. R., 2006, “The New Frontier in Heat Transfer: Microscale and Nanoscale Technologies,” Heat Transf. Eng., 27(9), pp. 1–3.

[2] Chunqiang S. et al.: Development and experimental investigation of a novel spray cooling system integrated in refrigeration circuit. Appl. Therm. Eng. 33–34(2012), 246–252.

[3] Agostini, B., Fabbri, M., Park, J. E., Wojtan, L., Thome, J. R., and Michel, B., 2007, “State of the Art of High Heat Flux Cooling Technologies,” Heat Transf. Eng., 28(4), pp. 258–281.

[4] Agostini B. et al.: State of the art of high heat flux cooling technologies. Heat Transf. Eng. 28(2007), 4, 258–281.

[5] Eivind Grøstad, Design and fabrication of micro-nano enhanced surfaces for controlling Leidenfrost point, Norwegian University of Science and Technology Trondheim, Norway

[6] Manuel Auliano, Maria Fernandino, Peng Zhang, Carlos Alberto Dorao, The Leidenfrost phenomenon on silicon nanowires, Norwegian University of Science and Technology Trondheim, Norway, (2016), DOI: 10.13140/RG.2.2.35318.19529

[7] Wroclaw University of Technology, Department of Thermodynamics, Wybrzeże Wyspiańskiego 27, 50-370 Wrocław, Poland Method of high heat flux removal by usage of liquid spray cooling, archives of thermodynamics Vol. 34(2013), No. 3, 173–184 DOI: 10.2478/aoter-2013-0023

[8] Andrew Griesmer, The Leidenfrost Effect, November 12, 2013, COMSOL BLOG, https://www.comsol.com/blogs/Leidenfrost-effect/

[9] Jearl Walker, Boiling and the Leidenfrost effect, Cleveland State University, (1994)

[10] Ivan U. Vakarelski1,2, Neelesh A. Patankar3 , Jeremy O. Marston1 , Derek Y. C. Chan4,5 & Sigurdur T. Thoroddsen1,2, Stabilization of Leidenfrost vapor layer by textured superhydrophobic surfaces, doi:10.1038/nature11418, 274 NATURE, vol 489,13 september (2012).

[11] Laurent Maquet, Leidenfrost effect at its limits, University Libre de Bruxelles Ecole Polytechnique TIPs, Doctor of Philosophy In the subject of physics (2016-2017)

[12] L.H.J. Wachters, N.A.J. Westerling, The heat transfer from a hot wall to impinging water drops in the spheroidal state, Chem. Eng. Sci. 21 (1966) 1047–1056.

[13]J. D. Bernardin, i. Mudawar, The Leidenfrost Point: Experimental Study and Assessment of Existing Models, Boiling and Two-Phase Flow Laboratory, School of Mechanical Engineering, Purdue University, West Lafayette, IN 47907, 896 / Vol. 121, NOVEMBER (1999).

[14] D. Quéré, “Wetting and Roughness,” Annual Review of Materials Research, vol. 38, no. 1, pp. 71–99, 2008.

[15] Wenzel, RN (1936). "Resistance of Solid Surfaces to Wetting by Water". Ind. Eng. Chem. 28 (8): 988–994. doi:10.1021/ie50320a024.

[16] Zisman, W.A, Contact Angle, Wettability and Adhesion. 1964, Advances in Chesmistry, American Chemical Society, pp. 1-6

[17] Scientific, Blloln. OneAttension Theta user manual Rev2.31.

[18] D. Attinger, C. Frankiewicz, A. R. Betz, T. M. Schutzius, R. Ganguly, A. Das, C.-J. Kim, and C. M. Megaridis, “Surface engineering for phase change heat transfer: A review,” MRS Energy & Sustainability, vol. 1, p. E4, 2014.

[19] E. a. Vogler, “Structure and reactivity of water at biomaterial surfaces.” Advances in colloid and interface science, vol. 74, pp. 69–117, 1998.

[20] Wenzel, R.N. Resistance of Solid Surfaces to Wetting by Water. 1936, Ind. Eng. Chem., pp. 688-994

[21]Cassie, A.B.D. and S.Baxter. Wettability of Porous Surfaces. 1944, Trans. Faraday Soc., pp. 546-551.

[22] Anti-Icing Superhydrophobic Coatings, Liangliang Cao, Andrew K. Jones, Vinod K. Sikka, Jianzhong Wu and Di Gao, Langmuir, 2009, Department of Chemical and

Petroleum Engineering, University of Pittsburgh, Pittsburgh, Pennsylvania 15261 25 (21), pp 12444–12448, DOI: 10.1021/la902882b.

[23] Dropwise condensation on superhydrophobic surfaces with two tier roughness. Chen, C-H. et al. 2007, Applied Physics Letters.

[24] W. Zhang, T. Yu, J. Fan, W. Sun, and Z. Cao, "Droplet impact behavior on heated micro-patterned surfaces," Journal of Applied Physics, vol. 119, no. 11, p. 114901, 2016.

[25] Amir Faghri, Yuwen Zhankg, Jhon R.Howell, Advanced Heat and Mass Transfer, chapter 8.2. Pool boiling regimen. (2013)

[26] Autor, Dragonfly Masterclass [Magic Marks]. (2014 20th January). Pool Boiling Heat Transfer - Magic Marks [video file]. https://www.youtube.com/watch?v=N1yZwRcQSZw&index=32&list=WL&t=73s

[27] Gangtao Liang, Issam Mudawar, Review of drop impact on heated walls, Article in International Journal of Heat and Mass Transfer · March 2017, DOI: 10.1016/j.ijheatmasstransfer.2016.10.031

[28] J.D. Bernardin, C.J. Stebbins, I. Mudawar, Mapping of impact and heat transfer regimes of water drops impinging on a polished surface, Int. J. Heat Mass Transfer 40 (1997) 247–267.

[29] J.D. Bernardin, C.J. Stebbins, I. Mudawar, Effects of surface roughness on water droplet impact history and heat transfer regimes, Int. J. Heat Mass Transfer 40 (1997) 73–88.

[30] Vijay K. Narasimhan, Thomas M. Hymel, Ruby A. Lai, and Yi Cui,Hybrid Metal_Semiconductor Nanostructure for Ultrahigh Optical Absorption and Low Electrical Resistance at Optoelectronic Interfaces, VOL. 9 NO. 11, (2015)

[31] R.-Q. Zhang, Y. Lifshitz, and S.-T. Lee, "Oxide-Assisted Growth of Semiconducting Nanowires," Advanced Materials, vol. 15, no. 78, pp. 635-640, Apr. 2003.

[32] Micro-chem, 1254 CHESTNUT STREET NEWTON, MA 02464 (2001)

[33] Vijay K. Narasimhan, Thomas M. Hymel, Ruby A. Lai, and Yi Cui, Hybrid Metal Semiconductor Nanostructure for Ultrahigh Optical Absorption and Low Electrical Resistance at Optoelectronic Interfaces, Department of Materials Science and Engineering, Stanford University, 476 Lomita Mall, Stanford, California 94305, United States, 7 (2015)

[34] Changsong Ding, Gaurav Soni, Payam Bozorgi, Brian D. Piorek, Carl D. Meinhart, and Noel C. MacDonald, A Flat Heat Pipe Architecture Based on Nanostructured Titania, Journal of Microelectromechanical Systems 19(4):878 - 884 · September 2010 DOI: 10.1109/JMEMS.2010.2051019

[35] Ivan U. Vakarelski1* , Joseph D. Berry2, 3, Derek Y. C. Chan4, 5 , Sigurdur T. Thoroddsen1, Leidenfrost vapor layers reduce drag without the crisis in high viscosity liquids, University of Science and Technology (KAUST).

[36] Improvements of the heat transfer systems, Univesity of Sevilla, Library of engineers, proyect 5036.

[37] P. Hrabovský, P. Nemec and M. Malcho, Compare Cooling Effect of Different Working Fluid in Thermosyphon, University of Žilina, Faculty of Mechanical

[38] Ruander Cardenas and Vinod Narayanan, Comparison of Deionized Water and FC-72 in Pool and Jet Impingement Boiling Thermal Management, IEEE TRANSACTIONS ON COMPONENTS, PACKAGING AND MANUFACTURING TECHNOLOGY, VOL. 2, NO. 11, NOVEMBER (2012).

[39] Z. Anxionnaz, M. Cabassuda, C. Gourdona, P. Tochonb, Heat exchanger/reactors (HEX reactors): Concepts, technologies: State-of-the-art, a Laboratoire de Génie Chimique, UMR 5503 CNRS/INPT/UPS, 5 rue P. Talabot, BP 1301, 31106 Toulouse Cedex 1, France b Atomic Energy Commission-GRETh, 17 avenue des Martyrs, F-38054 Grenoble Cedex 9, France.

A. DRAWINGS

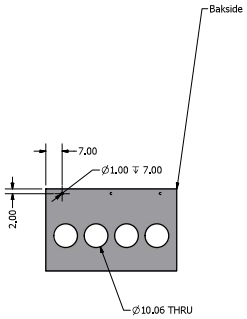

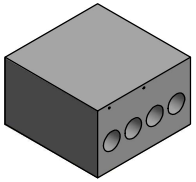

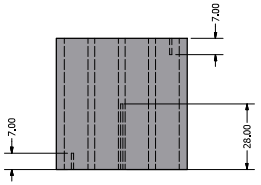

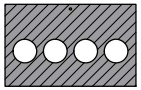

SECTION A-A
SCALE 1 : 1

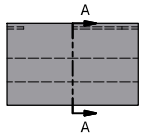

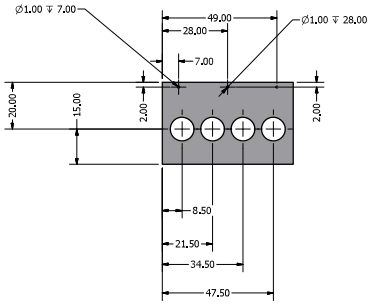

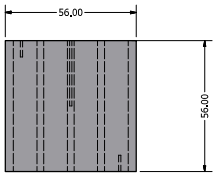

DRAWN elvigro	29.04.2016			
CHECKED		TITLE		
QA				
MFG				
APPROVED		SIZE D	DWG NO Block_Manuel	REV
		SCALE 1 : 1	SHEET 1 OF 1	

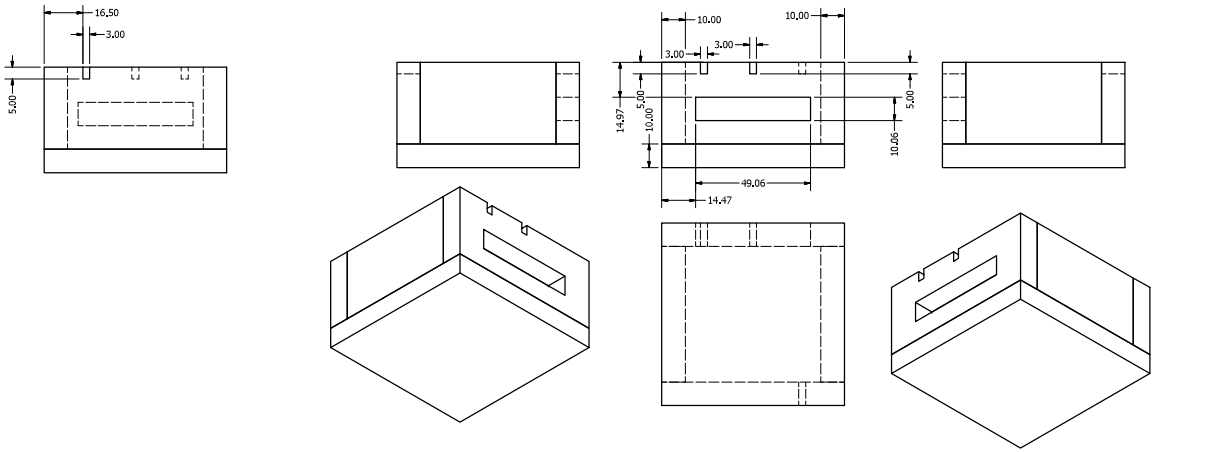

DRAWN elvigro	29.04.2016	
CHECKED		
QA		TITLE
MFG		
APPROVED		
		SIZE D / DWG NO Assembly - 2inch - Insulation / REV
		SCALE 1 : 1 / SHEET 1 OF 1

B. DATASHEETS

FASTCAM SA3

HIGH-G HIGH SPEED VIDEO SYSTEM

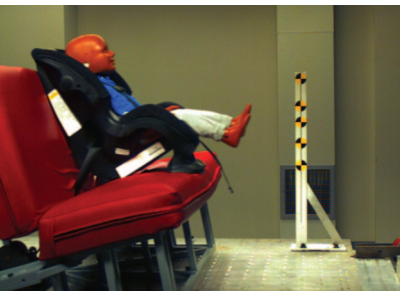


A rugged, megapixel High-Speed imaging system for General Application and Automotive Safety Test recording

2,000fps operation at 1024 x 1024 pixels

Designed referring to SAE-J211 to provide ruggedness and reliability, the Photron FASTCAM SA3 offers high performance recording for a broad range of applications in research and development and automotive safety testing.

Like the award winning FASTCAM MH4 multi-head camera system the FASTCAM SA3 ensures system stability under High-G conditions and long term system reliability.

The FASTCAM SA3 offers remote control through user selectable camera controls on rear panel, Gigabit Ethernet communications or through optional RS422 keypad with built-in 5" LCD display.

The FASTCAM SA3 provides exceptional light sensitivity, image quality and color fidelity through genuine 12-bit ADC, with extra record time provided by selecting 8-bit record mode.

Two FASTCAM SA3 models are available, Model 60K and Model 120K. Both systems offer higher frame rates at reduced image resolution and two microsecond global shutter.

Benefits

- Performance:

  FASTCAM SA3 Model 60K
  1024 x 1024 pixel resolution at frame rates up to 1,000 fps, and at reduced resolution up to 60,000 fps

  FASTCAM SA3 Model 120K
  1024 x 1024 pixel resolution at frame rates up to 2,000 fps, and at reduced resolution up to 120,000 fps

- User selectable Variable Framerate / Resolution
- Suitable for operation in HiG environments. Operation tested to 100G, 10ms, 6 axis
- 17µm pixel size to ensure high light sensitivity for demanding frame rate or low light applications
- 2µs global shutter selectable independent of frame rate.
- Composite video output for real time monitoring during set up, recording and playback
- Optional remote keypad control with integrated viewfinder
- 2GB, 4GB or 8GB memory options
- 8-bit recording mode increases record duration by 50%
- High performance Gigabit Ethernet interface
- Optional battery backup to protect data in the event of unexpected power loss (Pictured below)

Photron

www.photron.com

FASTCAM SA3

HIGH SPEED VIDEO SYSTEM

TARGET APPLICATIONS:

- Onboard vehicle impact testing
- Military test ranges where a sealed unit is beneficial
- Particle Image Velocimetry (PIV)
- Digital Image Correlation (DIC)
- Biomechanics

Specifications: Frame Rate / Resolution Table

FRAME RATE (fps)	MAXIMUM RESOLUTION				RECORD DURATION (12-BIT)											
					TIME (Sec.)						FRAMES					
	Model 60K		Model 120K		Model 60K			Model 120K			Model 60K			Model 120K		
	Horizontal	Vertical	Horizontal	Vertical	2GB	4GB	8GB	2GB	4GB	8GB	2GB	4GB	8GB	2GB	4GB	8GB
1,000	1,024	1,024	1,024	1,024	1.36	2.72	5.45	1.36	2.72	5.45	1,361	2,726	5,457	1,361	2,726	5,457
1,500	896	736	1,024	1,024	1.44	2.89	5.78	0.90	1.81	3.63	2,164	4,335	8,677	1,361	2,726	5,457
2,000	768	608	1,024	1,024	1.52	3.06	6.12	0.68	1.36	2.72	3,057	6,123	12,255	1,361	2,726	5,457
2,500	640	544	896	896	1.64	3.28	6.57	0.71	1.42	2.85	4,100	8,212	16,436	1,778	3,561	7,127
3,000	512	512	896	736	1.81	3.63	7.27	0.72	1.44	2.89	5,445	10,906	21,829	2,164	4,335	8,677
5,000	384	352	640	544	2.11	4.23	8.46	0.82	1.64	3.28	10,560	21,152	42,335	4,100	8,212	16,436
6,000	384	288	512	512	2.15	4.30	8.62	0.90	1.81	3.63	12,907	25,852	51,743	5,445	10,906	21,829
7,500	384	224	512	416	2.21	4.43	8.87	0.89	1.78	3.58	16,595	33,239	66,527	6,701	13,423	26,866
10,000	256	192	384	352	2.90	5.81	11.64	1.05	2.11	4.23	29,041	58,168	116,423	10,560	21,152	42,335
15,000	256	112	384	224	3.31	6.64	13.30	1.10	2.21	4.43	49,785	99,718	199,582	16,595	33,239	66,527
20,000	256	80	256	192	3.48	6.98	13.97	1.45	2.90	5.82	69,700	139,605	279,415	29,041	58,168	116,423
25,000	256	64	256	144	3.48	6.98	13.97	1.54	3.10	6.20	87,125	174,506	349,269	38,722	77,558	155,230
30,000	256	48	256	112	3.87	7.75	15.52	1.65	3.32	6.65	116,167	232,675	465,692	49,785	99,718	199,582
50,000	384	16	256	64	4.64	9.30	18.62	1.74	3.49	6.98	232,334	465,351	931,384	87,125	174,506	349,269
60,000	128	16	256	48	11.61	23.26	46.56	1.93	3.87	7.76	697,002	1,396,053	2,794,154	116,167	232,675	465,692
75,000	-	-	256	32	-	-	-	2.32	4.65	9.31	-	-	-	174,250	349,013	698,538
100,000	-	-	384	16	-	-	-	2.32	4.65	9.31	-	-	-	232,334	465,351	931,384
120,000	-	-	128	16	-	-	-	5.80	11.63	23.28	-	-	-	697,002	1,396,053	2,794,154

Sensor 12-bit ADC (Bayer system color, single sensor) with 17µm pixel size

Shutter Global electronic shutter from 16.7ms to 2µs independent of frame rate

Lens Mount Interchangeable F-mount and C-mount using supplied adapters (Optional High-G block mount available)

Extended Dynamic Range Selectable in twenty steps (0 to 95% in 5% increments) to prevent pixel over-exposure

Memory 2GB (standard), 4GB (optional) and 8GB (optional)

Video Outputs NTSC/PAL composite VBS (BNC). Ability to zoom, pan and scroll within image via keypad (option). Live video during recording

Camera Control Through optional keypad with integrated viewfinder and Gigabit Ethernet or RS-422

User Preset Switch User selectable camera function control mounted on the camera's rear panel

Low Light Mode Low light mode for simple camera adjustment when working in low ambient light, high frame rate or short exposure modes

Triggering Selectable positive or negative TTL 5Vp-p or switch closure

Trigger Delay Programmable delay on selected input and output triggers, 100ns resolution

Timing Internal clock or external source

IRIG Time Code IRIG/GPS timing is recorded in real time on every frame

Event Markers Ten user entered event markers mark specific events within the image sequence in real time. Immediately accessible through software

Variable Framerate/ Resolution User selectable Variable Framerate/Resolution function adjustable in 128 x 16 pixel steps

Selectable Recording Bit Depth User selectable 12-bit (high-dynamic range) or 8-bit (50% frame increase) recording mode

Trigger Modes Start, End, Center, Manual, Random, Random Reset

Saved Image Formats JPEG, AVI, TIFF, BMP, RAW, PNG, MOV, and FTIF. Images can be saved with or without image or comment data

Data Display Frame Rate, Shutter Speed, Trigger Mode, Date or Time, Status (Playback/Record), Real Time, Frame Count, Resolution and LUT

Partitioning Up to 8 memory partitions may be set by the user

High-G Tested to 100G, 10ms, six-axis

Operating Temperature 0-40 degrees C (32-104 degree F)

Mounting 1 x 1/4-20 UNC, 6 x M5 on all four sides

Dimensions 120mm (4.72")H x 120mm (4.72")W x 215.8mm (8.50")D *excluding protrusions

Weight 9.48 lbs (4.3kg)

Power Requirements 100V-240V AC ~ 1.5A, 50-60Hz optional DC operation 22-32VDC, 60VA

Specifications subject to change without notice

PHOTRON USA, INC.
9520 Padgett Street, Suite 110
San Diego, CA 92126-4446
USA
Tel: 858.684.3555 or 800.585.2129
Fax: 858.684.3558
Email: image@photron.com
www.photron.com

PHOTRON (EUROPE) LIMITED
The Barn, Bottom Road
West Wycombe, Bucks, HP14 4BS
United Kingdom
Tel: +44 (0) 1494 481011
Fax: +44 (0) 1494 487011
Email: image@photron.com
www.photron.com

PHOTRON LIMITED
Fujimi 1-1-8
Chiyoda-Ku, Tokyo 102-0071
Japan
Tel: +81 (0) 3 3238 2107
Fax: +81 (0) 3 3238 2109
Email: image@photron.co.jp
www.photron.co.jp

Photron

SLOW MOTION IMAGING SOLUTIONS

omega.com®
OMEGA®

OT-201

OMEGATHERM® Thermally Conductive Silicone Paste

INSTRUCTION SHEET

M0066/1104

Introduction

OMEGATHERM® 201 is a thermally conductive, "Heat Sink" silicone grease. It has a very high thermal conductivity coupled with high insulation resistance and high dielectric strength. The term heat sink compound or thermal joint compound is used to describe this type of material. It does not harden on long exposure to elevated temperatures, but retains its past-like consistency. It is rated for continuous use between -40°F and +392°F (40°C and 200°C).

OMEGATHERM® is available in four quantity sizes, from a ½ oz. jar to a 2 lb. can, as outlined below.

OMEGATHERM® 201 Part Numbers and Sizes	
OT-201-½ one ½ oz. jar	**OT-201-2** one 2 oz. jar
OT-201-16 one 16 oz. can	**OT-201-32** one 32 oz. can

OMEGATHERM 201 provides an excellent means of conducting heat and expanding the heat-path area from a surface to a temperature measurement sensor, thus increasing the speed of response and improving accuracy.

OMEGATHERM 201 improves the heat transfer between a solid state relay and its finned heat dissipating heat sink. Apply a thin layer of "201" thermal compound to the bottom of the solid state relay (SSR), then securely mount the SSR on the finned heat sink with the supplied screws.

Instructions for Use

Although OMEGATHERM 201 does not normally settle in its container, storage for long periods of time at elevated temperature may result in a slight separation of the conductive fillers from the silicone oil. If this condition is seen to exist, the fillers may be easily mixed by hand or mechanical mixing.

OMEGATHERM 201 may be dispensed through a nozzle using any appropriate hand operated or automatic equipment. For some applications, it will be convenient to apply thin films with a stiff brush.

To CLEAN OT-201 from surfaces, use a solvent containing Alcohol, MEK, or Xylene. Repeated use is required to completely clean silicon grease from surface.

Applications

A. Surface Measurement Probes-dab a small amount on the surface and push the thermocouple into this area.

B. Temporary Temperature Monitoring of Surfaces and Bodies-For applications to 392°F (200°C). OT-201 works well with insulated wire thermocouples. Simply dab this paste on the surface or into a cavity, put the sensor in the paste, and tape to hold.

C. Thermocouple Wells (to 200°C)-improve the response time of your thermowell assemblies. Simply put enough OMEGATHERM 201 into the bottom of the wells to cover the active length of the sensor. This application holds for vertical wells or those canted down.

D. NOT FOR USE IN A VACUUM. OT-201 will outgas if used in a vacuum.

Hygiene

MAY CAUSE IRRITATION.

1. Avoid contact with skin and eyes.
2. Wash thoroughly after handling.

First Aid

1. In case of contact, wash skin thoroughly with soap and water.
2. For eyes, flush with water for 15 minutes and consult physician immediately.

FOR INDUSTRIAL USE ONLY.

Typical Properties

Color:	Off-white
Temperature Range of Use:	-40° to +392°F (40° to +200°C)
Consistency:	Thick, smooth paste
Volume Resistivity:	10^{14} ohm-cm
Dielectric Strength:	500 volts/mil (19.7 kv/mm)
Thermal Conductivity:	16 (BTU) (in)/(hr) (ft^2) (°F) 0.0055 (cal)/(cm)/(sec) (cm^2) (°C)
Specific Gravity:	2.53 g/cc
Weight Loss:	0.2% (24 hours/100°C
Shelf life:	1 Year (Storage at 35°F or below will approximately double the shelf life).
Solvents:	Alcohol or MEK or Xylene Solvents

This information is not a warranty and assumes no legal responsibility. Actual suitability for a particular purpose is to be determined by the user.

omega.com®
OMEGA®

OMEGAnet® Online Service omega.com	Internet e-mail info@omega.com

Servicing North America:

U.S.A.: ISO 9001 Certified
One Omega Drive, Box 4047
Stamford, CT 06907-0047
Tel: (203) 359-1660 FAX: (203) 359-7700
e-mail: info@omega.com

Canada:
976 Bergar
Laval (Quebec) H7L 5A1, Canada
Tel: (514) 856-6928 FAX: (514) 856-6886
e-mail: info@omega.ca

For immediate technical or application assistance:

U.S.A. and Canada: Sales Service: 1-800-826-6342 / 1-800-TC-OMEGA®
Customer Service: 1-800-622-2378 / 1-800-622-BEST®
Engineering Service: 1-800-872-9436 / 1-800-USA-WHEN®
TELEX: 996404 EASYLINK: 62968934 CABLE: OMEGA

Mexico: En Español: (001) 203-359-7803 e-mail:espanol@omega.com
FAX: (001) 203-359-7807 info@omega.com.mx

Servicing Europe:

Benelux:
Postbus 8034, 1180 LA Amstelveen, The Netherlands
Tel: +31 (0)20 3472121 FAX: +31 (0)20 6434643
Toll Free in Benelux: 0800 0993344
e-mail: sales@omegaeng.nl

Czech Republic:
Frystatska 184, 733 01 Karviná, Czech Republic
Tel: +420 (0)59 6311899 FAX: +420 (0)59 6311114
Toll Free: 0800-1-66342 e-mail: info@omegashop.cz

France:
11, rue Jacques Cartier, 78280 Guyancourt, France
Tel: +33 (0)1 61 37 2900 FAX: +33 (0)1 30 57 5427
Toll Free in France: 0800 466 342
e-mail: sales@omega.fr

Germany/Austria:
Daimlerstrasse 26, D-75392 Deckenpfronn, Germany
Tel: +49 (0)7056 9398-0 FAX: +49 (0)7056 9398-29
Toll Free in Germany: 0800 639 7678
e-mail: info@omega.de

United Kingdom: ISO 9002 Certified
One Omega Drive, River Bend Technology Centre
Northbank, Irlam, Manchester
M44 5BD United Kingdom
Tel: +44 (0)161 777 6611 FAX: +44 (0)161 777 6622
Toll Free in United Kingdom: 0800-488-488
e-mail: sales@omega.co.uk

It is the policy of OMEGA Engineering, Inc. to comply with all worldwide safety and EMC/EMI regulations that apply. OMEGA is constantly pursuing certification of its products to the European New Approach Directives. OMEGA will add the CE mark to every appropriate device upon certification.

The information contained in this document is believed to be correct, but OMEGA accepts no liability for any errors it contains, and reserves the right to alter specifications without notice.
WARNING: These products are not designed for use in, and should not be used for, human applications.

MADE IN USA

WARRANTY/DISCLAIMER

OMEGA ENGINEERING, INC. warrants this unit to be free of defects in materials and workmanship for a period of **13 months** from date of purchase. OMEGA's WARRANTY adds an additional one (1) month grace period to the normal **one (1) year product warranty** to cover handling and shipping time. This ensures that OMEGA's customers receive maximum coverage on each product.

If the unit malfunctions, it must be returned to the factory for evaluation. OMEGA's Customer Service Department will issue an Authorized Return (AR) number immediately upon phone or written request. Upon examination by OMEGA, if the unit is found to be defective, it will be repaired or replaced at no charge. OMEGA's WARRANTY does not apply to defects resulting from any action of the purchaser, including but not limited to mishandling, improper interfacing, operation outside of design limits, improper repair, or unauthorized modification. This WARRANTY is VOID if the unit shows evidence of having been tampered with or shows evidence of having been damaged as a result of excessive corrosion; or current, heat, moisture or vibration; improper specification; misapplication; misuse or other operating conditions outside of OMEGA's control. Components in which wear is not warranted, include but are not limited to contact points, fuses, and triacs.

OMEGA is pleased to offer suggestions on the use of its various products. However, OMEGA neither assumes responsibility for any omissions or errors nor assumes liability for any damages that result from the use of its products in accordance with information provided by OMEGA, either verbal or written. OMEGA warrants only that the parts manufactured by the company will be as specified and free of defects. OMEGA MAKES NO OTHER WARRANTIES OR REPRESENTATIONS OF ANY KIND WHATSOEVER, EXPRESSED OR IMPLIED, EXCEPT THAT OF TITLE, AND ALL IMPLIED WARRANTIES INCLUDING ANY WARRANTY OF MERCHANTABILITY AND FITNESS FOR A PARTICULAR PURPOSE ARE HEREBY DISCLAIMED. LIMITATION OF LIABILITY: The remedies of purchaser set forth herein are exclusive, and the total liability of OMEGA with respect to this order, whether based on contract, warranty, negligence, indemnification, strict liability or otherwise, shall not exceed the purchase price of the component upon which liability is based. In no event shall OMEGA be liable for consequential, incidental or special damages.

CONDITIONS: Equipment sold by OMEGA is not intended to be used, nor shall it be used: (1) as a "Basic Component" under 10 CFR 21 (NRC), used in or with any nuclear installation or activity; or (2) in medical applications or used on humans. Should any Product(s) be used in or with any nuclear installation or activity, medical application, used on humans, or misused in any way, OMEGA assumes no responsibility as set forth in our basic WARRANTY/DISCLAIMER language, and, additionally, purchaser will indemnify OMEGA and hold OMEGA harmless from any liability or damage whatsoever arising out of the use of the Product(s) in such a manner.

RETURN REQUESTS / INQUIRIES

Direct all warranty and repair requests/inquiries to the OMEGA Customer Service Department. BEFORE RETURNING ANY PRODUCT(S) TO OMEGA, PURCHASER MUST OBTAIN AN AUTHORIZED RETURN (AR) NUMBER FROM OMEGA'S CUSTOMER SERVICE DEPARTMENT (IN ORDER TO AVOID PROCESSING DELAYS). The assigned AR number should then be marked on the outside of the return package and on any correspondence.

The purchaser is responsible for shipping charges, freight, insurance and proper packaging to prevent breakage in transit.

FOR **WARRANTY** RETURNS, please have the following information available BEFORE contacting OMEGA:
1. Purchase Order number under which the product was PURCHASED,
2. Model and serial number of the product under warranty, and
3. Repair instructions and/or specific problems relative to the product.

FOR **NON-WARRANTY** REPAIRS, consult OMEGA for current repair charges. Have the following information available BEFORE contacting OMEGA:
1. Purchase Order number to cover the COST of the repair,
2. Model and serial number of the product, and
3. Repair instructions and/or specific problems relative to the product.

OMEGA's policy is to make running changes, not model changes, whenever an improvement is possible. This affords our customers the latest in technology and engineering.

OMEGA is a registered trademark of OMEGA ENGINEERING, INC.

3M™ Thermal Management Fluids

Safe Sustainable Cooling Performance

Dielectric heat transfer solutions for the electronics industry

3M

Reliable performance. Environmentally sustainable options.

Thermal management issues are becoming increasingly important to electronics and semiconductor manufacturers. New designs put more demands on the dielectric fluids used to maintain proper temperatures. Environmental issues have become a critical factor in fab/plant operating decisions. And system maintenance is always an issue. In short, selection of a heat transfer fluid for your semiconductor processing and electronics equipment can no longer be an afterthought. Long-term, high-performance solutions are needed.

Whether for single-phase or two-phase systems, 3M has a broad range of thermal management fluids and technical support you need to make the right choice for your particular needs. Customers have used 3M products in many applications, including thermal test and immersion cooling of electronics. 3M experts are available to help you choose the right thermal management fluid to improve reliability, address environmental concerns, and lower your overall operating costs.

Cool Solutions for Today's Electronics

All values determined at 25°C unless otherwise specified

3M™ Thermal Management Fluids Properties

3M™ Novec™ Engineered Fluids

	Unit	Novec 7000	Novec 7100	Novec 7200	Novec 7300	Novec 7500	Novec 7600
Boiling Point	°C	34	61	76	98	128	131
Pour Point	°C	-122	-135	-138	-38	-100	-98
Molecular Weight	g/mol	200	250	264	350	414	346
Critical Temperature	°C	165	195	210	243	261	260
Critical Pressure	MPa	2.48	2.23	2.01	1.88	1.55	1.67
Vapor Pressure	kPa	65	27	16	5.9	2.1	0.96
Heat of Vaporization	kJ/kg	142	112	119	102	89	116
Liquid Density	kg/m^3	1400	1510	1420	1660	1614	1540
Coefficient of Expansion	K^{-1}	0.0022	0.0018	0.0016	0.0013	0.0013	0.0011
Kinematic Viscosity	cSt	0.32	0.38	0.41	0.71	0.77	1.1
Absolute Viscosity	cP	0.45	0.58	0.58	1.18	1.24	1.65
Specific Heat	J/kg-K	1300	1183	1220	1140	1128	1319
Thermal Conductivity	W/m-K	0.075	0.069	0.068	0.063	0.065	0.071
Surface Tension	mN/m	12.4	13.6	13.6	15.0	16.2	17.7
Solubility of Water in Fluid	ppm by weight	~60	95	92	67	45	410
Solubility of Fluid in Water	ppm by weight	<50	12	<20	<1	<3	<10
Dielectric Strength, 0.1" gap	kV	~40	~40	~40	~40	~40	~40
Dielectric Constant @ 1kHz	–	7.4	7.4	7.3	6.1	5.8	6.4
Volume Resistivity	Ohm-cm	10^8	10^8	10^8	10^{11}	10^8	10^{10}
Global Warming Potential	GWP	420	297	59	210	100	700

For test methods and variability, contact 3M Technical Service

3M™ Fluorinert™ Electronic Liquids

	Unit	FC-3284	FC-72	FC-84	FC-770	FC-3283	FC-40	FC-43
Boiling Point	°C	50	56	80	95	128	155	174
Pour Point	°C	-73	-90	-95	-127	-50	-57	-50
Molecular Weight	g/mol	299	338	388	399	521	650	670
Critical Temperature	°C	161	176	202	238	235	270	294
Critical Pressure	MPa	1.94	1.83	1.75	2.47	1.22	1.18	1.13
Vapor Pressure	kPa	35	30	11	6.6	1.4	0.43	0.19
Heat of Vaporization	kJ/kg	105	88	90	86	78	68	70
Liquid Density	kg/m^3	1710	1680	1730	1793	1820	1850	1860
Coefficient of Expansion	K^{-1}	0.0016	0.0016	0.0015	0.0015	0.0014	0.0012	0.0012
Kinematic Viscosity	cSt	0.42	0.38	0.53	0.79	0.75	1.8	2.5
Absolute Viscosity	cP	0.71	0.64	0.91	1.4	1.4	3.4	4.7
Specific Heat	J/kg-K	1100	1100	1100	1038	1100	1100	1100
Thermal Conductivity	W/m-K	0.062	0.057	0.060	0.063	0.066	0.065	0.065
Surface Tension	mN/m	13	10	12	15	15	16	16
Solubility of Water in Fluid	ppm by weight	14	10	11	14	7	<7	7
Solubility of Fluid in Water	ppm by weight	<5	<5	<5	<5	<5	<5	<5
Dielectric Strength, 0.1" gap	kV	>40	>40	>40	>40	>40	>40	>40
Dielectric Constant @ 1kHz	–	1.9	1.8	1.8	1.9	1.9	1.9	1.9
Volume Resistivity	Ohm-cm	10^{15}	10^{15}	10^{15}	10^{15}	10^{15}	10^{15}	10^{15}

For test methods and variability, contact 3M Technical Service

For discussion on GWP, refer to additional content in this brochure.

3M™ Novec™ 649 Engineered Fluid

	Unit	Novec 649
Boiling Point	°C	49
Pour Point	°C	-108
Molecular Weight	g/mol	316
Critical Temperature	°C	169
Critical Pressure	MPa	1.88
Vapor Pressure	kPa	40
Heat of Vaporization	kJ/kg	88
Liquid Density	kg/m^3	1600
Coefficient of Expansion	K^{-1}	0.0018
Kinematic Viscosity	cSt	0.40
Absolute Viscosity	cP	0.64
Specific Heat	J/kg-K	1103
Thermal Conductivity	W/m-K	0.059
Surface Tension	mN/m	10.8
Solubility of Water in Fluid	ppm by wt	20
Dielectric Strength, 0.1" gap	kV	>40
Dielectric Constant @ 1kHz	–	1.8
Volume Resistivity	Ohm-cm	10^{12}
Global Warming Potential	GWP	1

Novec 649 fluid is an advanced heat transfer fluid with the lowest Global Warming Potential (GWP) in the Novec family. It belongs to a new class of fluoroketone fluids which are being explored for their use in thermal management applications such as direct and indirect heat transfer systems and Organic Rankine Cycle (ORC) systems.

3M heat transfer fluids, sold under the 3M™ Novec™ Engineered Fluids and 3M™ Fluorinert™ Electronic Liquids brands, are available in a wide range of boiling points (34°C up to 175°C) and freezing points (-38°C down to -138°C), to meet your specific requirements.

3M™ Thermal Management Fluids Kinematic Viscosity

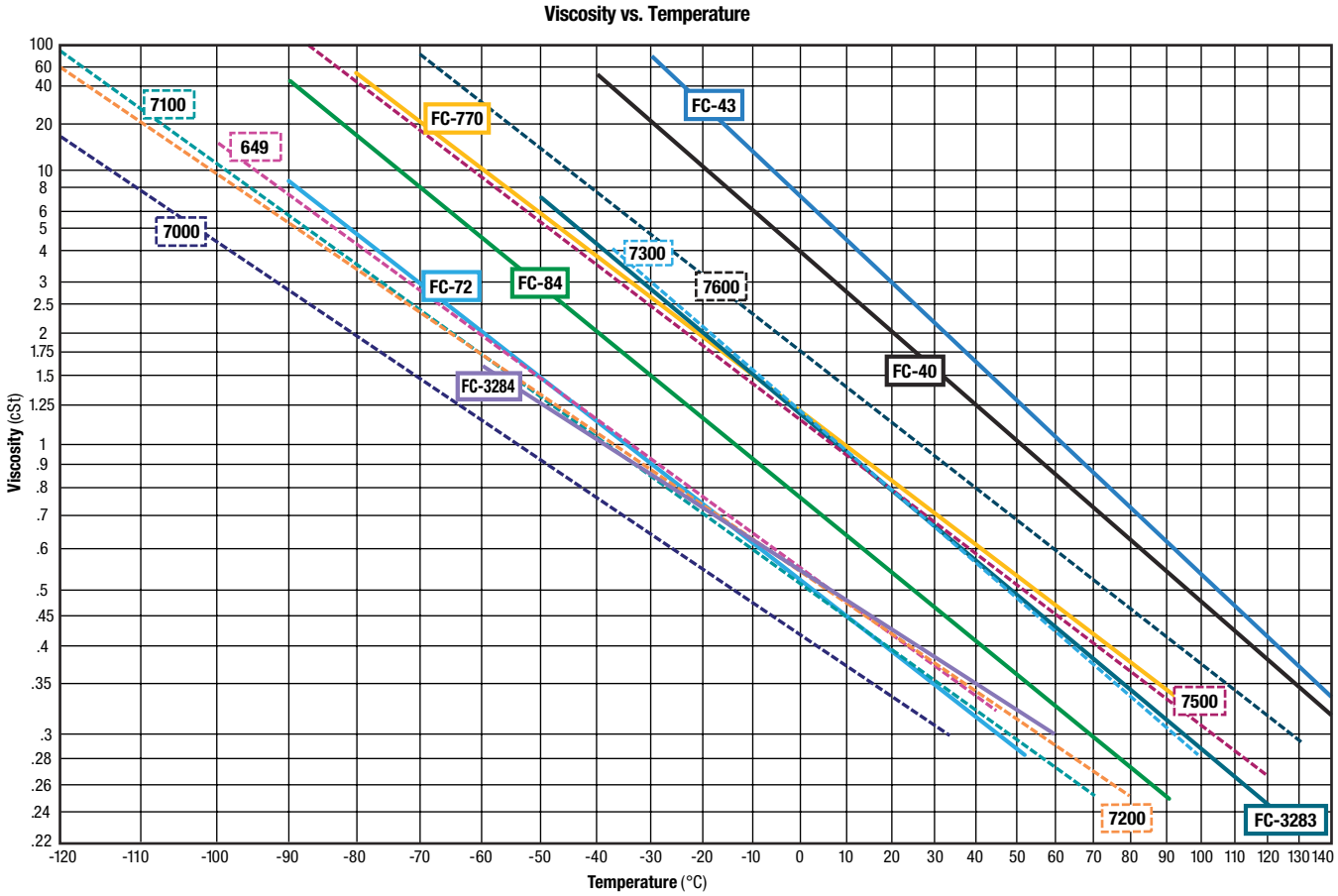

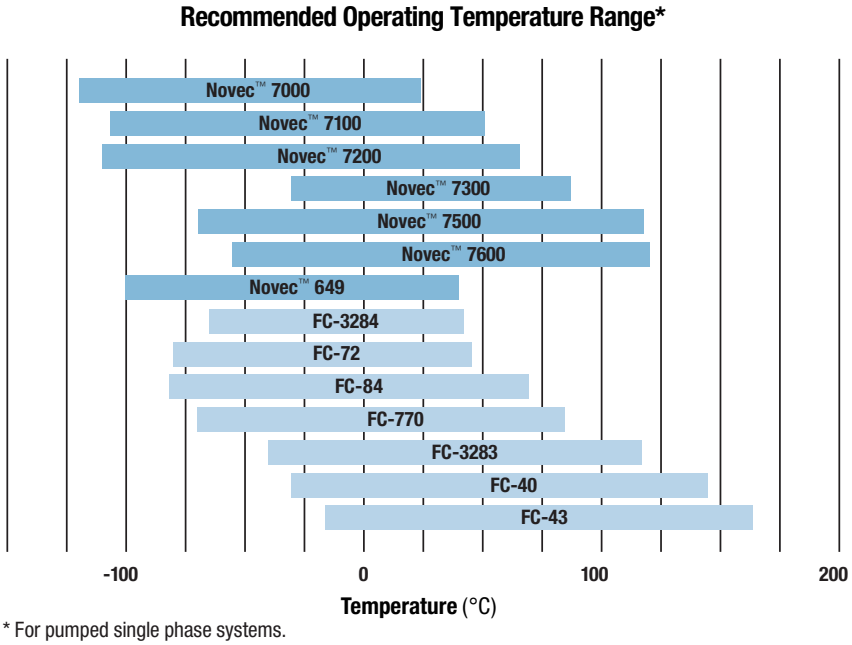

* For pumped single phase systems.

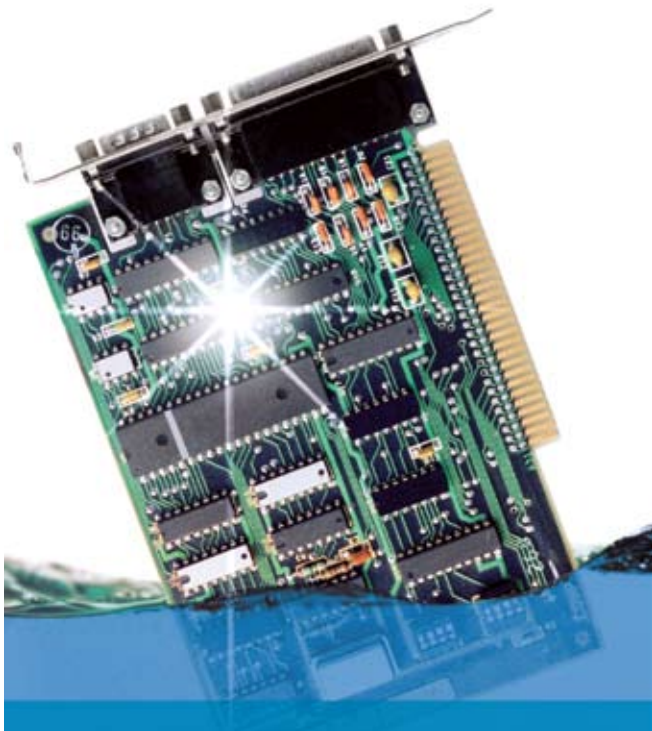

3M™ Novec™ Engineered Fluids

3M™ Novec™ Engineered Fluids are a family of low-Global Warming materials designed to deliver on the Novec promise of safe, sustainable chemistry.

Performance

Novec Engineered Fluids have excellent properties for heat transfer applications:

- Excellent dielectric properties
- Wide range of boiling points
- Good materials compatibility

These fluids require little maintenance and offer dependable performance. They have high resistivity and will not damage electronic equipment or integrated circuits in the event of a leak or other failure.

Environmental profile

Novec Engineered Fluids also offer favorable environmental and worker safety properties:

- Low toxicity
- Nonflammability
- Low Global Warming Potential (GWP)
- Zero Ozone Depletion Potential (ODP)

The chemical inertness and non-corrosivity of Novec Engineered Fluids make them safe for workers to handle, while the environmental properties mean they can be used both now and in the future while leaving behind a smaller footprint on the world.

The next generation of heat transfer fluids

The favorable environmental, health and safety properties of Novec fluids have made them a long-term, sustainable solution. Novec fluids have been recognized by a number of industry and regulatory bodies around the world, including 3M™ Novec™ Engineered Fluids 7100 and 7200 being approved for “use without restriction” under the U.S. EPA’s Significant New Alternatives Policy (SNAP).

Novec fluids are already widely used as heat transfer fluids in the semiconductor industry, where they are used for temperature control of manufacturing equipment while reducing a facility’s greenhouse gas emissions. They have also been used in direct contact dielectric test applications.

Safe
Reliable
Sustainable
Chemistries

3M™ Fluorinert™ Electronic Liquids

3M™ Fluorinert™ Electronic Liquids are part of a family of fully-fluorinated compounds known as perfluorocarbons, or PFCs. Fluorinert liquids are premier heat transfer fluids, and have long been used as heat transfer media for extreme cooling applications.

Originally used for direct contact cooling due to their stability, Fluorinert liquids are also used in a variety of semiconductor operations such as automated testing, etching, deposition, photolithography and more. Fluorinert liquids offer:

- Excellent dielectric properties
- Wide range of boiling points
- Good materials compatibility
- Low toxicity
- Nonflammability
- Zero Ozone Depletion Potential (ODP)

In addition, you have the assurance that comes from dealing with 3M, a company with over 40 years of experience addressing industrial-strength cooling needs.

While they are non-ozone depleting, high-performance Fluorinert liquids do have high global warming potentials (GWP) and long atmospheric lifetimes. Because emission of materials with these properties could have a significant impact on the environment, users must take care to carefully manage and minimize emissions. 3M recommends that users of Fluorinert liquids limit emissions by employing good conservation practices, and by implementing recovery, recycling and/or proper disposal procedures.

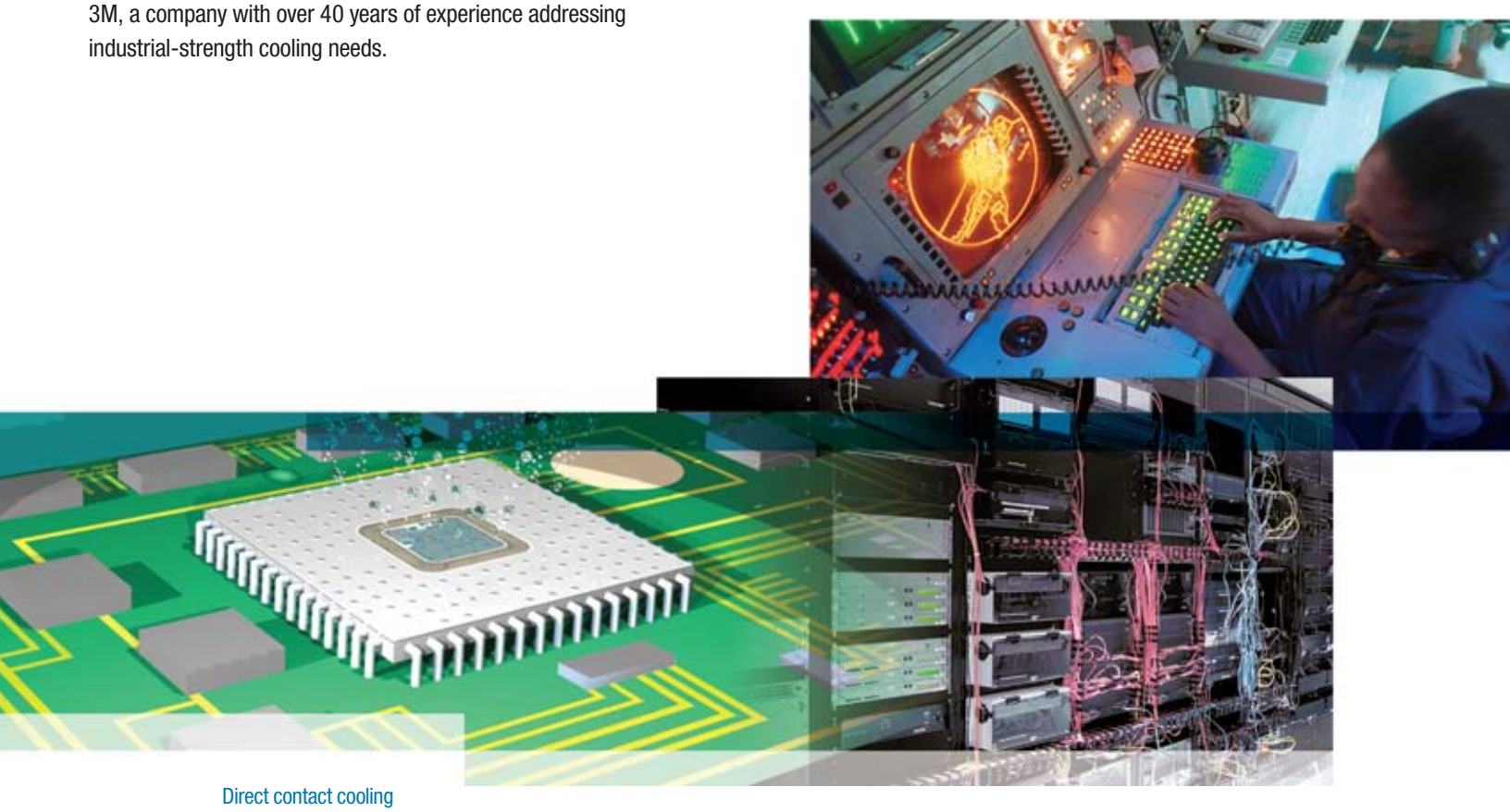

Direct contact cooling with 3M™ Fluorinert™ Electronic Liquids helped enable the development of dense electronics, such as supercomputers and power converters.

Material Compatibility

3M™ Novec™ Engineered Fluids and 3M™ Fluorinert™ Electronic Liquids are compatible with a wide variety of materials used in heat transfer equipment. As with any design, selection of these materials is very important. A 3M specialist in this area can help you make the proper choice.

Polymers

Most of the materials commonly considered “hard” plastics will perform well with both Novec fluids and Fluorinert liquids.

Elastomers

Elastomers should be limited to those that are not heavily plasticized. 3M engineers can assist you with recommendations and testing on specific compounds.

More Options More Answers

The hidden benefit: 3M experience

The use of fluorochemicals in heat transfer systems is a science that 3M has studied like no other company. Bringing this extensive knowledge to bear on your heat transfer equipment is a major part of our Thermal Management program ... and a major benefit of purchasing 3M™ Novec™ Engineered Fluids or 3M™ Fluorinert™ Electronic Liquids.

Here are just some of the services that 3M can provide to help you utilize these innovative fluids in your heat transfer equipment:

Heat Transfer Seminar/Design Assistance

Given free of charge at qualifying customer sites, this seminar teaches appropriate design procedures by discussing material compatibility, sources of leakage, pumping, component selection, environmental issues and more. The content of these seminars can be tailored to the specific interests of the audience. 3M has conducted seminars at numerous customer locations.

Compatibility Testing

3M engineers can evaluate parts with advanced testing methods to help you determine if a component or material is suitable in your design.

On-Site Consultations

Working side-by-side with equipment designers and end users, 3M engineers frequently help customers tighten-up equipment and optimize system performance.

Analytical Services

3M has state-of-the-art analytical resources which are used to help answer customer questions.

The 3M™ Novec™ Brand Family The Novec brand is the hallmark for a variety of patented 3M products. Although each has its own unique formula and performance properties, all Novec products are designed in common to address the need for safe, effective, sustainable solutions in industry-specific applications. These include precision and electronics cleaning, heat transfer, fire protection, lubricant deposition and several specialty chemical applications.

3M™ Novec™ Engineered Fluids ▪ 3M™ Novec™ Aerosol Cleaners ▪ 3M™ Novec™ 1230 Fire Protection Fluid ▪ 3M™ Novec™ Electronic Coatings ▪ 3M™ Novec™ Electronic Surfactants

Electronics Markets Materials Division
3M Electronics
3M Center, Building 224-3N-11
St. Paul, MN 55144-1000
www.3M.com/electronics
1-800-810-8513

Please recycle. Printed in USA.
Issued: 4/09
98-0212-2649-7

Safety Data Sheet

Document Group:	10-3789-4	**Version Number:**	33.00
Issue Date:	12/01/16	**Supercedes Date:**	08/05/15

SECTION 1: Identification

1.1. Product identifier

3M™ Fluorinert™ Electronic Liquid FC-72

Product Identification Numbers

ID Number	UPC	ID Number	UPC
98-0211-0216-9	00-51135-09194-4	98-0211-0217-7	00-51135-09195-1
98-0211-0267-2	00-51135-09209-5	98-0212-4823-6	00-51138-99198-2
98-0212-4842-6	0-00-51138-99222-4	ZF-0002-0321-4	
ZF-0002-0354-5		ZF-0002-0802-3	
ZF-0002-1162-1		ZF-0002-1872-5	

1.2. Recommended use and restrictions on use

Recommended use

For Industrial Use Only. Not Intended for Use as a Medical Device or Drug., Testing Fluid or Heat Transfer Fluid for Electronics.

Restrictions on use

Fluorinert™ Electronic Liquids are used in a wide variety of applications, including but not limited to precision cleaning of medical devices and as lubricant deposition solvents for medical devices. When the product is used for applications where the finished device is implanted into the human body, no residual Fluorinert solvent may remain on the parts. It is highly recommended that the supporting test results and protocol be cited during FDA registration.

3M Electronics Markets Materials Division (EMMD) will not knowingly sample, support, or sell its products for incorporation in medical and pharmaceutical products and applications in which the 3M product will be temporarily or permanently implanted into humans or animals. The customer is responsible for evaluating and determining that a 3M EMMD product is suitable and appropriate for its particular use and intended application. The conditions of evaluation, selection, and use of a 3M product can vary widely and affect the use and intended application of a 3M product. Because many of these conditions are uniquely within the user's knowledge and control, it is essential that the user evaluate and determine whether the 3M product is suitable and appropriate for a particular use and intended application, and complies with all local applicable laws, regulations, standards, and guidance.

1.3. Supplier's details

MANUFACTURER:	3M
DIVISION:	Electronics Materials Solutions Division
ADDRESS:	3M Center, St. Paul, MN 55144-1000, USA
Telephone:	1-888-3M HELPS (1-888-364-3577)

1.4. Emergency telephone number
1-800-364-3577 or (651) 737-6501 (24 hours)

SECTION 2: Hazard identification

2.1. Hazard classification
Not classified as hazardous according to OSHA Hazard Communication Standard, 29 CFR 1910.1200.

2.2. Label elements
Signal word
Not applicable.

Symbols
Not applicable.

Pictograms
Not applicable.

2.3. Hazards not otherwise classified
None.

SECTION 3: Composition/information on ingredients

Ingredient	C.A.S. No.	% by Wt
PERFLUORO COMPOUNDS, C5-18	86508-42-1	100 (typically 100)

SECTION 4: First aid measures

4.1. Description of first aid measures

Inhalation:
Remove person to fresh air. If signs/symptoms develop, get medical attention.

Skin Contact:
Wash with soap and water. If signs/symptoms develop, get medical attention.

Eye Contact:
Flush with large amounts of water. Remove contact lenses if easy to do. Continue rinsing. If signs/symptoms persist, get medical attention.

If Swallowed:
No need for first aid is anticipated.

4.2. Most important symptoms and effects, both acute and delayed
See Section 11.1. Information on toxicological effects.

4.3. Indication of any immediate medical attention and special treatment required
Not applicable

SECTION 5: Fire-fighting measures

5.1. Suitable extinguishing media
Non-combustible. Use a fire fighting agent suitable for surrounding fire.

5.2. Special hazards arising from the substance or mixture
Exposure to extreme heat can give rise to thermal decomposition.

Hazardous Decomposition or By-Products

Substance	Condition
Carbon monoxide	During Combustion
Carbon dioxide	During Combustion

5.3. Special protective actions for fire-fighters
When fire fighting conditions are severe and total thermal decomposition of the product is possible, wear full protective clothing, including helmet, self-contained, positive pressure or pressure demand breathing apparatus, bunker coat and pants, bands around arms, waist and legs, face mask, and protective covering for exposed areas of the head.

SECTION 6: Accidental release measures

6.1. Personal precautions, protective equipment and emergency procedures
Ventilate the area with fresh air. For large spill, or spills in confined spaces, provide mechanical ventilation to disperse or exhaust vapors, in accordance with good industrial hygiene practice. Observe precautions from other sections.

6.2. Environmental precautions
Avoid release to the environment. For larger spills, cover drains and build dikes to prevent entry into sewer systems or bodies of water.

6.3. Methods and material for containment and cleaning up
Contain spill. Working from around the edges of the spill inward, cover with bentonite, vermiculite, or commercially available inorganic absorbent material. Mix in sufficient absorbent until it appears dry. Collect as much of the spilled material as possible. Place in a closed container approved for transportation by appropriate authorities. Clean up residue with an appropriate solvent selected by a qualified and authorized person. Ventilate the area with fresh air. Read and follow safety precautions on the solvent label and SDS. Seal the container. Dispose of collected material as soon as possible.

SECTION 7: Handling and storage

7.1. Precautions for safe handling
Do not breathe thermal decomposition products. Avoid skin contact with hot material. Store work clothes separately from other clothing, food and tobacco products. Keep away from reactive metals (eg. Aluminum, zinc etc.) to avoid the formation of hydrogen gas that could create an explosion hazard. No smoking: Smoking while using this product can result in contamination of the tobacco and/or smoke and lead to the formation of hazardous decomposition products.

7.2. Conditions for safe storage including any incompatibilities
Store away from heat.

SECTION 8: Exposure controls/personal protection

8.1. Control parameters

Occupational exposure limits
No occupational exposure limit values exist for any of the components listed in Section 3 of this SDS.

8.2. Exposure controls

8.2.1. Engineering controls
Provide appropriate local exhaust when product is heated.

8.2.2. Personal protective equipment (PPE)

Eye/face protection
None required.

Skin/hand protection
No chemical protective gloves are required.

Respiratory protection

Use a positive pressure supplied-air respirator if there is a potential for over exposure from an uncontrolled release, exposure levels are not known, or under any other circumstances where air-purifying respirators may not provide adequate protection.

Thermal hazards
Wear heat insulating gloves when handling hot material to prevent thermal burns.

SECTION 9: Physical and chemical properties

9.1. Information on basic physical and chemical properties

General Physical Form:	Liquid
Specific Physical Form:	Liquid
Odor, Color, Grade:	Colorless, odorless liquid.
Odor threshold	*No Data Available*
pH	*Not Applicable*
Melting point	*Not Applicable*
Boiling Point	50 - 60 ºC
Flash Point	No flash point
Evaporation rate	> 1 [*Ref Std:* BUOAC=1]
Flammability (solid, gas)	Not Applicable
Flammable Limits(LEL)	None detected
Flammable Limits(UEL)	None detected
Vapor Pressure	232 mmHg [@ 20 ºC]
Vapor Density	Approximately 11.7 [@ 20 ºC] [*Ref Std:* AIR=1]
Density	1.7 g/ml
Specific Gravity	1.7 [*Ref Std:* WATER=1]
Solubility in Water	Nil
Solubility- non-water	*No Data Available*
Partition coefficient: n-octanol/ water	*No Data Available*
Autoignition temperature	*No Data Available*
Decomposition temperature	*Not Applicable*
Viscosity	0.4 centistoke [@ 20 ºC]
Molecular weight	*No Data Available*
Volatile Organic Compounds	[*Details:* Exempt]
Percent volatile	100 %
VOC Less H2O & Exempt Solvents	[*Details:* Exempt]

SECTION 10: Stability and reactivity

10.1. Reactivity
This material may be reactive with certain agents under certain conditions - see the remaining headings in this section.

10.2. Chemical stability
Stable.

10.3. Possibility of hazardous reactions
Hazardous polymerization will not occur.

10.4. Conditions to avoid
Heat

10.5. Incompatible materials
Finely divided active metals
Alkali and alkaline earth metals

10.6. Hazardous decomposition products

Substance	Condition
Hydrogen Fluoride	At Elevated Temperatures - greater than 200 ºC
Perfluoroisobutylene (PFIB)	At Elevated Temperatures - greater than 200 ºC

Refer to section 5.2 for hazardous decomposition products during combustion.

If the product is exposed to extreme condition of heat from misuse or equipment failure, toxic decomposition products that include hydrogen fluoride and perfluoroisobutylene can occur.

SECTION 11: Toxicological information

The information below may not be consistent with the material classification in Section 2 if specific ingredient classifications are mandated by a competent authority. In addition, toxicological data on ingredients may not be reflected in the material classification and/or the signs and symptoms of exposure, because an ingredient may be present below the threshold for labeling, an ingredient may not be available for exposure, or the data may not be relevant to the material as a whole.

11.1. Information on Toxicological effects

Signs and Symptoms of Exposure

Based on test data and/or information on the components, this material may produce the following health effects:

Inhalation:
Vapors from heated material may cause irritation of the respiratory system. Signs/symptoms may include cough, sneezing, nasal discharge, headache, hoarseness, and nose and throat pain.

Skin Contact:
Contact with the skin during product use is not expected to result in significant irritation.

Eye Contact:
Contact with the eyes during product use is not expected to result in significant irritation.

Ingestion:
No known health effects.

Toxicological Data
If a component is disclosed in section 3 but does not appear in a table below, either no data are available for that endpoint or the data are not sufficient for classification.

Acute Toxicity

Name	Route	Species	Value
PERFLUORO COMPOUNDS, C5-18	Dermal		LD50 estimated to be > 5,000 mg/kg
PERFLUORO COMPOUNDS, C5-18	Inhalation-Vapor (4 hours)	Rat	LC50 > 41 mg/l
PERFLUORO COMPOUNDS, C5-18	Ingestion	Rat	LD50 > 5,000 mg/kg

ATE = acute toxicity estimate

Skin Corrosion/Irritation

Name	Species	Value
PERFLUORO COMPOUNDS, C5-18	Rabbit	No significant irritation

Serious Eye Damage/Irritation

Name	Species	Value
PERFLUORO COMPOUNDS, C5-18	Rabbit	No significant irritation

Skin Sensitization

For the component/components, either no data are currently available or the data are not sufficient for classification.

Respiratory Sensitization

For the component/components, either no data are currently available or the data are not sufficient for classification.

Germ Cell Mutagenicity

Name	Route	Value
PERFLUORO COMPOUNDS, C5-18	In Vitro	Not mutagenic

Carcinogenicity

For the component/components, either no data are currently available or the data are not sufficient for classification.

Reproductive Toxicity

Reproductive and/or Developmental Effects

For the component/components, either no data are currently available or the data are not sufficient for classification.

Target Organ(s)

Specific Target Organ Toxicity - single exposure

For the component/components, either no data are currently available or the data are not sufficient for classification.

Specific Target Organ Toxicity - repeated exposure

Name	Route	Target Organ(s)	Value	Species	Test Result	Exposure Duration
PERFLUORO COMPOUNDS, C5-18	Inhalation	heart | endocrine system | bone, teeth, nails, and/or hair | hematopoietic system | liver | immune system | nervous system | eyes | kidney and/or bladder | respiratory system	All data are negative	Rat	NOAEL 49,821 ppm	13 weeks
PERFLUORO COMPOUNDS, C5-18	Ingestion	heart | endocrine system | hematopoietic system | liver | nervous system |	All data are negative	Rat	NOAEL 2,000 mg/kg/day	28 days

		kidney and/or bladder | respiratory system				

Aspiration Hazard
For the component/components, either no data are currently available or the data are not sufficient for classification.

Please contact the address or phone number listed on the first page of the SDS for additional toxicological information on this material and/or its components.

SECTION 12: Ecological information

Ecotoxicological information

Please contact the address or phone number listed on the first page of the SDS for additional ecotoxicological information on this material and/or its components.

Chemical fate information

Please contact the address or phone number listed on the first page of the SDS for additional chemical fate information on this material and/or its components.

SECTION 13: Disposal considerations

13.1. Disposal methods
Dispose of contents/ container in accordance with the local/regional/national/international regulations.

Dispose of waste product in a permitted industrial waste facility. Combustion products will include HF. Facility must be capable of handling halogenated materials.
Empty and clean product containers may be disposed as non-hazardous waste. Consult your specific regulations and service providers to determine available options and requirements.

EPA Hazardous Waste Number (RCRA): Not regulated

SECTION 14: Transport Information

For Transport Information, please visit http://3M.com/Transportinfo or call 1-800-364-3577 or 651-737-6501.

SECTION 15: Regulatory information

15.1. US Federal Regulations
Contact 3M for more information.

311/312 Hazard Categories:

Fire Hazard - No Pressure Hazard - No Reactivity Hazard - No Immediate Hazard - No Delayed Hazard - No

15.2. State Regulations
Contact 3M for more information.

15.3. Chemical Inventories
The components of this material are in compliance with the provisions of Australia National Industrial Chemical Notification and Assessment Scheme (NICNAS). Certain restrictions may apply. Contact the selling division for additional information.

The components of this product are in compliance with the new substance notification requirements of CEPA.

The components of this material are in compliance with the China "Measures on Environmental Management of New Chemical Substance". Certain restrictions may apply. Contact the selling division for additional information.

The components of this material are in compliance with the provisions of the Korean Toxic Chemical Control Law. Certain restrictions may apply. Contact the selling division for additional information.

The components of this material are in compliance with the provisions of Japan Chemical Substance Control Law. Certain restrictions may apply. Contact the selling division for additional information.

The components of this material are in compliance with the provisions of Philippines RA 6969 requirements. Certain restrictions may apply. Contact the selling division for additional information.

The components of this product are in compliance with the chemical notification requirements of TSCA.

Contact 3M for more information.

15.4. International Regulations
Contact 3M for more information.

This SDS has been prepared to meet the U.S. OSHA Hazard Communication Standard, 29 CFR 1910.1200.

SECTION 16: Other information

NFPA Hazard Classification
Health: 3 **Flammability:** 0 **Instability:** 0 **Special Hazards:** None

National Fire Protection Association (NFPA) hazard ratings are designed for use by emergency response personnel to address the hazards that are presented by short-term, acute exposure to a material under conditions of fire, spill, or similar emergencies. Hazard ratings are primarily based on the inherent physical and toxic properties of the material but also include the toxic properties of combustion or decomposition products that are known to be generated in significant quantities.

HMIS Hazard Classification
Health: 0 **Flammability:** 0 **Physical Hazard:** 0 **Personal Protection:** X - See PPE section.

Hazardous Material Identification System (HMIS® IV) hazard ratings are designed to inform employees of chemical hazards in the workplace. These ratings are based on the inherent properties of the material under expected conditions of normal use and are not intended for use in emergency situations. HMIS® IV ratings are to be used with a fully implemented HMIS® IV program. HMIS® is a registered mark of the American Coatings Association (ACA).

Document Group:	10-3789-4	**Version Number:**	33.00
Issue Date:	12/01/16	**Supercedes Date:**	08/05/15

DISCLAIMER: The information in this Safety Data Sheet (SDS) is believed to be correct as of the date issued. 3M MAKES NO WARRANTIES, EXPRESSED OR IMPLIED, INCLUDING, BUT NOT LIMITED TO, ANY IMPLIED WARRANTY OF MERCHANTABILITY OR FITNESS FOR A PARTICULAR PURPOSE OR COURSE OF PERFORMANCE OR USAGE OF TRADE. User is responsible for determining whether the 3M product is fit for a particular purpose and suitable for user's method of use or application. Given the variety of factors that can affect the use and application of a 3M product, some of which are uniquely within the user's knowledge and control, it is essential that the user evaluate the 3M product to determine whether it is fit for a particular purpose and suitable for user's method of use or application.

3M provides information in electronic form as a service to its customers. Due to the remote possibility that electronic

transfer may have resulted in errors, omissions or alterations in this information, 3M makes no representations as to its completeness or accuracy. In addition, information obtained from a database may not be as current as the information in the SDS available directly from 3M

3M USA SDSs are available at www.3M.com